NTNU

Norwegian University of
Science and Technology

On Developing a Digital Twin for Fault Detection in Drivetrains of Offshore Wind Turbines

Sigrid Siksjø Johansen

Marine Technology
Submission date: June 2018
Supervisor: Amir Nejad, IMT

Norwegian University of Science and Technology
Department of Marine Technology

NTNU – Trondheim
Norwegian University of
Science and Technology
Department of Marine Technology

MSC THESIS IN MARINE TECHNOLOGY
SPRING 2018

On Developing a Digital Twin for Fault Detection in Drivetrains of Offshore Wind Turbines

Sigrid Siksjø Johansen

Background:

The development trend in offshore wind turbines is towards larger turbines in deeper water. Thus, drivetrains designed for offshore wind turbines are expected to have higher reliability and availability than those designed for land-based turbines. In addition fault detection and condition monitoring becomes more important and essential for offshore wind turbines as the cost of maintenance and repair is by far higher than the land-based ones. "Digital twin - the future of engineering" as cited by DNV-GL, is a model-based approach to anticipate the behaviour of a system or a machine through its virtual image.
The aim of the project is to employ state-of-the art tools and methods to build a digital twin of a representative rotating system in the lab and to perform a sensitivity study of the different modal parameters in order to model the system faults.

Assignment:

The following tasks should be addressed in the thesis work:
1. Carry out a literature review on digital twin development. Discuss advantages and disadvantages compared with data-based methods.

2. Study faults and fault detection methods in drivetrains.

3. Develop a digital twin of the test rig from the MCMR lab.

4. Carry modal analysis in the lab to identify the system parameters.

5. Test different modelling methods, discuss challenges.

6. Measure vibration signals from the lab and compare with the model.

7. Model bearing fault in the digital twin, discuss fault modelling methods.

8. Discuss the results, conclude the work and give recommendations for future work.

9. Write the MSc thesis report.

In the thesis the candidate shall present his personal contribution to the resolution of problem within the scope of the thesis work.

Theories and conclusions should be based on mathematical derivations and/or logic reasoning identifying the various steps in the deduction.

The candidate should utilize the existing possibilities for obtaining relevant literature.

NTNU – Trondheim
Norwegian University of
Science and Technology
Department of Marine Technology

The thesis should be organized in a rational manner to give a clear exposition of results, assessments, and conclusions. The text should be brief and to the point, with a clear language. Telegraphic language should be avoided.

The thesis shall contain the following elements: A text defining the scope, preface, list of contents, summary, main body of thesis, conclusions with recommendations for further work, list of symbols and acronyms, reference and (optional) appendices. All figures, tables and equations shall be numerated.

The supervisor may require that the candidate, in an early stage of the work, present a written plan for the completion of the work. The plan should include a budget for the use of computer and laboratory resources that will be charged to the department. Overruns shall be reported to the supervisor.

The original contribution of the candidate and material taken from other sources shall be clearly defined. Work from other sources shall be properly referenced using an acknowledged referencing system.

The thesis shall be submitted electronically (pdf) in DAIM:

- Signed by the candidate
- The text defining the scope (this text) (signed by the supervisor) included
- Computer code, input files, videos and other electronic appendages can be uploaded in a zip-file in DAIM. Any electronic appendages shall be listed in the main thesis.

The candidate will receive a printed copy of the thesis.

Supervisor:
Amir R. Nejad (Amir.Nejad@ntnu.no)
Marine Technology Department
Deadline for thesis report: June 2018 (check the exact date at DAIM)

Abstract

This master thesis considers fault detection of drivetrains in offshore wind turbines through digital twin approach. A literature review regarding current operations concerning maintenance approaches in today's practices are covered. The main reasons for downtime in a wind turbine are discussed, and it is argued that faults in the gearbox are a significant contributor to downtime and should receive serious attention regarding fault detection and maintenance. Operation and maintenance costs should and could be reduced. There is an excessive industrial interest to evaluate improved maintenance schemes.

State-of-the-art fault detection in drivetrains is discussed, founded in condition monitoring and data-based schemes. It is debated that a model-based approach of a digital twin could be recommended for fault detection of drivetrains. By employing a digital twin fault detection would be extended to a more diagnostic and predictive maintenance programme, and costs could be reduced.

A holistic model system approach is considered to be more accurate, and the methodologies of digital twin design are covered. Designing the model introduces several pitfalls depending on the relevant system, and the advantages, disadvantages and appropriate applications are discussed in extent. For a drivetrain in an offshore wind turbine it is found that multi-body simulation is advised for the creation of a digital twin model.

A digital twin of a simple drivetrain test rig is made, and different modelling approaches were implemented to investigate levels of accuracy. Reference values were derived empirically by attaching sensors to the drivetrain during operation in the test rig. Modelling with a low fidelity model shows a high accuracy, however it would lack several segments required for a digital twin. The higher fidelity model shows that finding the stiffness parameter proves challenging, due to high stiffness sensitivity as the experimental modelling demonstrates.

For fault detection by digital twin approach to be reliable, both the digital twin and its fault modelling have to be reliable. The aim is to have a model reliable to such a degree that vibration data and fault detection would be performed on the digital twin. Two fault modelling approaches were performed in this thesis; altering stiffness in the bearing force, and using an input force vector in the bearing representing the bearing reaction force. Altering stiffness, based on the limited data attained, would not in this specific case be applicable, possibly because of high stiffness sensitivity and existing faults. The input force vector method showed imperfections in output response, and it is recommended to work further on to correct these flaws. However, this approach have a higher potential in the aim for digital twin modelling. The input force vector could be implemented in a real-time, online and dynamic digital twin. This could be done through use of an inverse method from the equation of motion (EOM) to a dynamic file input in SIMPACK. In this thesis a stochastic process is proposed, still other approaches could also be effective.

Sammendrag

Denne masteroppgaven vurderer feilsøking av drivverk i offshore vindturbiner ved hjelp av en digital tvilling. En litteraturgjennomgang om operasjoner vedrørende vedlikeholdsmetoder i dagens praksis er dekket. Hovedårsakene til nedetid i en vindturbin diskuteres, og det hevdes at feil i girkassen er en betydelig bidragsyter til nedetid og bør følges nøye opp når det gjelder feildetektering og vedlikehold. Drifts- og vedlikeholdskostnader bør og kan reduseres. Det er av stor industriell interesse å vurdere oppgraderinger av vedlikeholdsprogram.

Det er diskutert state-of-the-art feilgjenkjenning i drivverk, grunnlagt i tilstandsovervåking og databaserte ordninger. Det diskuteres at en modellbasert tilnærming til en digital tvilling kan anbefales for feilsøking av drivstasjoner. Ved å bruke en digital tvilling kan feildeteksjon bli utvidet til et mer diagnostisk og forutsigbart vedlikeholdsprogram, og kostnadene kan reduseres.

En helhetlig modell systemtilnærming anses å være mer nøyaktig, og metodene for digital tvilling design er dekket. Utformingen av modellen introduserer flere fallgruver avhengig av det aktuelle systemet, og fordelene, ulemper og hensiktsmessige anvendelser diskuteres i stor grad. For en drivkraft i en offshore vindturbin er det funnet at fler-kropps simulering anbefales for opprettelsen av en digital tvilling.

En digital tvilling av et enkel drivverk er laget, og ulike modellerings tilnærminger ble implementert for å undersøke nivåer av nøyaktighet. Referanseverdier ble avledet empirisk ved å feste sensorer til drivstasjonen under drift i testriggen. Modellering med lav gjengivelsesgrad viser høy nøyaktighet, men det ville mangle flere segmenter som kreves for en digital tvilling. Den modellen med høyere gjengivelsesgrad viser at det å finne stivhetsparameteren er utfordrende på grunn av høy stivhetsfølsomhet. Dette demonstrerer den eksperimentelle modelleringen.

For feilsøking ved digital tvilling tilnærming for å være pålitelig, må både den digitale tvilling og dens feilmodellering være pålitelig. Målet er å ha en modell som pålitelig i en slik grad at vibrasjonsdata og feildeteksjon vil bli utført på digital tvilling. To feilmodelleringsmetoder ble utført i denne oppgaven; endring av stivhet i opplager, og bruk av en kraftvektor i opplageret som representerer lagerreaksjonskraften. Endring av stivhet, basert på begrensede data, ville ikke i dette spesielle tilfellet være aktuelt, muli-

gens på grunn av høy stivhetsensitivitet og eksisterende feil. Kraftvektor-metoden viste feil i responsen, og det anbefales å arbeide videre for å rette opp disse feilene. Imidlertid har denne tilnærmingen et høyere potensial i målet for digital tvilling-modellering. Kraftvektoren kan implementeres i en sanntids, online og dynamisk digital tvilling. Dette kan gjøres ved bruk av en invers metode fra bevegelsesligningen (EOM) til en dynamisk filinngang i SIMPACK. I denne oppgaven er det foreslått en stokastisk prosess, men andre tilnærminger kan også være effektive.

Preface

This paper is a master thesis and a part of the study programme Marine Technology at the Norwegian University of Science and Technology (NTNU).

The work was carried out during the spring semester of 2018 and is the course *TMR4930 Marine Technology, master thesis*, at the Department of Marine Machinery. Supervisor for this thesis is Amir Rasekhi Nejad and the work load and the weighting is 30 ECTS. The work done in this master thesis is to be seen as a continuance of the project thesis that was written during autumn 2017. Chapters 1 through 2 is taken from from the project thesis.

The main focus in this master thesis has been with modelling of a digital twin of a drivetrain for the purpose of fault detection. This is motivated to be taken into use for an offshore wind turbine. The drivetrain was modelled in SIMPACK using co-simulation with MATLAB/Simulink. The literature study is for background and motivation for the work and to achieve insight of state-of-the-art in drivetrain modelling and fault detection. Conducting different modelling approaches has been interesting and time-consuming. When trying to model in a new software, it takes some time to understand the correlation between output and input, and there has been extensive troubleshooting regarding modelling both with flexible and rigid bodies in SIMPACK, and to resolve issues concerning co-simulation. However, this has been valuable time for me to attain the relevant knowledge needed to understand the resulting output.

My scope of work was formulated together with my supervisor Amir Rasekhi Nejad. The research and workload has been extensive, but has allowed me to answer the issue raised.

Trondheim, 27th June 2018

Sigrid Siksjø Johansen

Acknowledgment

I would first like to thank my supervisor and thesis advisor Amir Rasekhi Nejad. He has been crucial in keeping me on the right path in both my research and my work in SIMPACK. He steadily allowed the thesis to be my own work, but steered me in the right direction when he saw fit. His door was always open and he would gladly share his knowledge.

Furthermore, I would like to thank my peers at my office at NTNU, specifically Helene Rimstad for her input and our academic discussion regarding the master thesis subject. Additionally, I would like to thank Ashlee Espinoza as the second reader of this thesis, and I am gratefully indebted to her for her valuable comments on this thesis. Finally, I would also like to thank PhD student Shuaishuai Wang for his guidance in SIMPACK and helpful discussion regarding modelling.

S.S.J

Contents

List of Figures

List of Tables

Acronyms

AE acoustic emission

CACSD computer aided control system design

CPS cyber- physical system

DD direct drive

DOF degree of freedom

DTA digital twin aggregate

DTI digital twin incident

DTP digital twin prototype

EOM equation of motion

FE finite element

FEA finite element analysis

FEM finite element method

FFT fast-fourier transform

IoT internet of things

MCMR lab marine computational mechanics research lab

MBS multi-body simulation

O&M operation and maintenance

PI proportional-integral

RAMS reliability, availability, maintainability and safety

RMS root mean square

TCP/IP transmission control protocol/internet protocol

TESPAR time encoded signal processing and recognition

TLP tension leg platform

ULS ultimate limit state

DOF degree of freedom

Chapter 1

Introduction

1.1 Motivation

Renewable energy in general, and wind energy specifically, is increasing in capacity and is projected to continue to grow. With the expansion of wind turbines, an increased segment is found offshore. Moving from land based to offshore, wind turbines leads to more power extracted, less visual impact and less land displacement. However, new challenges arise, concerning technical issues and cost. There is an increased pressure to reduce costs where ever possible. In turbines, the operation and maintenance cost is a significant part of the budget, and a decrease in cost would make wind schemes more motivational to explore and invest in. Operation and maintenance costs could be reduced by optimizing the maintenance strategy used. By focusing on the drivetrain, gearbox and bearings, quality maintenance strategies would contribute significantly as they are heavily costly downtime for the turbines. A data-based condition monitoring approach will be out-staged by a model-based system that could be employed holistically. In this thesis, the model-based approach digital twin is suggested. Constructing a digital twin of the drivetrain could take the most sensitive parts of the offshore turbine to a sufficiently detailed level for the model simulation. Strategies in the maintenance market are presented and discussed, and predictive maintenance by employing a digital twin could avoid additional costs and make operation more profitable.

For fault detection by digital twin approach to be reliable, both the digital twin and its fault modelling have to be reliable. Thus, this thesis analyses and discusses different modelling and fault modelling approaches. The methodology is carefully assessed with regard to sensitive issues, such as stiffness values and fault modelling approaches. A recommencement is proposed for modelling drivetrain by digital twin approach.

1.2 Objective

The main objective of this thesis is to model a digital twin of a simple drivetrain that could be implemented in use for offshore wind turbine's drivetrain. By completion of this thesis a literature review on digital twin development, and a study of faults and fault detection should be comprised. A modal analysis is to be performed to identify system parameters and different modelling approaches to do so is to be performed, analyzed, discussed and compared. Vibration signals from the lab is to be compared with the model for verification. A one degree of freedom (DOF) model, five DOF model with rigid shaft and a five DOF model with flexible shaft is to be made. Fault detection will be done through use of fast-fourier transform (FFT) and fault modelling is considered both with altering stiffness and through altering the expression of response.

1.3 Background

Renewable energy is becoming a larger part of the energy mix, and wind energy is a significant part of this [1] [2]. Fundamentally, wind turbines turn kinetic energy from the wind to mechanical power, and then again to electrical power. This happens by a thrust force on the blades, lift and rotation of the main shaft. In the wind turbines nacelle the drivetrain is located, where the power is transferred. In the gearbox the rotational velocity is increased sufficiently for electricity generation. Hence, the energy from the blades is lead to a generator, which in turn has a connection to the electrical grid. Schematics of a wind turbine nacelle is illustrated in Figure 1.1.

1.3.1 History

Wind energy have historically been exploited in the use of wind mills to grind grain and to pump water. At the start of the 20th century the idea of using wind energy to produce electric energy arose. However, it was not until after the second World War the idea really caught on, and the most used turbine became the three bladed down-wind horizontal axis wind turbine (HAWT) [4]. Ever since, there have been a significant growth in the market, as shown in Figure 1.2 from the Global Wind Report 2015 [5]. The last 15 years there has been an increase of wind power capacity installed worldwide, and further increase in predicted [6].

Moving Offshore

Wind turbines are increasing in size and capacity, and moving offshore [5]. The benefit of having wind turbines offshore compared to onshore is that there are higher wind speeds available due to higher acceleration possible and less imperfections in surroundings. Higher wind speeds are related to increase in power by the power of three, so this

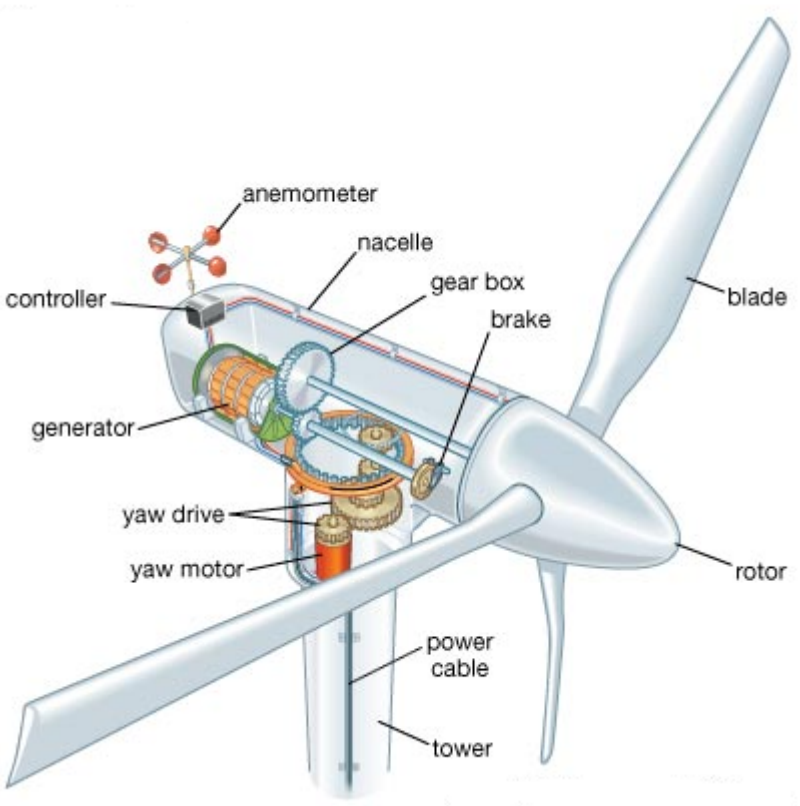

Figure 1.1: Schematics of a wind turbine [3]

advantage is significant [4]. There are also benefits of less noise, land displacement and visual impact. As the world is becoming more and more focused on reducing CO_2 due to climate change, technologies for renewable energy resources are maturing and growing [7]. There have been estimates of having an expansion of the offshore wind turbine market the next years, and by the current estimates a 60 GW increase in installed capacity by 2025 is probable. Most of this will most likely be installed in the UK, Germany and China [6]. To keep up the pace in this race it is important to have the engineering structures required and the analyzing tools fitted for both present and future expansive needs.

Challenges

Even though there are benefits from moving wind turbines offshore, there still are some challenges with the offshore scenario. Not only are the added hydrodynamic forces and connection to the grid an issue, but also corrosion as the turbines and their structures are in contact with seawater. What type of offshore wind turbine used has a large impact on the global forces and motions, as further described in Section 2.3.2. Additionally, there are

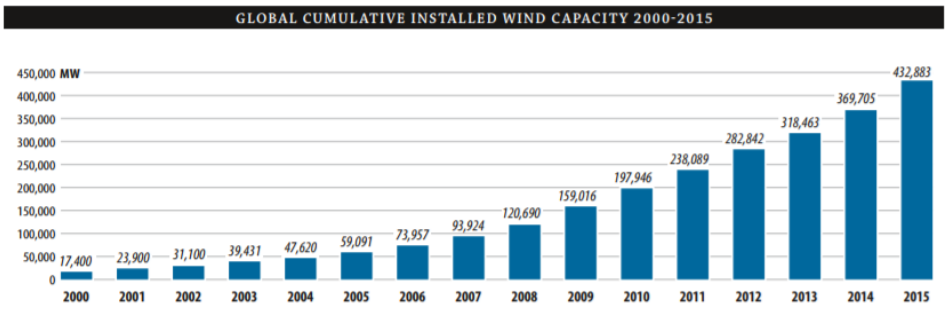

Figure 1.2: Wind capacity installed [5]

issues with installation and maintenance access due to rough weather and tight schedule from weather windows [8].

Operation and maintenance (O&M) is a costly component in a wind turbine budget, and consists of about 25% of overall energy generation cost, or about 75% to 90% of the investment cost of a 750 kW turbine [9][10]. Difficult-to-access locations and the high cost of the specialist personnel and access equipment needed, means that offshore O&M costs have been quantified as three to five times greater than those for onshore [11]. There is a significant potential for cost reduction by utilizing an improved maintenance and operation programme for this relatively new market.

1.3.2 Downtime

Several studies has been conducted in the literature regarding what components of a drivetrain that leads to the most downtime. Faulstich et. al considered the different parts of the wind turbine and their corresponding failure and downtime rates, see Figure 1.3 [12]. The study collected statistics from different databases. Wissenschaftliches Mess- und Evaluierungsprogramm (WMEP) database collected data between 1989 and 2006 containing failure statistics from 1500 wind turbines [13]. Landwirtschaftskammer Schleswig-Holstein (LWK) collected failure data between 1993 and 2006, and presents failure data from more than 650 wind turbines [14]. A Swedish survey of wind turbine failures was conducted between 1997 and 2005 [15]. These surveys are presented below. The gearbox comes out as a highly rated failure and downtime-component in the wind turbine, and is of extensive relevance for maintenance and operation issues.

Bearings are found to be a significant part of the root cause for failure [16]. Bearing faults are either caused by lubrication related cases or strength related cases [17]. They are of importance in further discussion of fault detection and modelling in Section 2 and Section 2.3.2.

To avoid the elevated expenses related to failure and downtime it is important to optimize maintenance and operations program. Then it is possible to achieve results that will be

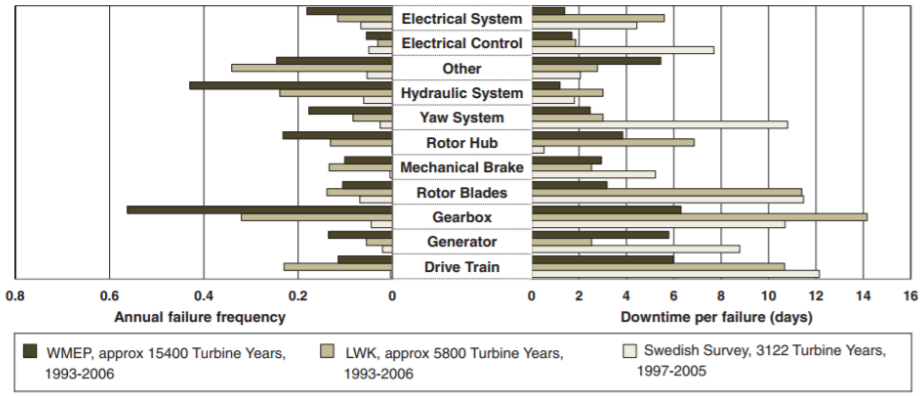

Figure 1.3: Failure and downtime rates [12]

more reliable and to speed up the time from analysis to action, both in design and in maintenance, more on this in Section 2.

1.3.3 Drivetrains in Wind Turbines

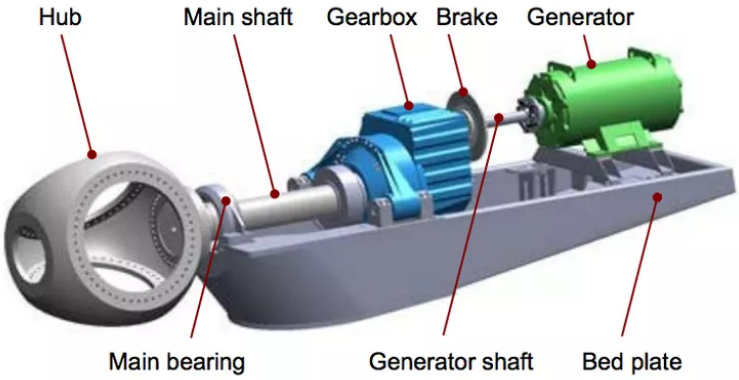

Figure 1.4: Typical geared drivetrain in offshore wind turbine [18]

Figure 1.4 shows a typical drivetrain in a wind turbine. Basically the rotor turns due to the rotating blades that rotates the shaft. The shaft is connected to the gearbox where the rotational speed is increased to appropriate speed for exporting power. As mentioned in Section 1.3.3 there are several possibilities for designing the drivetrain in wind turbines.

The European grid uses a frequency of 50 Hz and most used generators comprises four poles. The generator therefore would require the rotational speed found in Equation 1.1 in its rotor. In the equation, n is the rotational speed of the rotor in the generators stator, n_p

is the number of poles in the generator, and f is the frequency delivered by the generator. The gears are responsible for the velocity increase.

$$n = \frac{120f}{n_{\mathrm{p}}} = \frac{120 * 50}{4} = 1500rpm \tag{1.1}$$

Drivetrain Types

Generally, there are two types of drivetrains; with or without gearboxes. Considering Equation 1.1; say that the blades rotates with the velocity of 15 rpm. This results in the need for a speed ratio of 100 from the gearbox. However, it is possible to increase the number of poles in the same magnitude. That will indicate that there are 400 poles compared to 4 poles. This results in a large and heavy generator, but the need for a gearbox is eliminated. This type of drivetrain is called Direct Drive (DD). However, the most common type of drivetrain used in wind turbines are multi-stage gearboxes [11]. There are some arguments for the use of DD, due to the gearbox being a main contributor to downtime, as shown in Section 1.3.2. However, the DD wind turbines have more issues in electric sub-assemblies, blades and generator and Figure 1.5 shows the reliability per component in direct drive and multi-stage gearboxes [19].

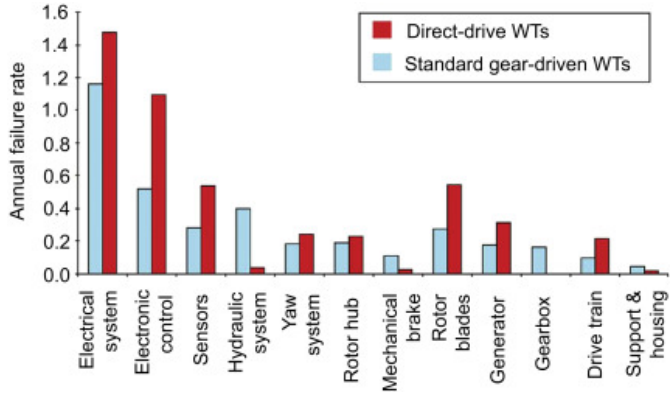

Figure 1.5: Annual failure rates for direct drive and gear driven wind turbines [19]

Traditionally, the downtime is significantly larger for blades, gearbox and generator than i.e. the electric sub assemblies [20]. In offshore wind turbines the downtime is less comparable to onshore, due to harsh weather and less access. The downtime will be of larger order than onshore, and all reliability could be more significant for the operation of the turbine [21].

The annual failure rate presented in Figure 1.5 shows a higher rate for DD drivetrains in almost all sections. Based on this, a drivetrain constituting of a gearbox has lower annular failure rates. The choice of a drivetrain should therefore be evaluated closely. Conclusively, drivetrains that includes a gearbox could be argued to have lower failure

rates, although they are argued to have a larger downtime contribution [20]. However, they are the most commonly used drivetrain type in the wind sector and will be further considered in this paper.

1.4 Structure of the Thesis

Below is an explanation of the flow of the thesis, and Figure 1.6 is a visualization of the outline.

Chapter 2: Literature Review This Section is an overview of the research and literature present in the field and shows the state-of-the-art within fault detection and modelling for a drivetrain in an offshore wind turbine. Limitations with data-based fault detection are discussed with a proposal of model-based fault detection as an alternative, digital twin in particular. The digital twin scheme is introduced and its advantages and challenges are presented.

Chapter 3: Modelling Analysis Theory The theories that lies behind the methods presented in Chapter 4: Methodology, are explained. Modal analysis, data presentation techniques, uncertainties, faults modelling and detection are covered, as well as acceptable vibration limits. Issues discovered in further chapters are also discussed with Chapter 3 as a backdrop. An experimental modelling approach is introduced along with different load cases that will be used in Chapter 4.

Chapter 4: Methodology The methodology is shown through use of different approaches when modelling a simple test rig drivetrain. The same drivetrain is modelled with different DOF and with resulting different fidelities. Two different fault modelling schemes are performed; altering stiffness in bearing force, and implementing a force input vector as the bearing response force input.

Chapter 5: Results Results from executing Chapter 4 are presented here in Chapter 5. Figures, plots and tables with significant value are included in this chapter, whereas residual results are shown in the Appendix.

Chapter 6: Discussion Where Chapter 5 displays the results, Chapter 6 comments and discuss the reason to imperfections in the results. Parallel to the work of methodology, theory and results a discussion of the validity and a loop for new methods and theories for approaches has been utilized. Thus, this has been a dynamic process. The final discussion chapter relates to the sensitivities, limitations, uncertainties and possible sources of error that are investigated, as well as prospects and potential that lies with the different approaches.

Chapter 7: Conclusion Key findings are presented that are found from Chapter 6 along with recommendation for further work.

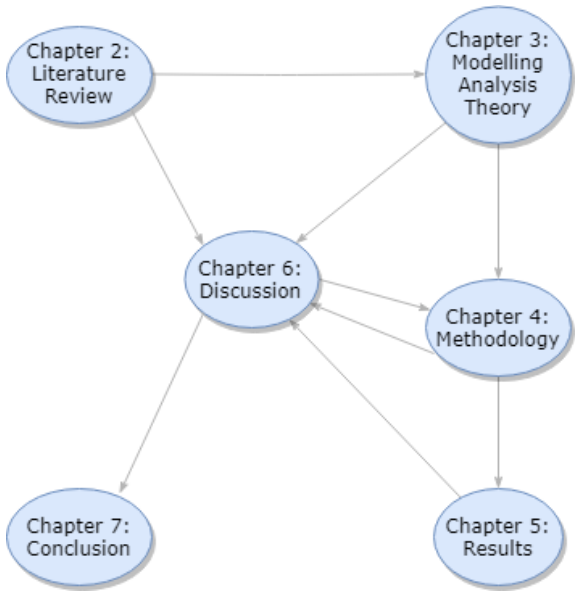

Figure 1.6: Flow chart of the structure of the thesis

Chapter 2

Literature Review

2.1 Fault Detection

2.1.1 General

Fault detection is the *"determination of faults present in a system and time of detection"*, whilst faults are *"unpermitted deviation of at least one characteristic property or variable of the system"* [22]. Fault detection has numerous approaches as will be presented in the following sections.

There are two maintenance actions available, corrective and preventive maintenance [23]. Corrective maintenance is of a run-to-failure nature and is more expensive, due to unscheduled downtime. Nevertheless, in some cases this is still a preferable strategy since there is no installation costs for the system. A simple example is the run-to-failure employed for light bulbs. Wind turbine operators on the other hand strive to avoid to resort to corrective maintenance due to a total higher cost from residual unwanted downtime cost [24].

A preventive maintenance scheme is the strategy to repair or replace system components before failure occurs. Preventive actions could e.g. be scheduling or condition monitoring employing fault detection. Scheduled maintenance is a safe way to avoid downtime because the intervals between maintenance are based on recommendations by the suppliers. In wind turbines inspections are often carried out every 6 months, and more complete inspections are carried out every 3 years [25]. However, scheduled maintenance could often lead to either under-maintaining, i.e. run-to-failure, or to over-maintaining, since this strategy does not take into concern current component condition. Condition monitoring on the other hand avoids this issue, building on that developing faults could be detected by change in system conditions. This makes condition based maintenance potentially cost saving [26]. Detection is done by a data-based approach, comprising sensors and other

data collecting systems to acquire acoustic emission, vibrations, strain measurement or oil particle data. Today, condition monitoring is the most used strategy for the wind turbine industry [27].

2.1.2 Wind Turbines

Applying condition monitoring requires a fault detecting sensor system. In a wind turbine there are several ways to achieve this. Visually it is possible to detect some defects such as discoloration as a result from temperature variations or deteriorating condition. Added noise from the drivetrain bearings may also indicate their physical condition [28]. Other cases are more intricate and needs a more refined scheme to indicate defects and faults. Installing fault detectors, and by comprising sensors and signal processing it is possible to get either periodically or continuously monitoring of a components condition. An offline monitoring is periodically retrieved, by sensors not integrated with the system. Online monitoring on the contrary is fully integrated with the system, and can collect condition data of the system continuously, or by any required time interval. For a wind turbine critical components should be monitored. These are mainly blades, the main bearing, generator and tower [29]. Maintenance tasks are planned according to the data acquired from sensors. For this to happen in a timely manner during operation, high quality data collecting systems are vital, along with relevant signal processing. Compared to corrective maintenance, condition monitoring is an asset for wind power system, and especially for offshore maintenance planning [30]. Reliability, availability, maintainability and safety (RAMS) could be improved by the increased efficiency in maintenance task planning, and reduce downtime and operational cost.

The different techniques for monitoring the condition of a system obviously varies on the nature of the system. Some solutions applied on different aspects on a wind turbine are listed below [31]. These approaches are further discussed in Section 2.1.3, 2.1.3 and 2.1.3 .

1. Vibration Analysis
2. Acoustic measurements
3. Operational Parameters
   (a) Oil analysis
   (b) Thermography
   (c) Strain measurement
   (d) Electrical effects
   (e) Physical condition of materials
   (f) Process parameters
   (g) Performance monitoring

2.1.3 Drivetrain

Drivetrain failure, and specifically gearbox and bearing-failure, leads to more downtime than other components and are of high significance as fault detection goes [12][29]. This section will therefore describe the state-of-the-art drivetrain condition monitoring tools, mainly focusing on vibration and acoustic emission analysis. These analyses are of most significance regarding analyzing these most sensitive parts in a drivetrain in a wind turbine [29].

Vibration Analysis

For rotating machinery, vibration analysis is the most used monitoring strategy. This strategy is employed both at gearbox, rotor and blades, but also at bearings and tower [27]. The tower and the bearings absorbs energy supporting axial and radial forces, and will receive a certain vibration planted from e.g. the gearbox or the rotor. Gearbox failure often start at the bearing as they have high probability of fatigue damage [32]. For wind turbines the monitoring is performed by evaluating the vibration at the wheels and bearings of the gearbox and generator. Especially the main bearing is considered, as it significantly influences the health of the other bearings [33].

Depending on the component analyzed, different frequency ranges should be used. For low frequencies a position transducer is applied, medium frequencies employ velocity sensors and high frequencies require accelerometers [34]. When selecting a sensor it is important to evaluate both dynamic range and sensitivity of the sensor. This is especially important for low frequencies where the amplitude from acceleration can be small. In the interest of deciding sensor type, ISO 13373-1 provides typically used transducers [35]. Furthermore, ISO 10816-21 provides standardized measurements, assists in evaluation of them and makes it possible to compare evaluations the vibration measurements in wind turbines. For this evaluation, specific zones are laid up with corresponding boundary conditions, however acceptance values needs to be confirmed with the manufacturer [36]. This is further specified in Section 3.6. Also, various bearings require a different specific total of sensors at different locations within the drivetrain. Frequency ranges relevant for wind turbines, and direction of measurement are procured in certification provided by DNV-GL [29].

Several distinctive ways of doing vibration analysis are analyzed in current literature on vibration analysis of drivetrains. Liu et al. propose fault diagnosis based on local mean decomposition technology, applied to the gear mesh frequency signal [37]. Feng et al. consider a diagnosis method based on amplitude and frequency demodulation [38]. Miao et al. considers a zoom interpolated discrete Fourier transform, found from multiple modulations [39]. Jayaswal et al. shows different vibration analysis techniques on bearings, and sees that bearing fault is found at an earlier stage by using vibration analysis. By employing FFT and studying the spectrum bearing condition is accessed [40]. Abdussiam et al. discuss the use of Time Encoded Signal Processing and Recognition (TESPAR) in

vibration analysis [41]. Dalvand et al. proposes an instantaneous frequency based method with envelope analysis of vibration signal [42].

Acoustic Measurements

The primary source of acoustic emission (AE) in a wind turbine is the generation and propagation of cracks. Acoustic monitoring is strongly related to vibration analysis, but there is a difference in how the sensors are attached. Vibration sensors are rigidly mounted onto the relevant component, whilst acoustic sensors ”listen” and are not rigidly attached to the component [34].

There have been several research studies on AE approaches. Elforjani and Mba demonstrated the use of acoustic emission technology for fault detection in bearings [43]. Ghazali et al. proposed a correlation between noise signal and wear response [44]. Early research from Tandon and Nakra in 1992 covered vibration and acoustic methods; time and frequency domain vibration measurements, sound measurements, shock pulse method and acoustic emission technique for bearing [45]. Later work by Tandon compares AE, stator current, vibration and shock pulse methods as fault detection schemes for bearings. It is evident from this research that acoustic emission detects fault at an earlier stage than e.g. vibration analysis [46]. Nienhaus et al. proposed using high frequency acoustic emission to discover faults on low speed roller bearings, where in this research AE proved more efficient at early fault detection [47].

Operational Parameters

Oil analysis should be performed as a supplement to other condition monitoring techniques [29], and is usually performed offline, but could also be monitored online continuously. If the samples show e.g. an excessive pollution, it could indicate disproportionate wear [34].

High temperatures should also be considered, and thermography is often used for fault detection, mainly for electronic components. Degeneration or excessive contact forces could lead to hot spots and should be monitored [31].

Furthermore, strain measurement could be considered, however not often applied for condition monitoring [48]. Electrical effects, physical condition of the components material, and process parameters are also of importance, alongside the implicit detection form through performance monitoring [31].

The angular velocity and the difference between rotation angle in output shaft and the generator input shaft could show useful information about the load variation in the gearbox [29]. Nejad et al. researched a prognostic way to determine fault detection by considering angular velocity errors and analyzing these in the frequency domain [49]. The result from this study is that bearing defects in intermediate and high-speed stages could be detected using this method, but at planetary stage fault detection prior severe faults, is challenging.

2.1.4 Limitations Data-Based Approach

Even though the condition monitoring scheme is an improvement from corrective and run-to-failure strategy for offshore wind turbines, there are issues raised with a data-based maintenance programme. Non-linear and significantly varying loads and rotational speed, combined with a strong dynamic integration of the turbine components, will have an influence on the data acquired. This represents a challenge for todays condition monitoring system. Both the procedure of vibration detection and the rougher operating environment offshore, adds complexity and could negatively affect the reliability of the monitoring system [50].

The most commonly used condition monitoring for gearboxes, bearings and drivetrains are based on vibration data. The data will have to be analyzed and this require an educated interpretation utilizing specialized knowledge. When a system reaches a certain complexity level it can be challenging to interpret data regardless of knowledge and experience. The risk of false or missed alarms are also significant [51].

In a wind turbine, different components are intertwined and a change in e.g. vibrations on one location may lead to an unexpected result in another location. For example, the holistic health of a gearbox is measured by the vibrations in the housing. However, it is not possible to find the origin of the fault. Drawing up a vulnerability map is possible, to see probabilistic fault root causes, as proposed by Nejad et al. [32]. Later work by Nejad et al. also shows that there is a direct linkage between defects at different components [52].

Data-based condition monitoring alone have challenges not to fall short meeting these challenges. A solution could be to employ sensors on all bearings and gears, but this is not cost effective or practical for the case of wind turbines. A more holistic approach to not only detect fault, but also diagnose them could be introduced, proposed generally by Isermann, and specifically for drivetrains in wind turbines by Nejad et al. [53] [33]. Coronado and Fischer discusses this, calling it a ”Holistic Condition Monitoring System” [50]. This approach is discussed further in Section 2.2.

2.1.5 Identifying Faults

In Section 2 the measurement techniques to discover faults were discussed. In this section the relevant method utilized in this thesis is in focus. There are several methods that could be of interest, such as reliability based maintenance, signal based fault detection or statistical fault detection [54]. However, as discussed in Section 2.2, a model based approach is preferred in the case of this thesis.

In a model based approach different signals are compared and evaluated to be able to identify faults. This is called analytic redundancy and the signals compared are one measured and one from the mathematical model [54]. Figure 2.1 shows the flow of model based approach of fault detection and identification (FDI). The residual in comparison

and the evaluation of this is the core of model-based FDI.

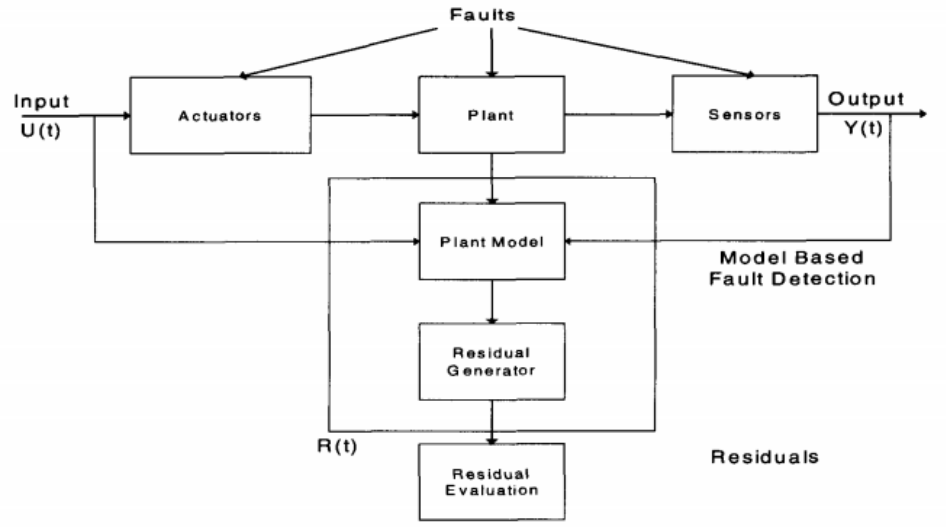

Figure 2.1: Model based approach flow [54]

The key is to be able to evaluate the residual generation in a sufficiently good way. There are several tools available to do this, and also it has to be emphasized that the relevant failure type will also have a say in the method used. In the literature there are mainly three different principles for the evaluation:

- Observer-based approach
- Parameter estimation technique
- Parity space approach

An observed based approach is build on the assumption that state estimation error is equal to zero if the operation is fault free, and other than zero whenever there are faults in the environment [55], [56]. This could be done through filters or observers. The outputs are evaluated by either Luenberger observers and reducing numbers of necessary observers, or Kalman filters; a control system that minimizes the co-variance of state estimation error [57] [58].

Parameter estimation technique is based on the faults affecting outputs through the system parameters [59]. This approach is therefore relying on generating estimates of parameters and analyzing the difference in those estimates when faults occur. The equation error methods that analyses the parameters directly uses least square estimation method. For output error approach, that computes error in output, a numerical optimization technique is often used [54].

Parity space is an approach that relies on checking for parity of measurements from the systems processes and generates a residual through comparison between model and process behavior [54]. A close correlation between the observer based techniques is been detected [60].

A case study by Simani in 2003 going through different processes and their applications, fault types such as sensor faults and process faults, FDI methods and residual evaluation showed that the observer bases approach was the largest contributor with about 70% of all the FDI method used, and that more than 50% of sensor related faults are detected through observer based approach [61].

The tools available and some of the mostly used for these model-based FDIs are

- State space parameter estimation
- Artificial neural networks
- Knowledge based systems
- Fuzzy interference systems
- Neuro-fuzzy systems

If there only is available output signals however, a signal-based or data based fault detection could be employed. That is, vibration data such as from rotating machinery. Typical signal-based approaches to detect faults are

- Bandpass filters
- Spectral analysis (FFT)
- Maximum-entropy estimation

In the modelled drivetrain in this thesis the only signal data is from optical sensor measuring vibration displacement data. This constrains the approach in this thesis to utilize signal-based approach, if not for the digital twin modelling. More specifically, the data achieved is applicable to be put through a FFT and spectral analysis. Thus, this method is considered the most efficient to detect fault with the data and nature of the drivetrain model.

2.2 Model-Based Approach

2.2.1 General

As discussed in Section 2.1.4 there are several challenges related to a data-based approach generally, and monitoring of a drivetrain in offshore wind turbines specifically. Issues regarding interpretation of data, false alarms and loss of overview could be solved by a

model-based scheme [33]. A model-based approach involves designing a digital model and using the model to interpret data received from sensors. Limiting the analysis backdrop to only data, level values or by analyzing trends will potentially reduce insight, and diagnosing the fault would normally be challenging. The model-based approach seeks to meet these issues, and relies on input and output signals and dynamic process models, for example built on state observers, parity equations and parameter estimation [53].

Decreasing costs of sensors and advancements on their technology, enables the potential to utilize sensor data in a more optimal way [26][62]. Furthermore, computer technology advancements and more sophisticated virtual models could in a larger degree be used as the master product model [63][64]. Merging models by a model-fusion approach opens up for integrated system engineering [65]. Conclusively, it could be possible to build a comprehensive model based on solid data from fault detection, import it to a model comprising the whole system, and be able to get an integrated analysis of the system.

2.2.2 Digital Twin

The model mentioned above will have a holistic system approach. However, when introducing dynamic conditions it will be insufficient for predicting the maintenance requirements for the system in question. To achieve this, a so called digital twin could be build. A digital twin is a virtual representation of the system containing all information available on site. This means that all descriptive condition information found on site are available in a digital model in a virtual and dynamic environment completely matching the real life system [66]. For offshore wind turbines this would be advantageous due to the hard-to-access locations, and since it is a high value product. High value products are: *"technologically intensive, expensive and reliability critical requiring continuous maintenance throughout their life cycle"* [67].

Origin

The concept of a digital twin was first introduced by the NASA Apollo programme and has evolved as the present technologies continues to grow. NASA started publicly using the term digital twin by calling it: *"(..) an integrated multiphysics, multiscale simulation of a vehicle or system that uses the best available physical models, sensor updates, fleet history, etc., to mirror the life of its corresponding flying twin"* [68]. Some, however, argue that a professor at University of Michigan, Michael Grieves, proposed the digital twin first under his executive course Product Lifecycle Management (PLM) at the university. There he defined it as a system comprising three components; a physical product in real space, virtual product in virtual space and the required interconnection between these two [69][70].

Concept

The digital twin would virtually be experiencing the same environment as the twin on site, and evolve identically through out the life cycle. This model type could be an answer to the issues raised in Section 2.1.4, as data interpreting would be done by the twin. Data pre-processing would also have to be done in this scheme, defined by the nature of the system. The assets would be considered as a whole, all components included and implied faults could be predicted as the twin will have life cycle updates [71]. It is then possible to schedule appropriate maintenance and reduce downtime and costs. Furthermore, it would be possible to retrieve sensor data from anywhere on the digital twin, opposed to the data from the real twin that is restricted to the location of the sensors.

There are several definitions of a digital twin. The digital twin prototype (DTP) describes the information required to create an asset, similar to a recipe for manufacturing the asset. A digital twin instance (DTI) contains information about single physical instances and the current operational states monitored by sensors. A digital twin aggregate (DTA) is the aggregation of several DTIs, and allows a system approach [72] [69]. In the case of a drivetrain in an offshore wind turbine it could be concerned as a DTA.

An optimal digital twin, as described by Rosen et al., is comprising autonomy, modularity and connectivity. Autonomy is defined by Rosen et al. as *"Intelligent machines that execute high-level tasks without detailed programming and without human control"* [71]. All autonomy in this matter relies on an accurate virtual model, being the decision backdrop for actions and skills employed. Autonomy could be achieved with remote maintenance. This could be done by online collecting health data and executing software based tasks and upgrades to the physical asset.

The communication between the twins is enabled by the continued rise in connectivity [66]. Web technology is evolving, internet protocols and the rise of the of Internet of Things (IoT), which is the interconnection between objects, enhances intercommunication [73]. Rosen et al. suggest IoT in the following way: *"ubiquitous connectivity such as the Internet of Things facilitates closing of the digitalization loop, allowing next cycle of product design and production execution to be optimized for higher performance"* [71]. Data could be handled on an IoT platform, opening several opportunities for applications, making connectivity and data handling accessible.

Concerning a drivetrain in an offshore wind turbine, a digital twin for the drivetrain alone could be build. This is due to the logically permitted decoupled approach. Global forces will have to be of importance nevertheless, however excitation to resonance is unlikely from global forces [25]. Starting with a global model and analysis, the loading on the drivetrain could be obtained and by the detailed model gear loads and load response analysis will be performed simultaneously to get instant conditions.

Examples of Industrial Use Fedem Technology (SAP SE), a Trondheim based software company, has developed a digital twin and has it operating with several systems, e.g.

offshore wind turbines in the north of Norway. Figure 2.2 shows how the physical system ”twins” with the digital representation through intercommunicating with online sensor condition monitoring. An external load on the wind turbine is represented in the digital twin through an actuator and virtual sensors [74]. The data is collected and has to be pre-processed before treated by the twin. After the twin has evaluated it, some verification is in order between a physical strain gauge and the virtual supposedly equivalent. However, the analysis in the digital twin applied here is for large component experiencing heavy external loads, and structural integrity is more a focal point than in drivetrain design, it still is a sufficient way to illustrate the digital twin premise. This shows that the approach is feasible, and combining this with a digital twin of a drivetrain, a complete system model of an offshore wind turbine would be available.

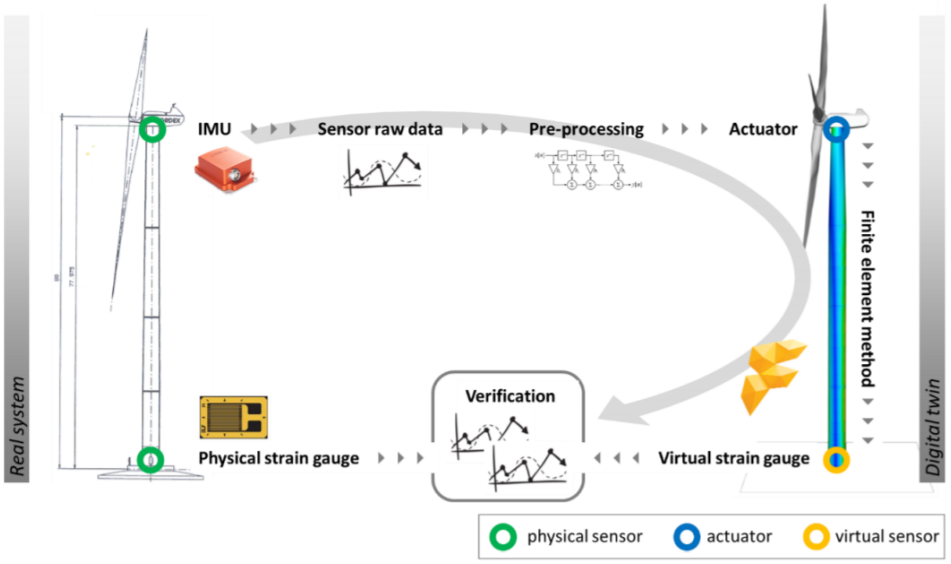

Figure 2.2: Digital Twin by Fedem Technology/SAP SE [74]

Larger companies than Fedem Technology has approached the digital twin scheme. For example, General Electric (GE) has conceptualized digital twins in general, and specifically for the wind energy sector. They empower it by an industrial industry platform named ”Predix”, to achieve the requires connectivity [75]. The industrial internet is meant to be comprising intelligent machines, advanced analytic and people at work. GE also considered the savings available in any industry if incorporating industrial internet combined with optimizing performance by using digital twins [76].

Applications

Digital twin has become known in several industries and they have a diverse set of applications. A digital twin could not only be used in monitoring a product and its life span, but

also in manufacturing and business models. In manufacturing, Industry 4.0 is pushing forward the evolutionary development, as it combines technological improvements like the cyber-physical system (CPS) with IoT to make new production systems available, called ”smart factories” [77]. Industry 4.0 is called the forth industrial revolution, and represents a shift from centralized to decentralized production processes [78]. The Industry 4.0 model is, simply put, similar to the digital twin approach as it is a fusion between digital and real world made possible by a virtual copy [79].

In the maritime industry it is not only drivetrains in offshore wind turbines that can take advantage of a digital twin. Large and complex vessels sail around the world and are dependent on high reliability and operability [80]. Both a digital twin for the life cycle monitoring and management, and Industry 4.0 approach for manufacturing is advantageous for a more energy-efficient and smart ship design [81]. Enabled by IoT and machine learning the digital twin is becoming a larger focus in shipping [82]. Machine learning constitutes of both the study and the modelling of learning processes; task-oriented, cognitive simulation and theoretical analysis [83]. Digital twins are also of considerable interest for the offshore oil and gas industry, and other industries with systems and operations in remote locations [84]. Having less access to more complex systems raises maintenance challenges, which is one of the current challenges that the digital twins are addressing.

Digital twins are not only used for manufacturing and system operability, but could also be used to connect back-end business applications such as accounting and human resources, to achieve certain business outcomes regarding supply chain operations [72]. One could also imagine digital twins being applicable for health care, by virtually representing hospitals and seeing how changes could affect operations, or a digital twin could even be employed by surgeons. Twins could also be utilized in designing ”smart cities”, to optimize urban sustainability by comprising spatial and temporal imperfections. Virtual Singapore is an example of a ”smart city”, aiming to improve e.g. accessibility and visualize landscape to harmonizing building projects [85].

Challenges

Model The digital twin of a drivetrain could be modelled and when including data acquired online from the on-site sensors, the condition of the drivetrain could be modelled. Where, and at what rate, the sensors would be collecting data could be based on what offshore wind turbine type the drivetrain is located in, guidelines from DNV-GL and ISO standards, and by considering the individual drivetrain hot spots for fatigue damage. Creating a sufficiently high-fidelity model will be a demanding issue and a general algorithm has yet to be made for fault diagnosis in a complete wind turbine [48][70]. Altogether, designing a digital twin is not straight forward to do. A drivetrain in a wind turbine is a complex system, containing a several subsystems and would require sophisticated design to be able to get an accurate twin.

Data Optimally the digital twin would constitute all information about the physical system. The amount of data acquired would be of a substantial size and containing both unstructured and diverse information. Hence, the connectivity would cause an architectural challenge for such big data analyses [66][81]. Anwer et al. [86] proposed a concept of Skin Model Shapes for design and manufacturing phase. This concept has been further conceptualized through other research and represents a digital and abstract model of the physical interface between an object and its environment and how to process data retrieved [62][87]. However, this approach is more relevant for manufacturing and mass production precision. For a drivetrain in an offshore wind turbine, the contact analysis is superiorly relevant and could be done numerically in a model-based approach as discussed in Section 2.3.1.

The digital twin could either be collecting data continuously or by intervals. If doing so continuously it might lead to excessive data. This could be exchanged with an assumption of the process being stationary and time independent for certain short time periods. Additionally, the whole drivetrain should not have to be implemented with sensors. This would be expensive and unpractical. A vulnerability map would aid in employing a sufficient amount of sensors, and their independent rate of monitoring [32].

Roy et al. discusses the effort that would have to be behind prognostics based on data from monitoring. The research debates a need for three components; confidence in accurate data, material degradation modelling and mastering the trade off between holistic overview and detail and precision [67].

Autonomy and Remote Maintenance Roy et al. further discusses that to achieve a remote, autonomous operated maintenance scheme further maturing of the technology has to be achieved, addressing current challenges in autonomous maintenance [67]. There are significant benefits for employing autonomous and remote maintenance in drivetrains in offshore wind turbines, and the system would increase its availability if this is done well [11].

Furthermore, remote maintenance could be executed by utilizing remotely controlled robots [67]. In a vessel, wind turbine or other complex and remote systems they could be controlled autonomously, enabled by visualizing in a digital twin, and perform maintenance tasks. This would be very advantageous for offshore wind turbines due to the short weather windows open for access, and the robots could be permanently installed. Remotely controlled maintenance robots are already widely used in nuclear industry [88]. In some designs the fault diagnosis conclusion could be sent back to the system to achieve autonomous maintenance by the robot, for routine tasks. Looking even further, it could be possible to achieve a maintenance technician operating in the virtual model enabled by virtual reality technology [89].

Connectivity Interconnecting the twin and sensors in an intelligent system by IoT have been researched by Xu et al., and three challenges were discovered. Firstly, there are

issues with communicating the data from the IoT sensor network. Secondly, there will be issues with non-stationary and non-linear fault prediction. Lastly, there will be a vast amount of data to process [90]. IoT is enabling efficient maintenance, however there will still be a need for a fundamental expertise of degradation mechanisms and root causes [67].

A dynamic linkage between the twins is challenging to achieve accurately [90]. Sensor data being continuously transferred from real life to the digital twin are introducing data processing challenges. Both interconnecting well and smart with an offshore installation are of focus to achieve interaction, as is one of the digital twin premises [70].

Furthermore, issues raised with trusting a digitally interconnected system are present. If unwanted sources were able to control or even read data in a digital twin system, it is of essence to have a high standard protection system to both avoid this from happening and to restrict damage and being able to reverse the situation. A significant effort for cyber securing the data network will have to be of high priority [91].

Motivation

The wind energy industry is showing an unprecedented effort to developing digital twins. The motivation lies with the benefits a digital twin provides; predictive system behaviour, simulations of rough environments, less downtime, less man hours for maintenance and improved lifespan for their systems [72]. This all leads to a decrease in expenses. Offshore wind turbines are in areas that are harder to reach and has to be approached in a certain weather window [20]. Additionally, offshore wind turbine farms are growing larger, more expensive and further away from land so the incentive for a decentralized maintenance programme is there in a much larger aspect than for the onshore wind turbines [16].

2.3 Methodology

2.3.1 General

A drivetrain is a complex multi-body system containing several rotating components. By a system-identification approach, an overall diagnosis of fault detection and data acquiring could be done [50]. To model a digital twin of the drivetrain properly, both the dynamic aspect, contact analysis and power transferring through gear teeth contact should be considered. Contact analysis can generally by done numerically by either finite element method (FEM) or by multi-body simulation (MBS) [92][93]. Other approaches has been researched such as the study of Nejad et al. [94]. This method is a base for ultimate limit state (ULS) design, and does not include internal dynamics which would have to be accounted for independently.

Digital Twin Approach

FEM is suitable for high accuracy and detailed numerical modelling, whilst MBS is significantly less time consuming [92]. MBS contain rigid and flexible bodies that are connected with force elements [95]. The flexible bodies could be modelled in FEM and imported into a MBS program [96][97]. However, this increase in detail level and additional information about internal dynamics makes the computation more complex and time consuming.

On one hand, rigid bodies replaced by DOF reduced flexible bodies could capture the greater part of the gearbox dynamic response [96]. But on the other hand, flexible modelling is less time consuming [98]. It could therefore be said to be a trade off between detail and fidelity, and computational time.

Added detail may not however lead to an increase in value of results [99]. MBS is found to be sufficiently accurate and definitively faster than FEM, and would be preferred in the making of a digital twin for a drivetrain in offshore wind turbines.

A certain level of DOF in the models components should be balanced against computational time, and Guo et al. recommends model requirements for wind turbine gearbox simulations, presented in Table 2.1 [99]. Table 2.1 also shows where Guo et al. proposes FEM used on certain components. It could possibly be necessary to evaluate in what degree simulation considerations are directly transferable to implementation for a digital twin, but as a first evaluation this is assumed to be the case.

Table 2.1: Multi-Body Simulation recommendations [99]

Component	Recommended Approach	DOF Requirement
Rotor/hub	Rigid body w/ lumped weight	N/A
Main shaft	Flexible Body, FE beams	Determined by convergence study
Main bearing	Stiffness matrices	5 (Excluding rotation)
Gearbox housing	Flexible body, condensed FE	Determined by convergence study
Planetary carrier	Flexible body, condensed FE	Determined by convergence study
Gearbox shafts	Rigid body	N/A
Gearbox support	Stiffness matrices	6
Gear	Rigid body	6
Gearbox bearings	Stiffness matrices	5 (Excluding rotation)
Spline	Stiffness matrices	2 (Tilting)
Bedplate	Rigid body or condensed FE	N/A
Generator coupling	Stiffness matrices	5 (Excluding rotation)

2.3.2 Gearbox, Bearings and Drivetrains

Gearbox components should be designed by following the offshore wind turbine design code and standard IEC 61400-4. IEC 61400-4 includes maintenance recommendations [100]. However, floating turbines are not included in the standard.

By utilizing the vulnerability map drawn up by Nejad et al. to a 5 MW reference gearbox, or by making one for a specific drivetrain, the most sensitive components to fatigue damage are detected, and would be the road map towards where the highest density of sensors should be located [32]. This sort of approach would be revealing as to where and how frequent sensor data should be collected in a digital twin. The vulnerability map drawn up of the reference 5 MW gearbox is found in Figure 2.3 and it is evident from this research that the bearings at the high-speed, third stage gear and close to the generator (HS-A and HS-B) is exposed to high fatigue damage probability. Evidently, these would be of high interest when choosing where and how often sensor data is collected in a digital twin of a drivetrain in an offshore wind turbine.

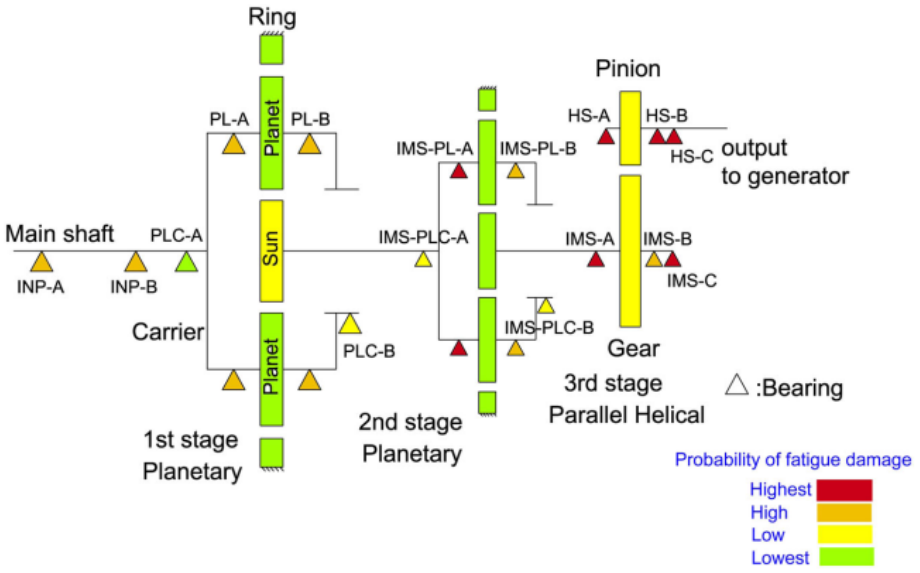

Figure 2.3: 5 MW gearbox vulnerability map [32]

Gearbox

A gearbox is modelled by flexible and rigid bodies connected with force element appropriate. So called ”joints” represent the bodies DOF, and each body has one joint, revealing its location and DOF. Force elements draws up how the forces are transferred between bodies and are represented e.g. as dampers, springs, contact mechanisms, gear teeth etc. The basis of multi-body simulation is found in various articles such as Shabana [101] and

Bauchau [95].

In a gear model, it is common to utilize a rigid body model and then simulate the contact as a spring, damper or error function for the gear backlash. Such a model is very applicable and could be of interest in a digital twin design. However, if the gear is relatively thin body deformation would influence dynamic behaviour and FEM method should be used for added detail [102].

Bearings

The life of the bearings designed should be modelled to follow life span analysis specified by ISO 281 [103]. In MBS, bearings will often be modelled as a force element. The force-deflection relationship could be linear, non-linear, and with or without clearance [104]. The force element on the bearing would be representing their stiffness [105]. However, finding this stiffness is of a challenging nature and various results would be achieved from various models [106]. This will become evident in this thesis as well, as discussed in Section 3.2.3. Because of this, a validation should be done with a more detailed approach like a FEM analysis, experimental data modelling or by other software [106].

Drivetrain

For a gearbox and drivetrain in an offshore wind turbine the type of structure and whether it is floating or not should be considered. Floating wind turbines have various global loads, depending on them being a tension leg platform (TLP), semi-submersible or a spar [52]. However, these loads are decoupled from the separate drivetrain multi-body simulation, and put as input forces. Significant variations in fatigue damage are demonstrated by Nejad et al. and should be carefully considered when designing the drivetrain [52].

Chapter 3

Modelling and Analysis Theory

3.1 Fast Fourier Transform

When analyzing the time data series of a response it is often practical to be able to consider which frequency bands the signal lies in. By performing a FFT it is possible to transform the data time series to a series on the form of frequencies, as visualized in Figure 3.1. The FFT is a discrete Fourier transform algorithm. When doing FFT of a decay test the natural frequency, f_n is discovered. This frequency band will be a distinct peak as it holds most signal in these tests [107].

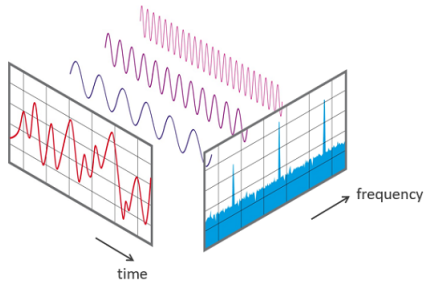

Figure 3.1: Fast Fourier Transform

3.2 Modal Analysis

3.2.1 Equation of Motion

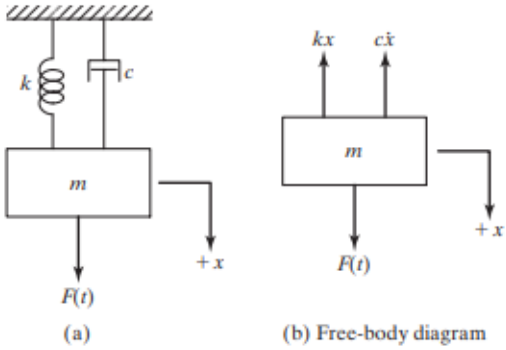

Figure 3.2: Spring-mass-damper system

When a force F(t) is applied to a viscously force damped spring-mass system, see Figure 3.2, the EOM is as presented in Equation 3.1. When the motion is a free-damped vibration it follows Equation 3.2. $x(t)$ is the displacement movement, m is the mass, k the stiffness and c is the damping of the system. This second order differential equation has a homogeneous solution $x_h(t)$ and a particular solution $x_p(t)$. The general solution is the sum of these. The homogeneous solution is shown in Equation 3.2, and this free vibration solution dies out over time under all three possible conditions of damping (overdamped, underdamped and critically damped) and through all initial conditions [108].

$$m\ddot{x} + c\dot{x} + kx = F(t) \tag{3.1}$$

$$m\ddot{x} + c\dot{x} + kx = 0 \tag{3.2}$$

After a certain time period, τ, the homogeneous solution $x_h(t)$ will die out. Thus, the dominant part for the general solution could be claimed to be the particular solution, and the phase when both homogeneous and particular solution applies is called the *transient* phase. When gathering deflection data $x(t)$ will be known and the transient and stable phase are detected. How fast the transient phase decays is dependent on characteristic values for the system; stiffness *k*, damping *c* and mass *m*. These values, their meaning and how to detect their magnitude are discussed in the following paragraphs.

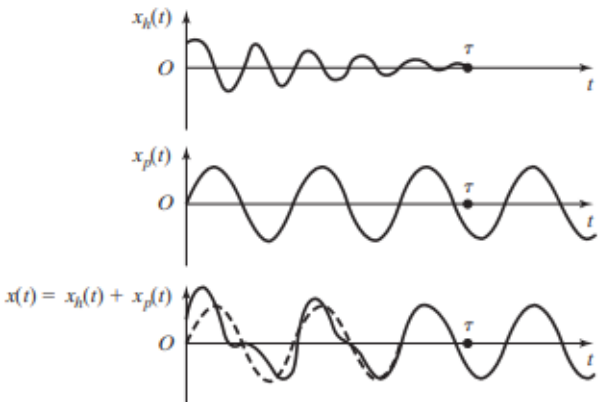

Figure 3.3: Homogeneous, particular and general solution of Equation 3.1 for an underdamped system.

3.2.2 Mass

The mass of the system, if not known, could be calculated by solving the EOM. However, to be able to do so all the other parameters and variables have to be known. On the other hand, one could also measure the mass. In most cases the individual masses are known and presented by the producers of the components. It is evident from Equation 3.3 that the mass has impact on the system's undamped natural frequency and is one of the characteristic values when determining the behaviour of a system.

$$w_n = \sqrt{\frac{k}{m}} \tag{3.3}$$

3.2.3 Stiffness

Considering the stiffness of a system that follows Equation 3.3, the translational stiffness could be derived when both mass and natural frequency is obtained. The natural frequency is found through decay analysis from testing the system and considering the transient phase fade. This decay test could for simple test rig drivetrains be performed through hammer stroke. A stroke by a hammer that interferes with the system invokes a transient phase. It could also be other interference or force exerted on the system to push it out from equilibrium, and then released for the purpose to induce a decay phase. The natural frequency is found through observing the periods in this transient, decaying phase and through spectral analysis of FFT the natural frequency f_n could be found. By converting this to angular velocity it is possible to solve Equation 3.4. The translational stiffness are different in the different sensors and directions, which will be considered in the modelling. The results found are shown in Section 5.3.2.

The natural angular velocity w_n is found by $w_n = 2\pi f_n$.

$$k = w_n^2 m \tag{3.4}$$

Torsional Stiffness

In the equation above the translational stiffness is found. However, the torsional stiffness is also of interest. There are various approaches as to how to calculate these which will be shown in the following paragraphs. Firstly, it is possible to calculate the torsional stiffness in the three different rotational orientations by Equation

$$k_t = \frac{T}{\Phi} = \frac{GJ}{L} \tag{3.5}$$

where k_t is the torsional stiffness, T is the applied torque in the rotational orientation in question, G is shear modulus (modulus of rigidity) and Φ is relative rotation. J is the polar second moment of area and L is the shaft length for this direction.

A second approach is through the stiffness matrix. Considering the whole stiffness matrix for the shaft, whilst assuming that the two bending planes shown in Figure 3.4 does not couple, it is possible to assemble this stiffness matrix. It is worth noting the sign in the matrix elements involving Θ and the related moments. Also, by assuming that the shaft is symmetric yields that the second moment of area is the same for both planes. The stiffness matrix then is:

$$K_e = \begin{bmatrix} 12 & 0 & 0 & 6l_e & -12 & 0 & 0 & 6l_e \\ 0 & 12 & -6l_e & 0 & 0 & -12 & -6l_e & 0 \\ 0 & -6l_e & 4l_e^2 & 0 & 0 & 6l_e & 2l_e^2 & 0 \\ 6l_e & 0 & 0 & 4l_e^2 & -6l_e & 0 & 0 & 2l_e^2 \\ -12 & 0 & 0 & -6l_e & 12 & 0 & 0 & -6l_e \\ 0 & -12 & 6l_e & 0 & 0 & 12 & 6l_e & 0 \\ 0 & -6l_e & 2l_e^2 & 0 & 0 & 6l_e & 4l_e^2 & 0 \\ 6l_e & 0 & 0 & 2l_e^2 & -6l_e & 0 & 0 & 4l_e^2 \end{bmatrix}$$

A third approach is by assuming a flexible shaft carrying masses at a and b distances from the bearings, a so-called *Jeffcott* or *De Laval* rotor. This assumption leads to rotational stiffness, that is moment about the vertical axis that leads to a rotation about the same axis, shown as

$$k_R = k_{\Psi\Psi} = k_{\Theta\Theta} = \frac{3EI(a+b)}{ab} \tag{3.6}$$

where E is the Young's modulus and I is the moment of inertia. The directions are as

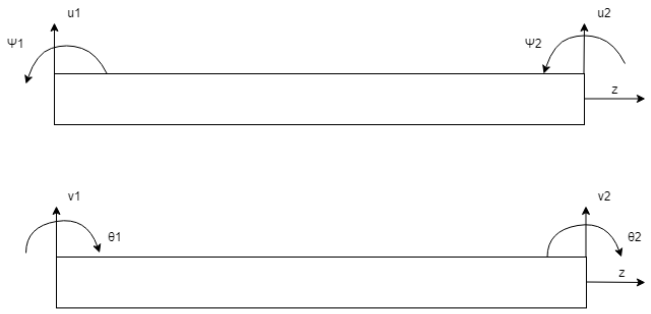

Figure 3.4: Local coordinates in the two bending planes

shown in Figure 3.4.

By this approach, it is possible to consider coupled stiffness such as when a moment gives a displacement in vertical direction the stiffness becomes on the form:

$$k_C = k_{u\Psi} = k_{v\Theta} = \frac{3EI(a^2 - b^2)}{a^2 b^2} \tag{3.7}$$

These three approaches performed are found from Friswell et. al [109] [110] [111]. The results are shown in Section 4.4.1.

3.2.4 Experimental Modelling

As there are several approaches to achieve the stiffness values, coupled or not, they all lead to different answers. These issues in modelling with correct stiffness have to be met in a comprehensive way. Also, the use of different software will lead to different answers as shown in Figure 3.5. When the modal analysis for the decay tests lead to different result for each analysis, it also motivates for investigation of the impact of the outputs from the analysis. Additionally, there is discussion in the literature as to how to achieve correct values for the stiffness in a rotating shaft as shown in Section 3.2.3. Conclusively, by implementing a sensitivity analysis of the stiffness utilized in the bearings in MBS, a picture is painted as to how well stiffness change will describe faults in a model as well.

Considering different approaches, assumptions and calculation methods, different answers for the stiffness will be produced. Three different approaches was discussed in Section 3.2.3. All of these three will result in different responses. An experimental approach could be a feasible solution to achieve a sufficiently accurate model. Clearly, this is a question of model fidelity versus computational time.

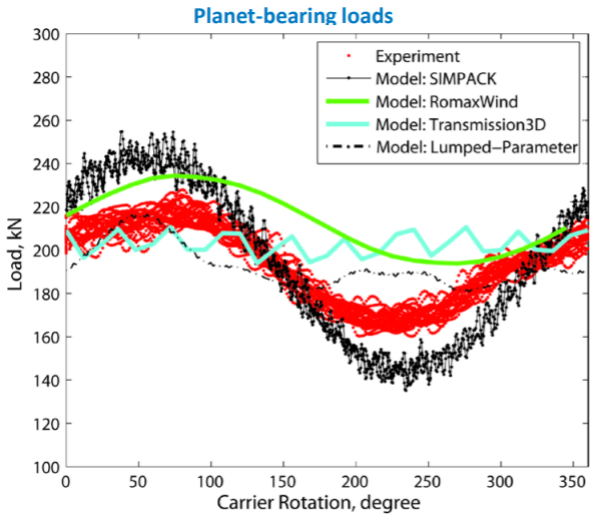

Figure 3.5: Different resultant loads with different modelling approaches [112]

Figure 3.5 shows a visualization of how different the result from different modelling approaches could be and also that the model could be made similar, but never completely accurate to a real life model. The figure shows bearing loads, which also are dependent on the stiffness in a non- linear way. Additionally, the figure shows that the results varies dependently on software modelling approaches and practices [112].

This chain of thought is the grounds to employ an experimental modelling for finding the stiffness values that could be feasible in further modelling. Figure 3.6 shows an example of a simplified shaft with two bearings that has stiffness K1 and K2. An experimental approach with different load cases of K1 and K2 is to be performed for the case of the drivetrain test rig in this thesis. The goal is to get a response as close to the real twin as possible. This will show the model sensitivity for stiffness change in the model.

The different load cases will be tried at different magnitudes, to explore the sensitivity and the degree of stiffness tuning needed for sufficiently accurate results.

Figure 3.6: Experimental model

Load Case 1: LC1

The first load case is at perfect system, when there are no faults present in a drivetrain so it is assumes that the values are the same.

$$k_1 = k_2 \tag{3.8}$$

Load Case 2: LC2

The second load case is a shaft with faults in X- direction in bearing 1. This is shown with an increased stiffness by:

$$\begin{aligned} k_{x1}* &> k_{x2} \\ k_{x1}* &= 1.05k_{x1} \end{aligned} \tag{3.9}$$

Incremental stiffness increases are done, such as $k_{x1}* = 1.05k_{x1}$ as shown in Table 3.1. The same increments are used in all the different load cases.

Table 3.1: Different increments for sensitivity analysis

Increment
1.05
1.10
1.15
1.20
1.25
1.30

Load Case 3: LC3

The third load case is a shaft with faults in X-direction in bearing 2. This is shown with an increased stiffness by

$$k_{x1} < k_{x2}* \tag{3.10}$$

Load Case 4: LC4

The fourth load case is a shaft with faults in Y-direction in bearing 1. This is shown with an increased stiffness by

$$k_{y1} > k_{y2}* \tag{3.11}$$

Load Case 5: LC5

The fifth load case is a shaft with faults in Y-direction bearing 2. This is shown with an increased stiffness by

$$k_{y1} < k_{y2}* \tag{3.12}$$

3.2.5 Damping

A system's viscous damping force is corresponding to the velocity $\dot{x}$ as shown in Figure 3.2, and could be expressed as $F = -c\dot{x}$. The damping constant *c* is negative since the damping works in opposite direction of to the velocity. The translation damping constant *c* is found through the Equation 3.13. The translational damping is found for one DOF at one location, so for several positions and directions of interest this should be considered.

$$c = 2m\zeta w_n \tag{3.13}$$

$$\delta = ln\frac{X1}{X2} = \frac{2\pi}{w_d}\frac{c}{2m} \tag{3.14}$$

Table 3.2: ζ for different damping conditions

	Value	Condition
ζ	0	Undamped
ζ	$[0, 1]$	Underdamped
ζ	> 1	Overdamped
ζ	1	Critically damped

Estimating of the damping coefficient depends on finding ζ. The ζ value considers the condition of damping for the system, presented in Table 3.2 and displayed in Figure 3.7. ζ depend on the logarithmic decrement, which considers the decrease of amplitude in a response. Equation 3.14 shows the general equation for the logarithmic decrement. The X1 and X2 values are the relevant amplitudes, w_d is the frequency of damped vibration, *c* is the damping constant and *m* is the mass. However, if ζ is small ($<< 1$) and damping is small this equation could be estimated to be:

$$\delta \approx 2\pi\zeta \tag{3.15}$$

It is shown that is irrelevant which of Equation 3.14 or 3.15 is used until ζ reaches a value about 0.3, which is shown in Figure 3.8. If there is access to the response data for the model to be investigated, it can be analyzed for which ζ value that could be relevant. Say that the response is oscillating, then complying to Figure 3.7 it can then be implied that $\zeta << 1$. In such a case, ζ is found through $\zeta \approx \frac{\delta}{2\pi}$.

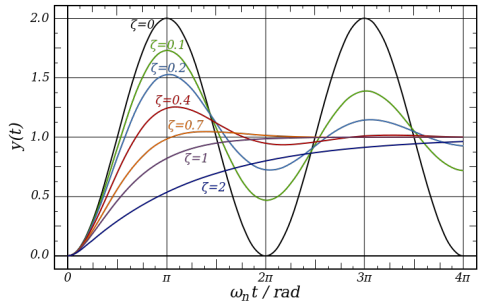

Figure 3.7: Damping ratios

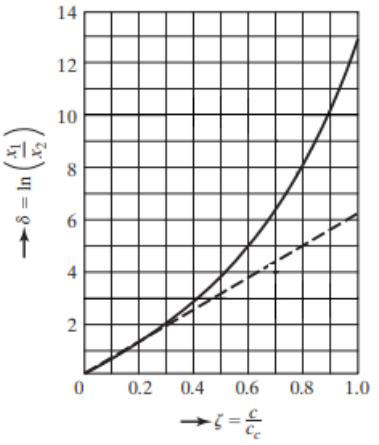

Figure 3.8: Logarithmic decrement variation over damping [108]

A system's rotational bearing is found through Equation 3.16, where the torque is divided by the angular velocity.

$$c_t = \frac{T}{w} \tag{3.16}$$

3.3 Uncertainties

Uncertainty has several meanings such as inaccuracy, likelihood of events etc. It is crucial to have an accurate representation for a given system, so it is possible to understand the limitations of validity. For the case of stiffness in a vibration system there will always be some sort of uncertainty. Uncertainties in reliability analysis are classified as

- Aleatory uncertainty - random or objective
- Epistemic uncertainty - subjective

An aleatory uncertainty is caused by randomness and is irreducible. An epistemic uncertainty is caused by lack of data or knowledge and is a reducible uncertainty. By being reducible it implies it is possible to reduce the uncertainty, in the case of epistemic more information will reduce the uncertainty. On the other hand random uncertainty is irreducible. Say a random person is going to guess a strangers birthday. The probability for the correct answer would then be 1/365. However, if someone that knew that stranger was asked, the probability would be higher, and the more knowledge and experience achieved the higher it could become. This epistemic uncertainty is regarded as reducible, and thus also requires careful attention [113]. For the case of the drivetrain test rig in this thesis, an epistemic uncertainty is relevant due to the characteristic values being more certain when a higher knowledge or experience base is introduced.

In a model of a physical asset it is necessary to in what degree of certainty the calculated data represents the measured data [114]. Such uncertainty could simply be expressed as shown in Equation 3.17.

$$\chi = \frac{X_{true}}{X_{model}} \tag{3.17}$$

Here, χ is model uncertainty of X, a physical variable. X_{true} is the measured X and X_{model} is the calculated. E.g. if χ turns out to be 1.05, it means that it possible to say that the modelled value is correct within a 5% margin.

3.4 Faults

3.4.1 Fault Detection

When the model has been optimized and is sufficiently accurate to simulate the real system without flaws, it is possible to consider fault detection. In a drivetrain there are several reoccurring faults. In the list below are some of the typical machinery defects that can be

detected through vibration analyses [115]. There are several more, but in this thesis these will be of interest.

- Misalignment
- Unbalance
- Bent shaft

3.4.2 Fault Types

Unbalance

A very common fault is an unbalanced shaft, however this is a fault that easily could be detected. ISO defines this by a *[..] condition which exists in a rotor when vibratory, force or motion is imparted to its bearings as a result of centrifugal forces.* An uneven mass distribution about the rotors center line gives characteristic vibration data, from FFT shown in Figure 3.9. Unbalanced mass is shown with a peak at 1xrpm. Figure 3.10 shows the unbalanced mass as an added mass in the black dot in the bearing, and the expressions attached are the backdrop for the expression derived for fault modelling of this fault, in Section 3.4.3.

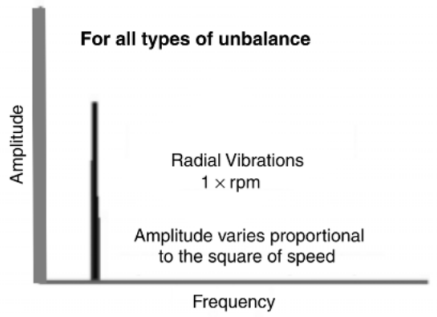

Figure 3.9: FFT analysis, effects of unbalance [115]

Misalignment

Misalignment is a common fault cause in a shaft, and the misalignment could be on the form of either angular or parallel misalignment. An angular misalignment is when the center line of two shafts meets an angle at the meeting point. This is shown in Figure 3.11. The characteristic FFT response is shown in Figure 3.12. A misalignment only due to angular misalignment does not happen often and the vibration data FFT could be an interpretation issue. However, angular misalignment is shown in the FFT as a

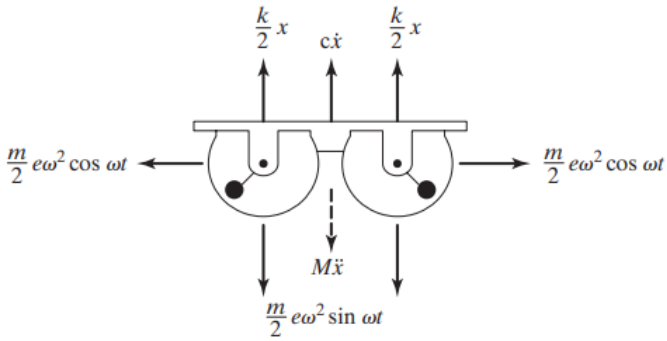

Figure 3.10: Rotating unbalanced mass with expressions for excitation in vertical and horizontal direction [116]

1xrpm frequency. Axial vibration, and perhaps coupling issues such as looseness, could be affecting the FFT to look like it does in Figure 3.12, and both 1x, 2x and 3xrpm could all be of dominating nature [115].

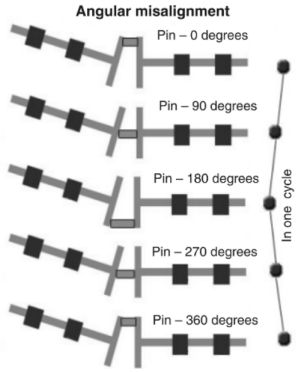

Figure 3.11: Angular misalignment [115]

A parallel misalignment is e.g. when the shaft and coupling hole is not centered, and there is a relative offset. Figure 3.13 shows how this could happen. The frequency this misalignment will excite is 2xrpm in the radial direction and Figure 3.14 shows that 2xrpm has dominance. However, both 1xrpm and 3xrpm indicates that the parallel misalignment is not working alone. Vibrations due to only parallel misalignment is not frequent, and it is normally observed in association with angular misalignment.

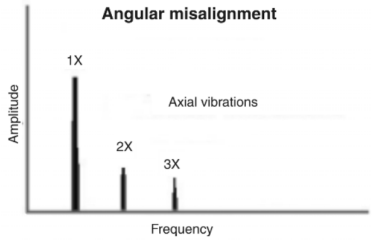

Figure 3.12: FFT of angular misalignment [115]

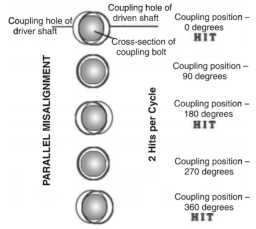

Figure 3.13: Parallel misalignment [115]

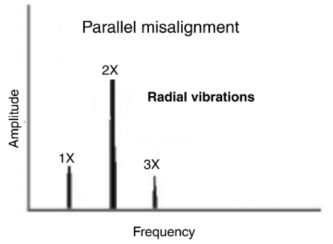

Figure 3.14: FFT of parallel misalignment [115]

Bent Shaft

If the shaft is bent, the vibration in both radial and axial directions are high. Axial could have higher magnitude than radial, and the FFT will normally have 1x and 2x parts. The bend is near the shaft center if the amplitude of 1x is the largest, and if the amplitude of 2x is highest then the bend is near the shaft end [115] [117].

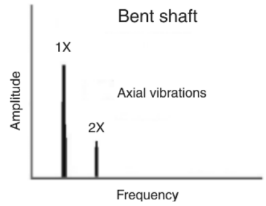

Figure 3.15: FFT analysis, effects of bent shaft [115]

3.4.3 Fault Modelling

Motivation

It is essential when the fault detection is done by digital twin model approach that these faults are modelled accurately in the digital twin. Then the twin is reliable for it's purpose in predicting faults in the long run and the modal detection of faults. In the digital twin it is possible to inspect all aspects and spots for the model or system in question. Knowledge about the real twin is restricted by the sensor locations. Consequently, this advantage of the digital twin is of significance, but the fault modelling should be done with careful attention for it to be reliable. If this is done with error, this error could lead to misinformation and the advantage is then turned into a disadvantage.

Stiffness

Fault modelling is discussed in the literature, and there has been use of an approach that model faults by altering the stiffness in the bearings[49]. It is also shown by Ghane et al. that bearing stiffness and it's damage and life expectancy has a direct link [118].

Force Vector

On the other hand, fault modelling could be done by other means than altering the stiffness in the bearings in the model. By employing a force vector or force system, not only single fault, but also multiple faults could be modelled. This has proved to be effective in fault detection and identification for both position, module and phase [119].

In vibration theory, typical response when a fault has occurred is found by Equation 3.18.

$$\begin{aligned} F(t) &= F(t)_{\text{unbalance}} + F(t)_{\text{misalignment}} + F(t)_{\text{other}} \\ &= Asin(wt) + Bsin(2wt) + Csin(3wt) \end{aligned} \tag{3.18}$$

These expressions for unbalance etc. is directly linked to the peak detection system in FFT, where a peak at 3xrpm would be implying a force vector with $sin(3wt)$ and so on.

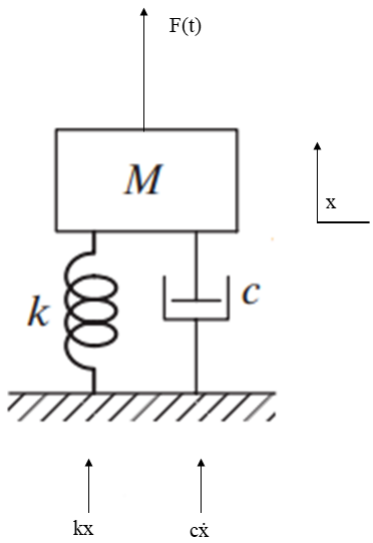

Figure 3.16: Response schematics of a one degree of freedom system

The EOM shown in Equation 3.19 shows a definition of bearing reaction F_R. Figure 3.16 visualizes how F_R is the bearing reaction, with the opposite forces, and on the form of damping and stiffness.

$$\begin{aligned} m\ddot{x} + c\dot{x} + kx &= F(t) \\ m\ddot{x} + F_R &= F(t) \\ F_R &= F(t) + m\ddot{x} \end{aligned} \tag{3.19}$$

This F_R could then be implemented in a model's bearing as force input. The issue then lies with finding the correct expressions for the fault force vector and systems. This could be done with solving the force system with combined faults and focusing on nodal displacements [119]. Or it could be done with a modal approach, where the system response is used to find the force system for the combined faults as described in Equation 3.18. In that case, the modal analysis in Section 3.2 becomes inessential for fault detection, as stiffness and damping coefficients would be redundant. It is possible to find the values for A, B and C in Equation 3.18, through analysis or an inverse method. The inverse method could possibly be a stochastic approach, by utilizing for example a Monte- Carlo method and programming the selection with an acceptable low error.

Unbalance Specifically, in the case of unbalance it is possible to calculate the value of the amplitude A. By considering displacement in one DOF, this could be expressed as $F(t) = me\omega^2 sin\omega t$. This is also shown in Figure 3.10[116].

By considering the EOM

$$m\ddot{x} + c\dot{x} + kx = F(t) = me\omega^2 sin\omega t \tag{3.20}$$

it is possible to derive a prediction of the response with regards to the response amplitude X, by the solution

$$\frac{MX}{me} = \frac{\frac{\omega}{\omega_n}^2}{\sqrt{(1 - \frac{\omega}{\omega_n}^2)^2 - (2\zeta\frac{\omega}{\omega_n})^2}} \tag{3.21}$$

where M is the mass of the system, X is the amplitude, m is the eccentric mass and e is the radius out to the eccentric masses. For each X it is possible to get the corresponding me values, and solve the EOM [116].

3.5 Monte Carlo Method

The only unknown parameters from Section 3.4.3 are the fault associated amplitudes A, B and C. By considering the spectral analysis, some relation between the different faults amplitude could be found, however this is only suggestive. To find the amplitudes a stochastic approach could be implemented. Monte Carlo method is a way that this could be done, a method often used in cases when determining analytic solutions is too time consuming.

By utilizing a Monte Carlo method, randomly generated numbers are used as inputs to generate a solution. The probability to achieve a specific solution is then found by finding the relation between number of times the solution was generated to the total number of trials. By increasing the number of trials, the probability becomes more accurately determined [120].

3.6 Acceptable Vibration Limits

It is possible to evaluate the vibration severity through comparing them to zone boundary layers. This comparison is done with the root mean square values of the mm/s velocities of the real time series data of the vibration, and the zones are found in ISO Standard ISO10816-1 and described as [121]:

- *Zone A: The vibration of newly commissioned machines normally falls within this zone*

- *Zone B: Machines with vibration within this zone are normally considered acceptable for unrestricted long-term operation*
- *Zone C: Machines with vibration within this zone are normally considered unsatisfactory for long-term continuous operation. Generally the machine may be operated for a limited period in this condition until a suitable opportunity arises for remedial action*
- *Zone D: Vibration values within this zone are normally considered to be of sufficient severity to damage the machine*

The table that shows the boundary ranges for vibration velocity is shown in Figure 3.17

	Range of typical zone boundary values for non-rotating parts r.m.s. vibration velocity mm/s			
0,28				0,28
0,45				0,45
0,71	Zone boundary A/B 0,71 to 4,5			0,71
1,12				1,12
1,8		Zone boundary B/C 1,8 to 9,3		1,8
2,8				2,8
4,5			Zone boundary C/D 4,5 to 14,7	4,5
7,1				7,1
9,3				9,3
11,2				11,2
14,7				14,7
18				18
28				28
45				45

NOTE 1 This table only applies to machines for which specific International Standards have not been developed and for which there is no suitable experience available.

NOTE 2 Small machines (e.g. electric motors with power up to 15 kW) tend to lie at the lower end of the range and large machines (e.g. prime movers with flexible supports in the direction of measurement) tend to lie at the upper end of the range.

Figure 3.17: Range of typical values for zone boundaries [121]

3.7 Flexible Multibody System Dynamics

There are several approaches when modelling a multibody nonlinear, i.e. flexible, system; convected coordinate system, finite segment method, large rotation vectors or absolute nodal coordinate formulation. For larger deformation a FE model or absolute nodal coordinate formulation more generally could be used. In that case a nonlinear EOM describes the flexible motion in an exact geometrical sense. This could lead to a significantly high computational time, but as discussed, in some situations time is traded off for accuracy.

However, the most commonly used is the floating frame of reference formulation. This is also used in the employed MBS software SIMPACK. Here, two coordinate sets are used for describing a deformable bodies' motion. The first set is the position of a selected body, while the second set is the bodies deformation in relevance to its own coordinate system [122]. The deformation is then a product of super-positioning. The super-positioning is between a larger referential motion and the smaller deformations. To be able to describe the displacements in such a multibody system, a linear combination of the estimated shape functions with the following time dependent weighting factors is performed. Thus, a way to achieve the shape functions appropriately is of the essence. This could be done by two different approaches:

- Nodal approach
- Modal approach

A nodal approach will utilize finite element (FE), with the local expressions weighted with the nodal deformations. This could be done by using absolute nodal displacement and coordinates, or by using an FE model. On the other hand, a modal approach will weight global eigenfunctions or static displacement with modal coordinates. By performing a modal approach, the system order is significantly reduced, however an issue with choosing the shape functions arises. Consequently, it is possible to assume that strain and displacements are small, and that the shortening and tilting effects caused by higher loads must be considered when calculating the displacements. A modal approach has fewer degrees of freedom and shortened computational time, which could be advantageous [123].

3.8 Inverse Method

There have been done research on several inverse methods that could be employed to find the response of a viscously damped system. Inverse problems are traditionally hard to solve in comparison the traditional direct method problems. Simply put, direct method goes from input to output, while the inverse goes from output to input. When extracting the output of a system, this is again used to model input to replicate output. Example on

inverse methods are e.g. neural networks [124]. Or it could also be for instance Jacobi matrices calculations by retrieving the eigenvalues [125].

For the case of the simple model drivetrain it is possible to retain the significant parameters in the equation of motion for the system, from modal analysis of the response. In a digital twin however, it is the model behaviour predictability of the system that is central. To achieve a predictive analysis, the function for the external force could be obtained, by an educated assumption.

For instance, assuming the drivetrain is unbalanced will yield a $F(t) = mesinwt$, and in Section 4.2 the inverse method is by analysis finding the me values. Verification of the model then happens by comparison with data from model tests. If the correct force is achieved in the model, it is possible to employ the model as a proper digital twin and to perform predictive analyses. However, for a system with more degrees of freedom other more elegant methods could be more time efficient to employ instead of doing so for each DOF. This would also be pointless, as a model with more DOF would have coupled effects and also, there rarely would be only an unbalance as the fault in a system as discussed in Section 3.4.2.

Chapter 4

Methodology

4.1 Modelling

For method verification reasons this thesis will consider a simple drivetrain test rig in a lab, equipped with optical sensors for vibration analyses that detects displacements. The drivetrain is shown in Figure 4.1. The sensors are placed to detect displacements in horizontal (X) and vertical (Y) direction as shown in Figure 4.2a and 4.2b. By utilizing this simple drivetrain instead of a gearbox, it is easier to detect flaws in the methodology approach. Further use of the method could then be employed and this method could be utilized for other and more intricate and complex models. Additionally, NTNU has this simple drivetrain available in real life for testing in lab. The lab is the *Marine Computational Mechanics Research Lab* (MCMR Lab) at NTNU Department of Marine Technology. This model is simplified and some assessments done in Section 2.3.1 where power transferring through gear teeth contact and contact analysis should be considered is ignored for the behalf of modelling verification. In this case, the model approach possibly could be used in further, more complex digital twins. Several modelling approaches of this simple drivetrain were tested, and the modelled drivetrain is shown in Figure 4.1. In the following sections both the theory behind and the methodology for the approaches are described. How strong these approaches are when detecting faults is also discussed, and a complete discussion for their application follows in Section 6.

Traditionally when a modal analysis is performed, the EOM (Equation 3.1), is solved. Resulting from these analyses the stiffness and damping coefficient are found. A disruptive impulse from the stroke of a hammer is introduced to the system and the following responses are retrieved. In what degree the motion slows down, decays, and goes back to original state is observed, and the vibration data shows the nature of this transient phase.

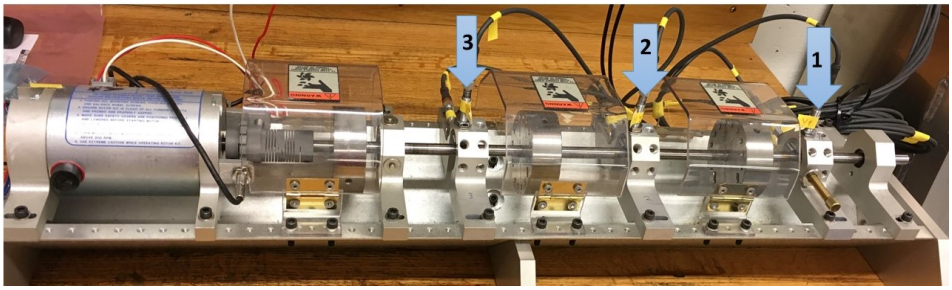

Figure 4.1: Simple drivetrain real model. The arrows shows the location of sensor 1, 2 and 3.

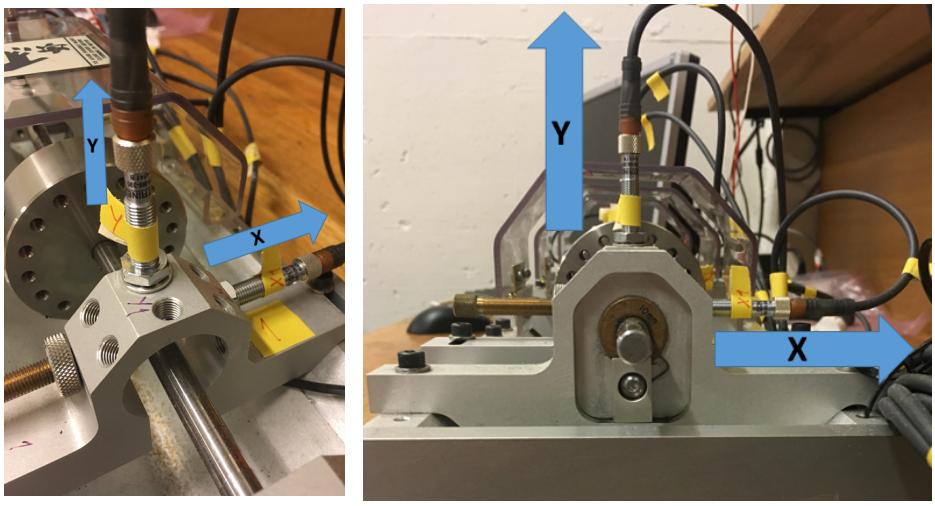

(a) Overview

(b) Frontview

Figure 4.2: X and Y direction if the simple drivetrain test rig that will be used in this thesis

4.2 Modelling of a 1 DOF drivetrain

When considering the model in one DOF, it is easier to model and it is faster to do calculations. The drivetrain is considered as shown in Figure 3.2.

4.2.1 Modal Analysis

After running the model at a constant angular velocity (ω) of 20 Hz, comparable results were available, shown in Section 5.1. When performing the modal analysis for the simple one DOF system, the theory in Section 3 was followed and implemented in coding in MATLAB. This relatively simple programming analyzes the response data from the decay hammer tests, and the results are shown in Table 5.3 in Section 5.2.1. The translational stiffness, which is the only relevant stiffness in the one DOF case, is found in each

direction X and Y, and at all three sensors. The same is the case for the damping. It is found from the response that ζ should be significantly less than 1. ζ is then found through $\zeta \approx \frac{\delta}{2\pi}$. The resulting values found are shown in Section 5.2.1.

By following Equations 3.20 and 3.21 it is possible to obtain the modelled amplitudes and compare the results. These results are shown in Section 5.2.1.

4.2.2 Experimental Modelling

Experimental modelling for the 1 DOF model will concern stiffness change as proposed in Section 3.2.4, however only load case 2 (or 3) and load case 5 (or 4) are relevant. This is due to that the stiffness applied in this case only regards one direction and one location at the time. Thus, there are no impact from one location of the shaft to the next. For this analysis the stiffness in X direction was increased, whilst the displacements there was calculated, and the likewise with Y direction. These results were then compared to the measured values and the model sensitivity revealed, presented in Section 5.2.2.

4.3 Modelling of a 5 DOF drivetrain

4.3.1 Modal Analysis

To include all dimensions and DOF, a modal analysis considering all DOF of the drivetrain was performed. As shown in Section 4.2, the characteristic values were found through the MBS with the motivation to perform a more complete analysis of the system. Therefore, the increased fidelity model considers three dimensions and up to six DOF.

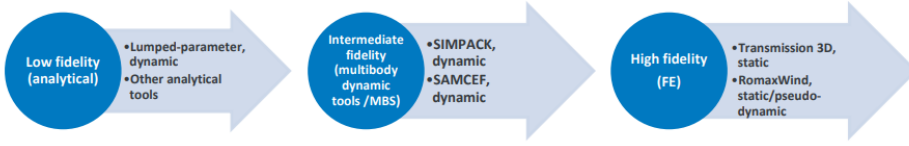

Figure 4.3: Modelling tools for increasing fidelity models

4.3.2 Multi-Body Simulation

The modelling of the drivetrain, is done in the MBS software SIMPACK. In this software it is possible both to model rotating systems, bearings, perform analysis and calculations, post-processing of data and to communicate with other software e.g. MATLAB, Abaqus or ANSYS. The digital model is shown in Figure 4.4.

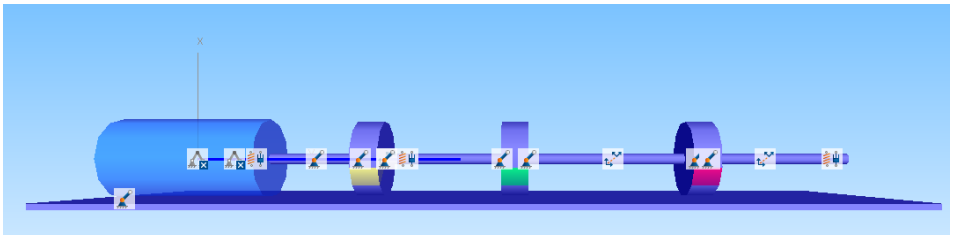

Figure 4.4: Digital twin

In the model all bodies could be chosen to be either rigid or flexible, and the degrees of freedom set in the joints will make allowances to vibrate in desired directions, as discussed in detail in Section 2.3.2. For this drivetrain comparable data from the sensors in horizontal (X) and vertical direction (Y) are retrieved from the real model. The shaft should therefore be able to show displacement in these directions. Furthermore, the shaft will have to be able to rotate due to the torque applied. This results in a minimum of three degrees of freedom. The kinematic tree for the digital drivetrain is shown below in Figure 4.5.

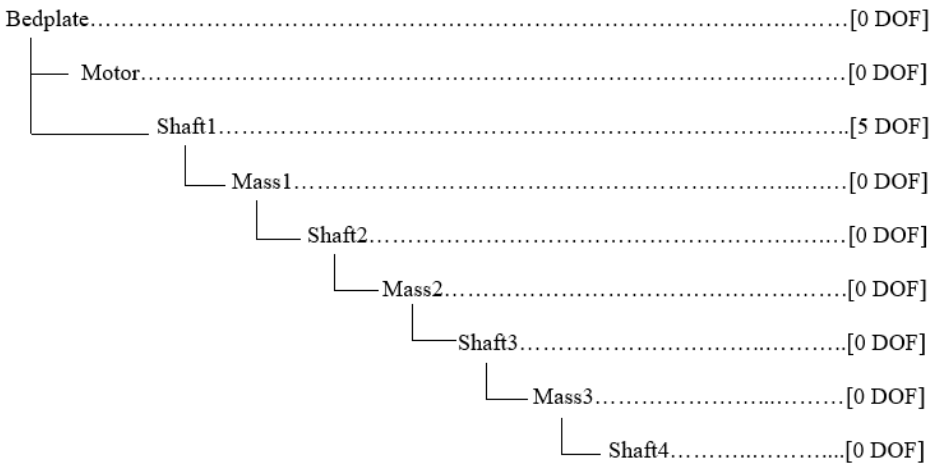

Figure 4.5: Kinematic tree

The bearings in the SIMPACK model are modelled as a force element *FE43 Bushing Cmp* with characteristic values for stiffness and damping. These values are found from the modal analysis. The MBS model accuracy is dependent on the level of precision of stiffness, mass and damping values. For digital twin approach it is therefore worth spending time on the modal analysis.

4.3.3 Degrees of Freedom

The bodies are connected through the kinematic tree as presented above in Figure 4.5. To be able to model the real drivetrain accurately it is important to consider each element correctly. The geometric values and position in regards to each other are copied to the digital model. To be able to model all masses well, and to have better control of the system the shaft is segmented into four smaller shafts interconnected with three masses. These masses are identical to those put on the real drivetrain. As shown in Figure 4.5 these segments are all connected to each other with zero DOF. In that way, all the translational and rotational movement are transferred through the whole system.

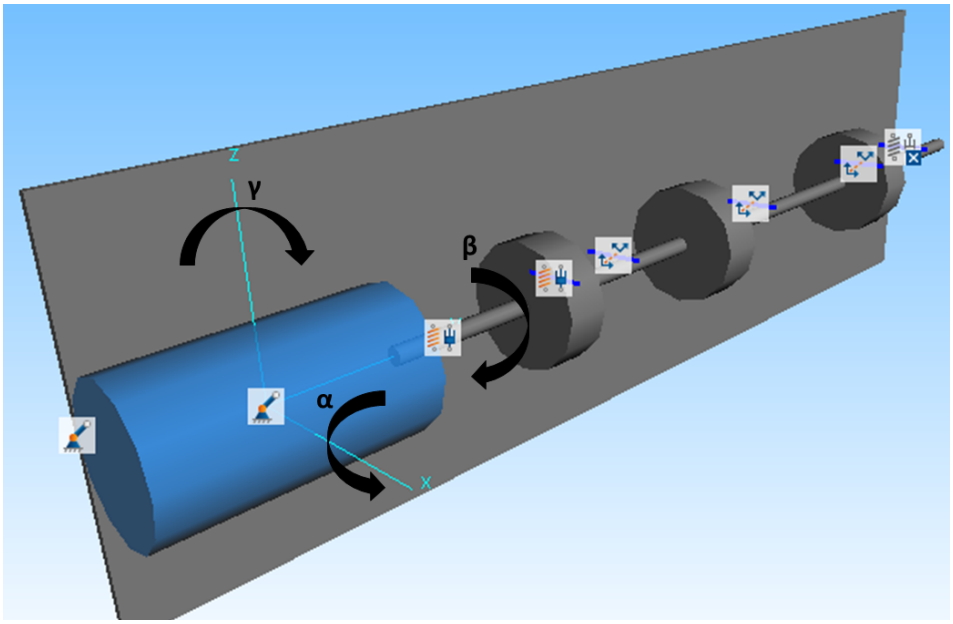

Figure 4.6: Rotational orientations

Extensional work has been done in order to determine which joint type in SIMPACK that was suitable. The joint type defines the DOF in the joint that attaches the bodies. I.e., the shaft joint type decides the DOF of the shaft body. In the early iterations all joints on the shaft have the same DOF. However, the solution of zero DOF in the attached bodies makes them behave as a continuous shaft, which is the desired result. Allowing three DOF in all these joints makes them free to have translational movement in relation to each other. When the bearing forces are employed, this results in unfavourable system behaviour, making it evident that this was not a feasible solution. By increasing this to a five DOF solution with freedom to move in rotational degrees in α and γ allows the model to more accurately simulate the real drivetrain test rig. These rotational directions are used in reference extensively further on in this thesis and they are shown in Figure 4.6.

Introducing freedom to move in these directions also introduces their relevant stiffness. There are several ways to do so, with varying results, as discussed in Section 3.2.3. The first method found in Section 3.2.3 proves more accurate in this drivetrain model and is used for further use and comparison. However, none of these calculations led to an accurate simulation.

4.3.4 Control System

In the model in SIMPACK the angular velocity is driven up if there is no torque control. Therefore, a control system is made to keep the angular velocity at desired ranges. This control is performed by a proportional-integral (PI) control system in MATLAB/Simulink by co-simulating between the software SIMPACK and MATLAB/Simulink. The sample rate is made identical for SIMPACK and MATLAB/Simulink. In MATLAB/Simulink a simple PI control system is built to keep the drivetrain torque at the correct level to achieve the globally required angular velocity. This is done by following the control as presented in Equation 4.1 and 4.2. The K_p and K_I values are found through the tuning and iteration based on Nyquist- Zigler method [126].

$$T_{\text{out}} = K_P e + K_I \int_0^t e dt \tag{4.1}$$

$$e = \omega - \omega_{\text{ref}} \tag{4.2}$$

The tuning done for a 20 Hz running drivetrain will have to be altered when the running speed is increased or decreased. This is done by changing the input wanted angular velocity and doing the tuning again. In Section 5.3.1 and Table 5.4 shows the tuning values found for frequencies from 20 to 50 Hz. The tuning for the control system has to be changed for rigid and flexible shaft. For the flexible system $K_P = 12/10$ and $K_I = 40/8$, whilst for the rigid system $K_P = 1/10$ and $K_I = 1/8$. In Figure 4.7 these values are shown for the rigid shaft run.

Co-Simulation

In the simple drivetrain in SIMPACK there is no angular velocity control so if not controlled, the angular velocity could increase infinitely in theory. The vibration data will then not be comparable to the real system. Therefore, a control system is needed as presented in Equation 4.1. The control system is based on error estimation, and to calculate the error, a reference value is needed. This reference value, ω_{ref} is the angular velocity the real system is running at.

It is possible to make the control system in MATLAB/Simulink by employing the Sim-

ulink add-on module SIMAT, that has the communication tools between SIMPACK and MATLAB. This is done by a separate s-function in Simulink/MATLAB. It is important to facilitate this communication through the same server ports and port ranges in both software, so it can be feasible to communicate through coupling in by Transmission Control Protocol/Internet Protocol (TCP/IP) tools. SIMPACK sends its output to Simulink/MATLAB through y-vectors, that will become a output in the SIMAT block in Simulink/MATLAB. Simply put; the co-simulation consists of data exchange at discrete time steps, and the module combines computer aided control system design (CACSD) with SIMPACK [127]. Then by employing the control system from Equation 4.1 and 4.2 Simulink/MATLAB will calculate a new input value in the SIMAT block. This input value is stored in SIMPACK as an u-input. SIMPACK in turn will calculate a new output value and this will go on for the each data set. The system is shown in Figure 4.7.

4.3.5 Inverse Method

Relevant inverse methods will be able to figure the response from the EOM of the drivetrain. In the drivetrain considered, the MBS software SIMPACK is used as the inverse method. SIMPACK is based on the implicit time integrator SODASRT2 and Newtoninan vector calculations for writing EOM. By letting SIMPACK do this, with the data from the modal analysis, the digital twin should operate and behave in the relatively same manner as the real twin, as long as all the values are correct. Other methods to solve this for could be by employing Lagrange method for calculating EOM. However, SIMPACK does not do this, so this should be done in other tools, possibly MATLAB or other programming languages.

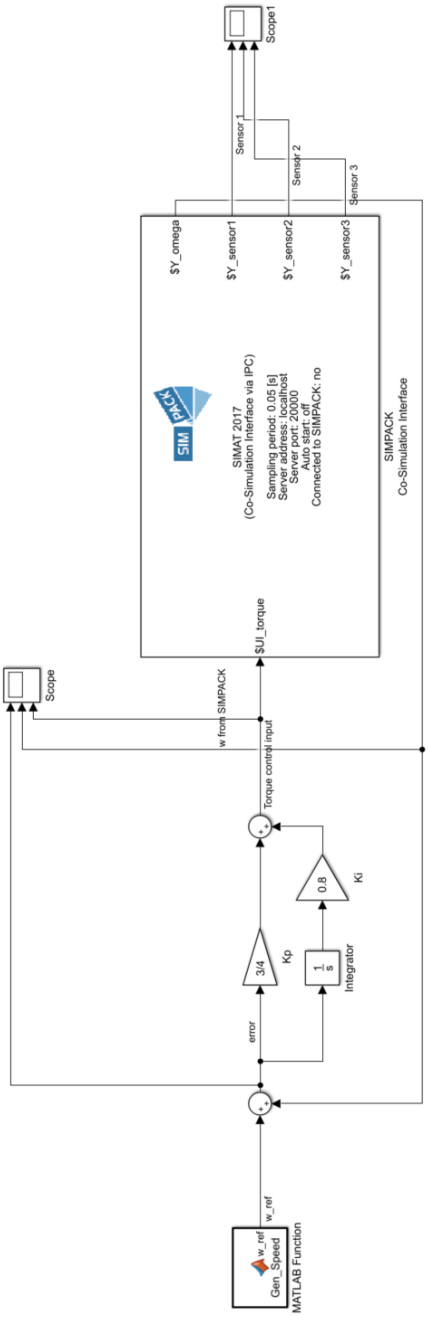

Figure 4.7: Control system from Simulink/MATLAB, connected to SIMPACK through SIMAT-block

4.4 Flexible Shaft

Motivated by accuracy and increased fidelity, flexible shafts are introduced. As discussed in Section 2.3.1 the shafts in drivetrains are typically modelled as flexible. This is because the shaft diameter is relatively small compared to the shaft length. In SIMPACK, this could be done in the digital twin model by employing SIMBEAM; an alternative for flexible modelling. SIMBEAM considers a bodies' flexible characteristics, by considering finite element analysis (FEA). By solving eigensystems and performing a calculation of static equilibrium in pre- calculation, a modal approach is feasible, as described in Section 3.7.

SIMBEAM uses this modal reduction that will describe deformation correctly up to second order, which is sufficient for many simulations [123][128]. The calculations were done using Timoschenkos approach, and the flexible bodies were given significant nodes and cohesive elements from node to node. Markers were put at the same locations as the nodes, for rotation data in nodes, as the rotation from joint to marker is transferred. The other bodies, such as the three masses, the motor and the bedplate are all considered as rigid bodies. Every simulation was run for 300 s, as a trade-off between excluding transient phase and computational time, especially for the case of experimental modeling and the different load cases.

The flexible bodies have characteristic material and cross- section values, shown in Table 4.1.

Table 4.1: Characteristic values flexible body

Material	Steel
Density	7850 [kg/m^3]
Poisson's ratio	0.32 [-]
Modulus of elasticity	200 [GPa]
Cross-section	circular, diameter 10 mm

4.4.1 Experimental Modelling

All the relevant load cases described in Section 3.2.4 was performed and the results from these are found in Section 5.3.3. A representative excerpt of all five load cases are shown by LC2 in Appendix G. Both the rotational and translational stiffness and damping found from Section 3.2.3 was implemented, in addition to tuning for accuracy. The stiffness parameter turns out to be complex to calculate, and this is partly why this experimental modelling approach is performed. Additionally, the results from the hammer tests as described in Section 3.2.3 shows a somewhat differing stiffness value, and it is of interest to see the degree of sensitivity of the model for each stiffness in the vibration orientations.

4.5 Rigid Shaft

In this section the shaft is modelled as rigid, meaning that all bodies in the MBS are defined as rigid, having no deformation or bending throughout each body. The joints following the *Shaft 1-* joint are applied as zero degrees of freedom, making the whole shaft simulated a one continuous object.

Two different approach was tried in the case of rigid shaft:

- 3 DOF
- 5 DOF

The different responses are shown in Section 5.3.3.

4.6 Modelling Faults

A way to model faults in multi body simulation is by reducing the stiffness in the bearings. If there is no fault the stiffness should be completely similar, however if there are any faults the stiffness will be different. Thus, to model the faulty bearings the stiffness could be reduced in E03 order as Nejad et al. has performed [49].

Sensors are put at the same place as the real twin has its sensors, so that the data achieved are comparable, and if there are faults in the model rig at run test 20 Hz this should be similar to the model faulty bearings. Nejad et al. performed iterative sensitivity analysis of a planet bearing, and concluded with a stiffness reduction of about 50% of the fault free bearing [49]. This research leads to a similar approach in this thesis. Several stiffness reduction schemes were tried, and a tuning was done to achieve as similar as possible results as the measured ones. More on this uncertainty in Section 3.3.

4.7 Force Vector - Flexible Shaft

The force vector inputs are the solutions to Equation 3.19: $F_R = F(t) + m\ddot{x}$, in both X and Y direction for bearing 1 and 2. Next, the vectors was utilized to be the input force in SIMPACK where F_R is input in the bearing force component. This approach assumes that there are fault occurring that results in peaks in FFT at 1 and 2 xrpm, thus it is a modelling approach for faulty systems. If this is introduced well and with good results, this program could be used for fault detection.

It is evident from the derivation from Equation 3.19 that parts of the modal analysis process actually could become redundant, as only the force and the acceleration is necessary and this could be an argument for the efficiency of this method. However, there are parameters not found in the EOM that still would be of interest. The challenge in this approach

lies with finding the different force vector input amplitude values, which then are the only unknown values. The scheme to do so is presented in Equation 4.3.

$$\begin{aligned} x(t) = Xsin(\omega t) \qquad \Phi = 0 \\ Z = -M\omega^2 Xsin(\omega t) + c\omega Xcos(\omega t) + kXsin(\omega t) \\ Y = Asin(\omega t) + Bsin(2\omega t) + m\ddot{x} \\ |Z - Y| = 0.0001 \end{aligned} \tag{4.3}$$

$x(t)$ is the response if the system, X is the amplitude ω is the rotational velocity in rad/sec, Φ is the phase, M is the mass, and A and B are the unknown amplitudes to be detected and implemented in this fault modelling approach. This was done for both directions X and Y. Sensor values from sensor 1 and 3 are assumed accurate enough to be employed in bearing 1 and 2.

4.7.1 Monte Carlo

Finding the expression for the force vector input only relies on finding the unknown left, the amplitudes. To figure out the amplitude values in the input force vector of the response of the EOM, a Monte Carlo method was used in MATLAB programming. The error between the response and the EOM was set to be less than or equal to 0.0001, as shown in Equation 4.3. A and B values were chosen randomly between 0.1 and 100 and an array of 3000 cells for each A and B was tried and paired. Additionally, the phase for Y was accounted for. In all, the results from this procedure is shown in Section 5.5.

Chapter 5

Results

5.1 Real Twin - Drivetrain Test Rig

In this section the results from a 20 Hz test of the drivetrain test rig model is presented. The displacement of each sensor value in X and Y direction is shown, and in Appendix C the velocities and accelerations are displayed. Also the FFT of the 20 Hz run is performed and showed below in Figure 5.7, showing a peak at 1xrpm and 2xrpm and a significantly smaller one at 3xrpm. This implies *already existing faults* in the drivetrain test rig, which again implies that the model values should include fault modelling such as stiffness change or force vector input. The implications from this are discussed in Section 6.Figures 5.8 to 5.10 shows the orbit plots for the sensors 1-3. The model was also run for an increasing rotational velocity to investigate the critical speed. As sensor 2 by its location in the middle between the two bearings, it has the most displacement, and is the one used for critical speed calculations. The model was run at 5 Hz incremental increases, and by this approach the maximum deflection and critical speed was found at 35 Hz. Nevertheless the lab coordinator refers to a critical speed at 33 Hz. This difference is possibly due to the coarse incremental increase.

Table 5.1: Average peaks from 20 Hz run, for further comparison

	Sensor 1	**Sensor 2**	**Sensor 3**
X	0.029 mm	0.052 mm	0.0123 mm
Y	0.028 mm	0.049 mm	0.0149 mm

In Section 3.6 the root mean square (RMS) values are described as revealing data for the severity of vibration. Therefore, the RMS values are found for the 20 Hz run at mm/s, and they are as shown in Table 5.2. From this it is evident that sensor 1 are within Zone A/B in both directions, as is sensor 3, but sensor 2 are in the limit area towards upper Zone

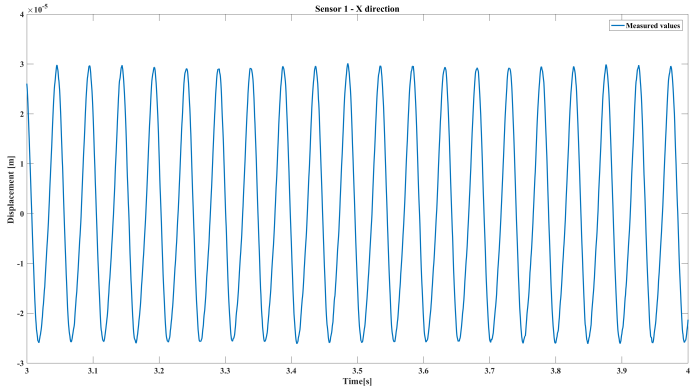

Figure 5.1: Displacement in X direction at sensor 1

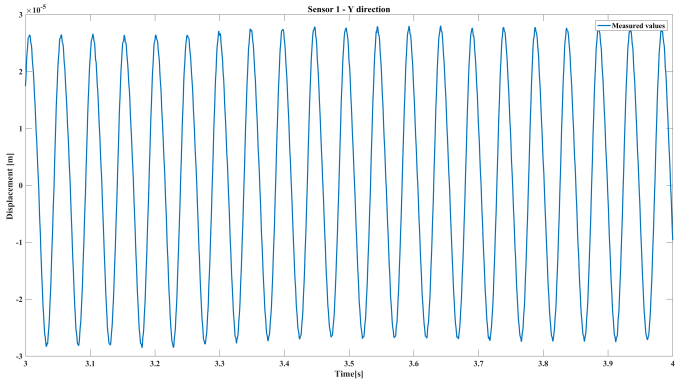

Figure 5.2: Displacement in Y direction at sensor 1

B/C.

	X1	**Y1**	**X2**	**Y2**	**X3**	**Y3**
rms values	2.5509	2.5169	4.6251	4.4612	1.3336	1.2818

Table 5.2: RMS values [mm/s] for sensor 1-3 in X and Y direction

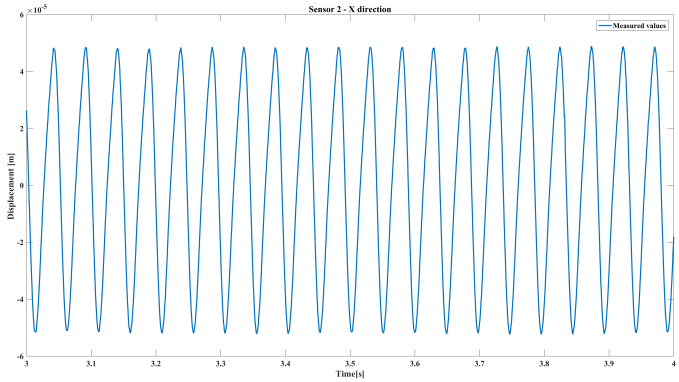

Figure 5.3: Displacement in X direction at sensor 2

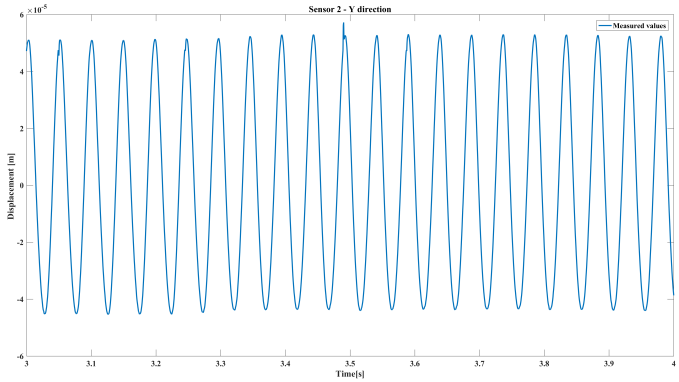

Figure 5.4: Displacement in Y direction at sensor 2 test run at 20 Hz

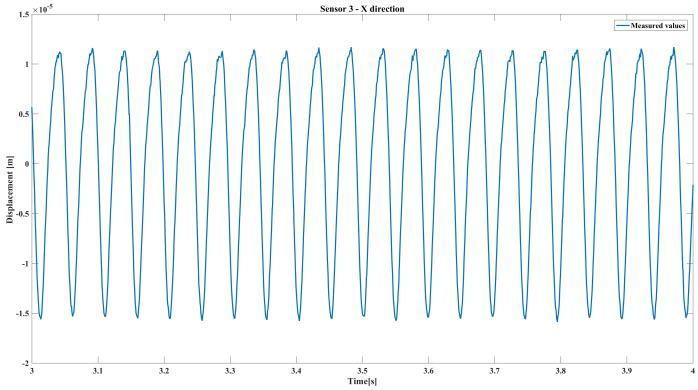

Figure 5.5: Displacement in X direction at sensor 3

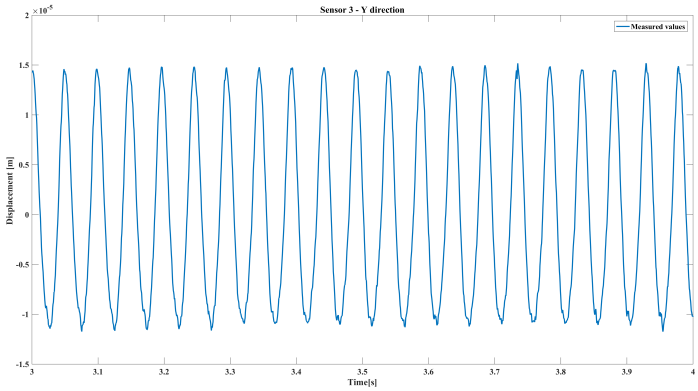

Figure 5.6: Displacement in Y direction at sensor 3

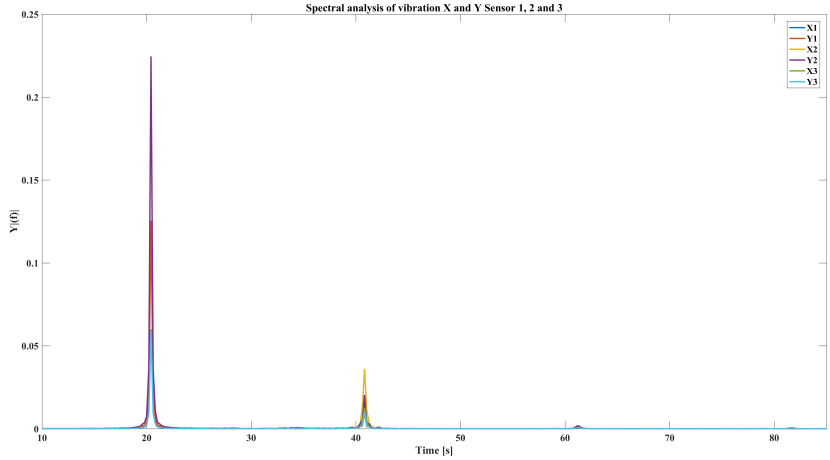

Figure 5.7: FFT of the 20 Hz run

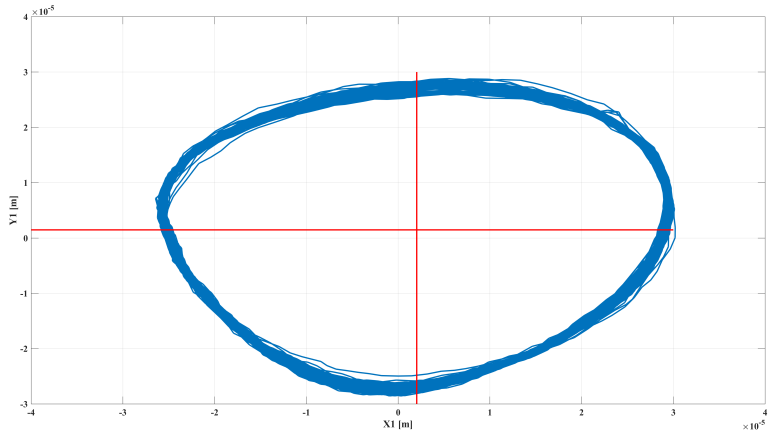

Figure 5.8: Orbit plot sensor 1, center lines for X and Y in red.

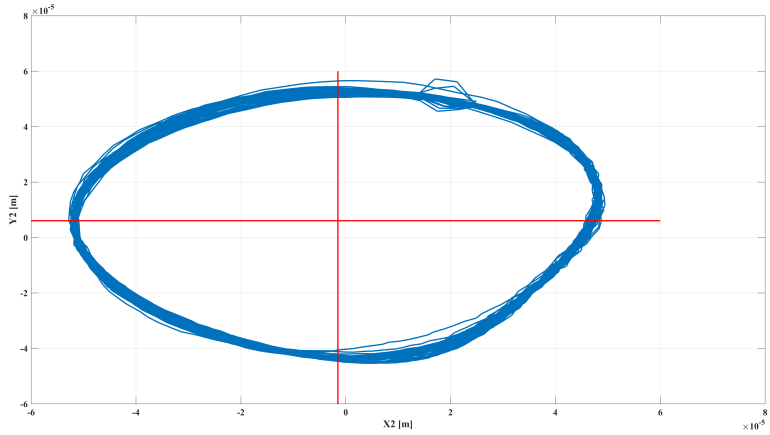

Figure 5.9: Orbit plot sensor 2, center lines for X and Y in red.

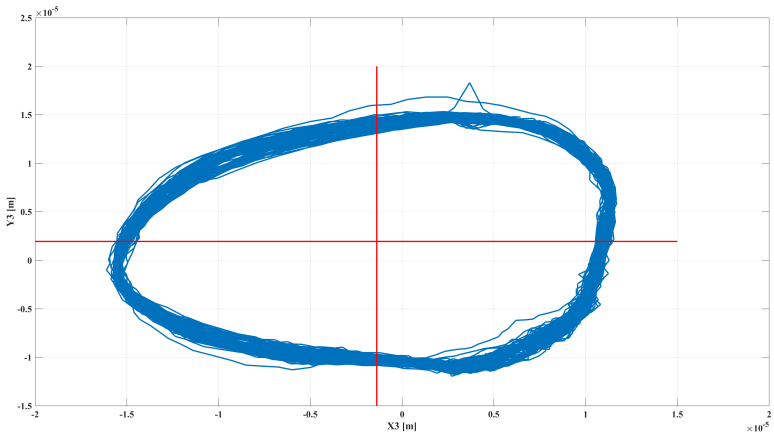

Figure 5.10: Orbit plot sensor 3, center lines for X and Y in red.

5.2 1 DOF Model

5.2.1 Modal Analysis

To simplify the data from Section 5.1 the average peak for Y directions at all three sensors are presented in Table 5.3. The natural frequency and the implied natural angular velocity, stiffness, me-values and damping coefficient are all found through use of simple programming in MATLAB and calculations described in Section 3 and 4.2.

Table 5.3: Results from modal analysis 1 DOF vertical (Y) direction

	Sensor 1	**Sensor 2**	**Sensor 3**
Average peak [mm]	0.027278	0.052388	0.01467
Natural angular frequency [rad/sec]	188.5	188.5	188.5
Stiffness [N/m]	8.5273e+05	8.5273e+05	8.5273e+05
ζ **[-]**	0.11462	0.095436	0.079212
Damping coefficient [Ns/m]	118.08	82.031	56.593

The rotational stiffness in is found to be 0.14, which could be considered to be quite low, however it is an important value for the system to retain a rotational speed. The performance of the digital twin is shown in full in Appendix D, and a representative excerpt from sensor 2 in Y and X direction is shown below in Figure 5.11, 5.12.

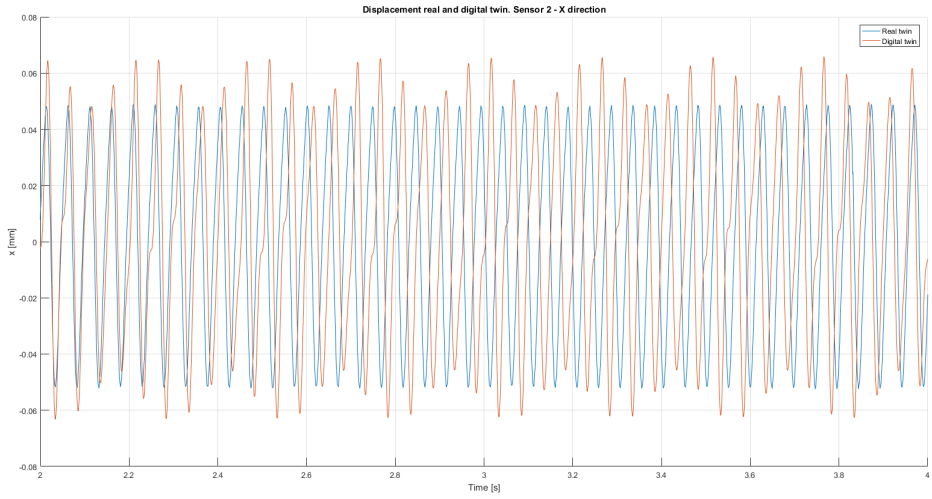

Figure 5.11: Performance for Digital Twin 1DOF Sensor 2 - X direction

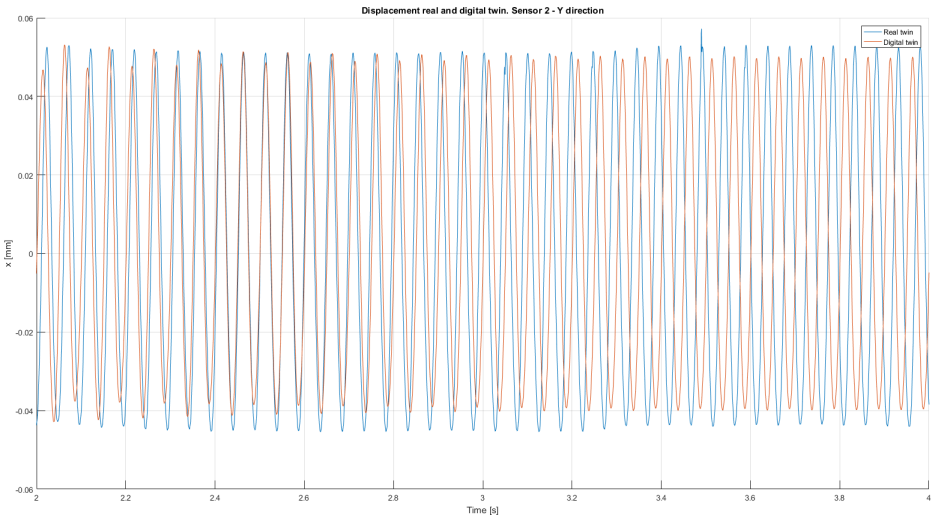

Figure 5.12: Performance for Digital Twin 1DOF Sensor 2 - Y direction

5.2.2 Experimental Modelling

Figure 5.13 shows the average percentage error for load case 2 and load case 5, sorted by incremental increase. The error is found as the average percentage error,

$$\frac{X_{Calculated} - X_{Measured}}{X_{Measured}} * 100 \tag{5.1}$$

for X-and Y- directions at all three sensors, relative to the measured values found from the run of the drivetrain test rig. The load cases are described in Section 3.2.4.

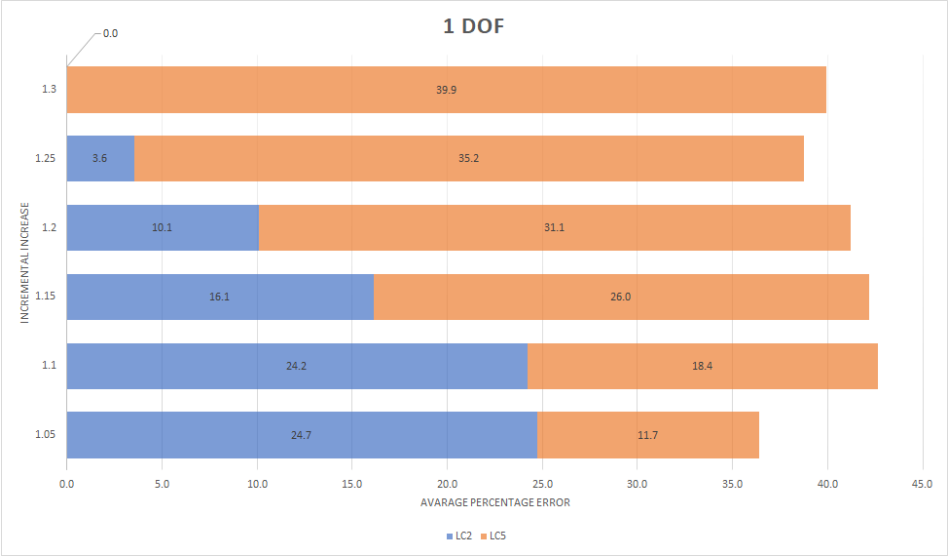

Figure 5.13: Load case 2 versus load case 5

5.3 5 DOF Model

5.3.1 Control System

The control system has to be tuned for each new running frequency, and below in Table 5.4 shows the tuning values. Additionally, the values for respectively rigid and flexible shaft modelling are shown. When the model was run at the higher frequencies, the vibration response increased up until 35 Hz, and decreased for a bit after that, until increased again at 50 Hz. The response from this is shown in Appendix H and the trend and response from these running test of the model show that the model has a critical speed at 35 Hz, which is close to the real drivetrain test rig critical speed as shown in Section 5.1.

5.3.2 Flexible Shaft

Modal Analysis

For each hammer test performed the associated natural frequency and stiffness at each sensor was computed. All the different values are presented in Appendix A. An excerpt is shown in Table 5.5, that is taken from hammer test number two. Figure 5.14 shows the FFT of hammer test number two and that the frequency peaks are at 30 and 36 Hz, which are the natural frequencies as calculated and shown in Table 5.5.

Table 5.4: Control system tuning results for different running frequencies

Stiffness	K_p	K_i
Rigid	1/10	1/8
Flexible	12/10	1/8
Force vector input	3/5	1/8000
Frequency	K_p	K_i
20	12/10	40/8
25	1/10	4/8
30	1/10	4/8
35	1/10	4/8
40	1/10	1/8
45	1/10	1/13
50	1/10	1/550

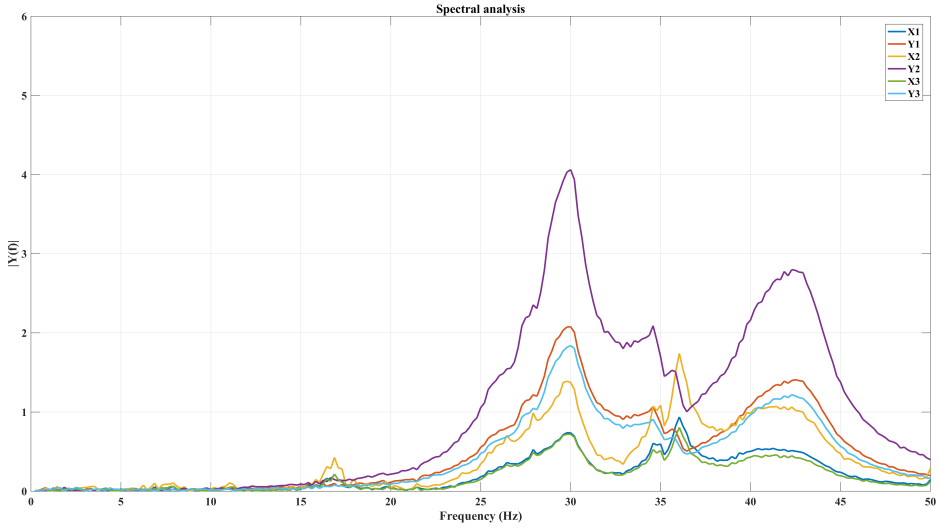

Figure 5.14: Spectral analysis hammertest 2

Table 5.5: Natural Frequency and Stiffness in hammer test 2

	X1	Y1	X2	Y2	X3	Y3
Damping Coefficient [Ns/m]	1.5972	78.72	0.15073	54.688	4.7996	37.728
Natural frequency [Hz]	36.042	30	36.042	30	36.042	30
Stiffness [N/m]	8.2052e+05	5.6849e+05	8.2052e+05	5.6849e+05	8.2052e+05	5.6849e+05

For each hammer test performed there was computed the relevant ζ values in both X and Y direction at sensor 1, 2 and 3. Additionally the damping coefficient was calculated in both directions at all sensors. All the different values are presented in Appendix A. An excerpt is shown in Table 5.6, that is taken from hammer test number two.

Table 5.6: ζ and Damping Constants in hammer test nr 2

	X1	Y1	X2	Y2	X3	Y3
ζ	0.014847	0.11462	0.0045607	0.095436	0.018535	0.079212
Damping Coefficient [Ns/m]	1.5717	94.114	0.15006	62.616	2.4759	43.547

Stiffness

As mentioned in Section 4.4.1, both the calculated stiffness values and the tuned values were implemented in the model. However, the tuned values through an iteration process proved more valuable and combined with an iterative process with damping values they proved to be have more similar output to the measured values. Why this could be is discussed in Section 6.3.3. After an extensive iteration process the values gave similar results between digital and real model, presented in Table 5.7 and Table 5.8. Figure 5.21 shows that the values in Y- direction are close to 1, i.e. accurate to the real model. On the other hand, in X- direction the accuracy is lower and the calculation overestimates the displacement.

Stiffness	Value
$\mathbf{K_{x1}}$	820520
$\mathbf{K_{x2}}$	820520
$\mathbf{K_{y1}}$	568490
$\mathbf{K_{y2}}$	568490
$\mathbf{K}_{\alpha 1}$	1000
$\mathbf{K}_{\alpha 2}$	1000
$\mathbf{K}_{\gamma 1}$	1000
$\mathbf{K}_{\gamma 2}$	1000

Table 5.7: Stiffness values after iteration process

Damping	Value
$\mathbf{C_x}$	11490 ($\sim$1.4% K_x)
$\mathbf{C_y}$	7960 ($\sim$1.4% K_y)

Table 5.8: Damping values after iteration process

Figures 5.15-5.20 shows the displacement calculated using flexible SIMPACK model, compared to the measured values on the drivetrain test rig.

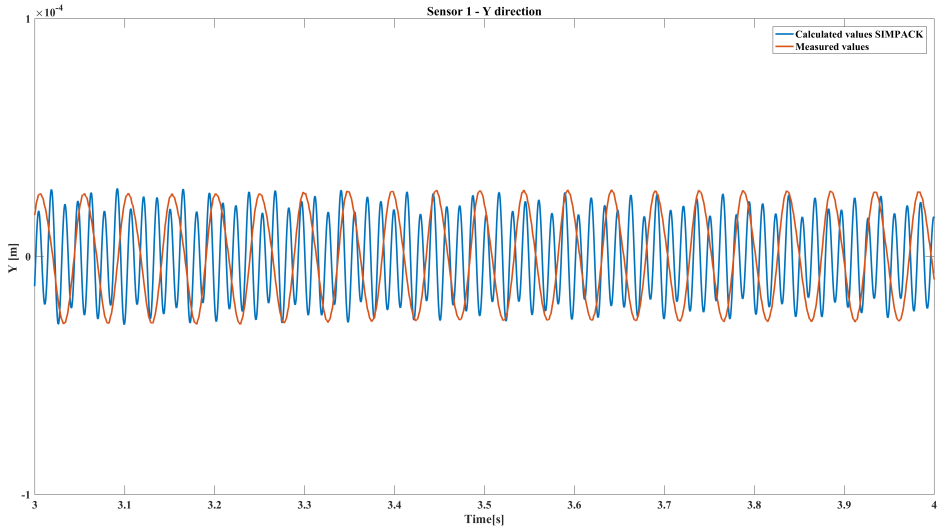

Figure 5.15: Compared displacement in sensor 1 - Y direction

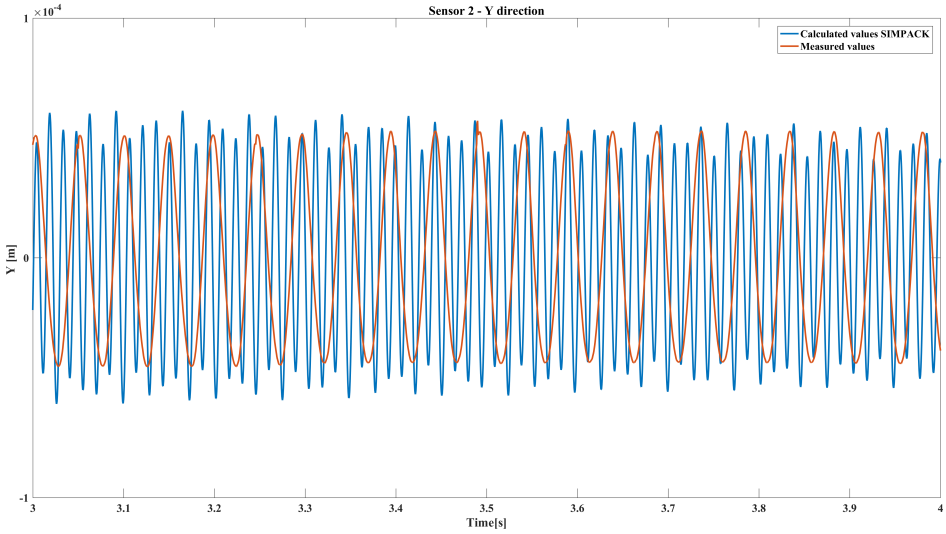

Figure 5.16: Compared displacement in sensor 2 - Y direction

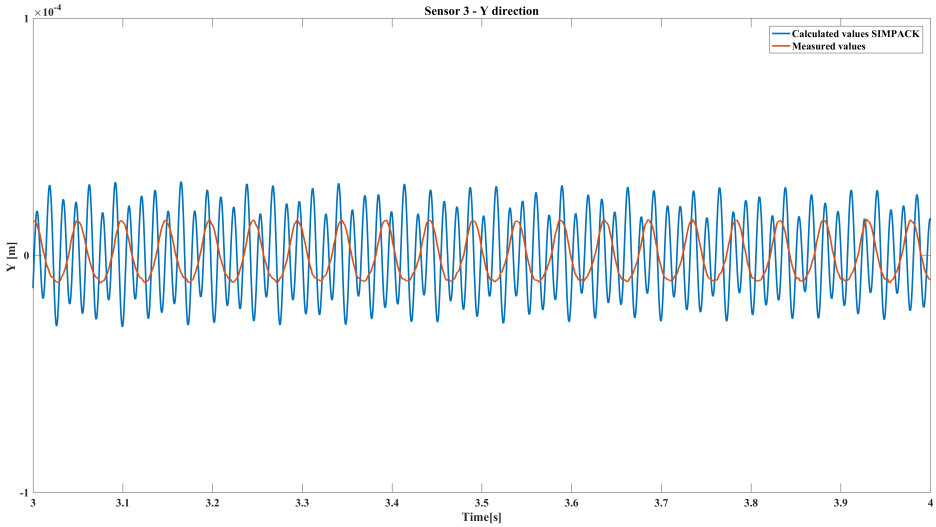

Figure 5.17: Compared displacement in sensor 3 - Y direction

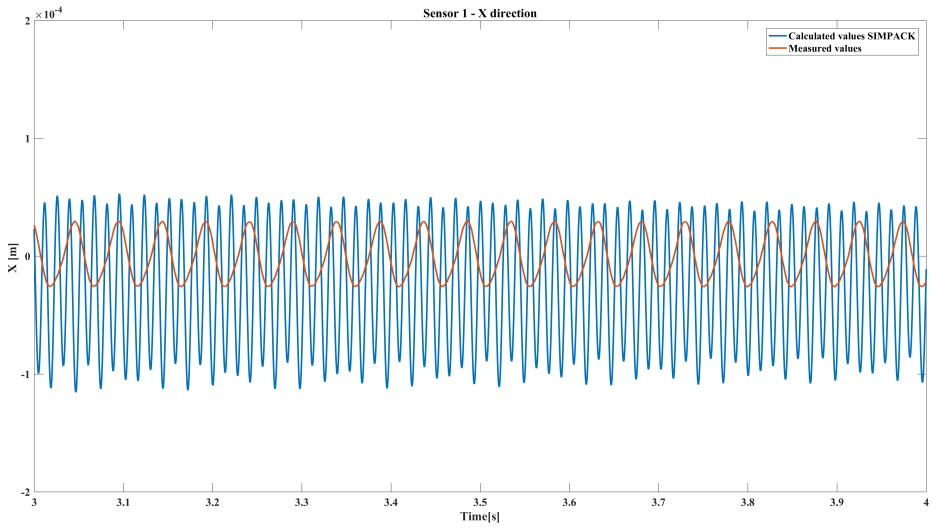

Figure 5.18: Compared displacement in sensor 1 - X direction

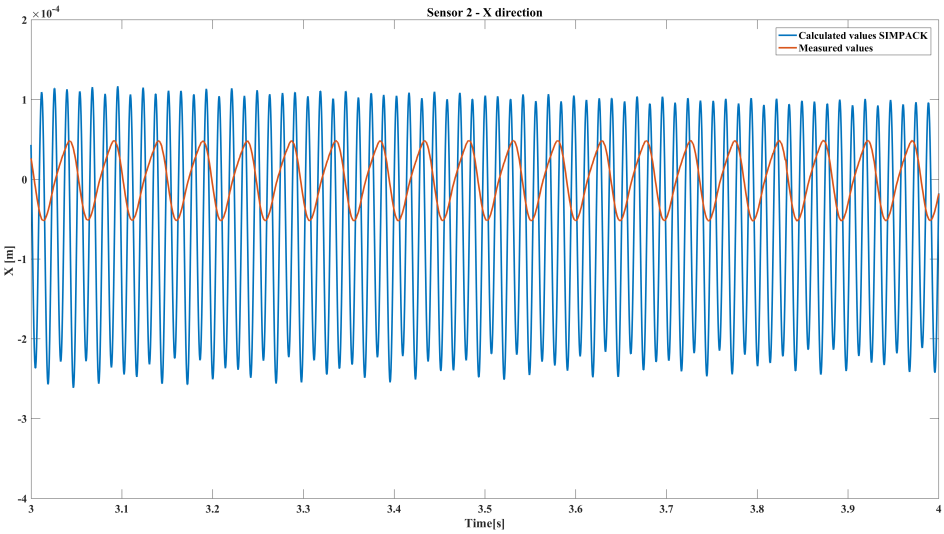

Figure 5.19: Compared displacement in sensor 2 - X direction

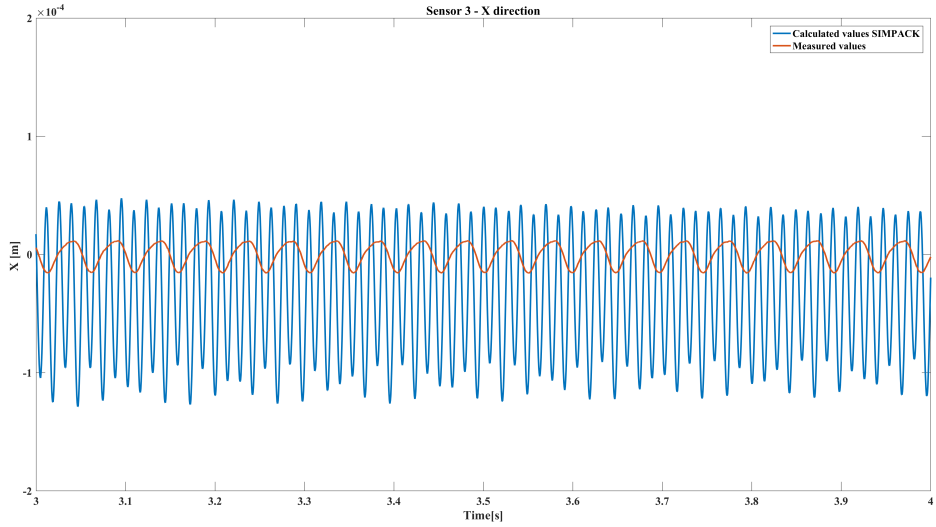

Figure 5.20: Compared displacement in sensor 3 - X direction

Experimental modelling

In Figure 5.21 the accuracy is measured in relation to the attained data. The load cases are described in Section 3.2.4. At value 1 in Y-axis the output from the model calculated is exactly the same as the measured data. The different sensors and orientations are put on the X-axis that is Sensor 1 in X direction is found as ”X1” and so on. It is evident that the ”Accuracy” for Y directions seem more accurate, however the fit is relatively similar as to what the measured values are. This is shown in Figures 5.15-5.20 above. In LC2 there is a negative offset which diminishes over the incremental increases. However, the general accuracy also decreases, as shown in Figure 5.22.

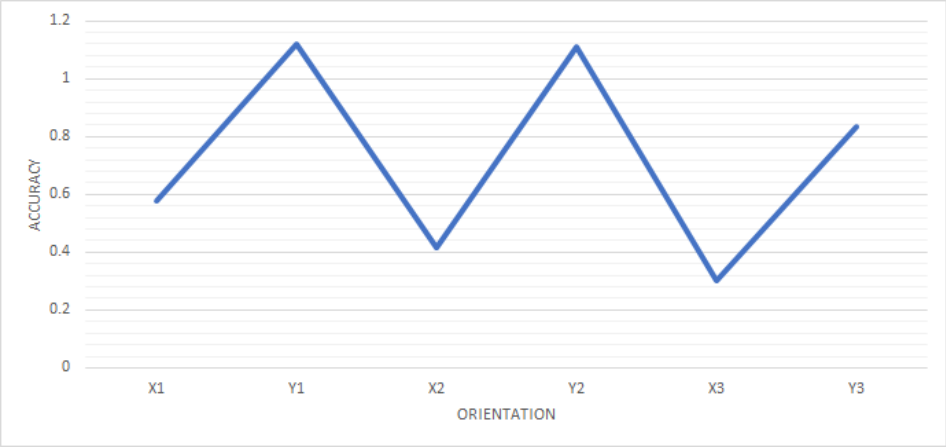

Figure 5.21: Load case 1 with the accuracy for all three sensors on X and Y direction. At accuracy equal to one, the measured and calculated values are the same.

Load Cases

In Figure 5.23, 5.25, 5.27 and 5.29 the top upper amplitude is shown for increasing increment in each load case. In all load cases the increases stiffness leads to increased displacements. Figure 5.22, 5.24, 5.26 and 5.28 shows the average accuracy relative to the measured values, where 1 means completely similar response. An representative excerpt of all five load cases are shown by LC2 in Appendix G.

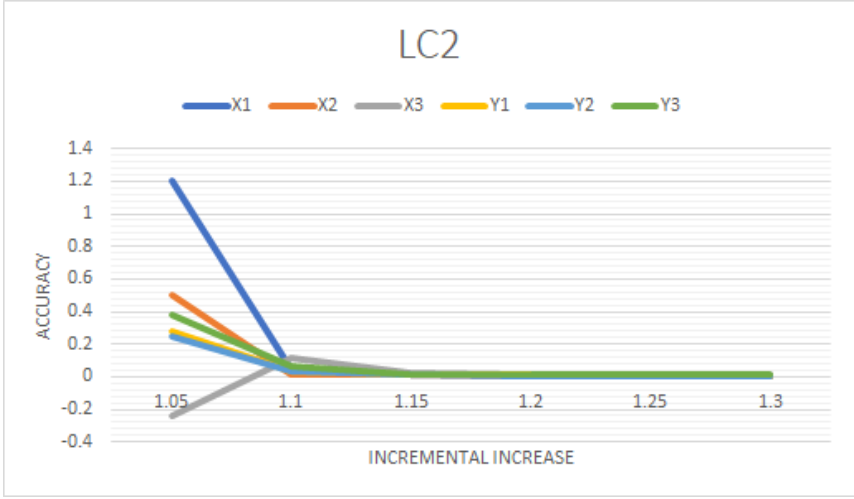

Figure 5.22: Load case 2: At accuracy equal to one, the measured and calculated values are the same

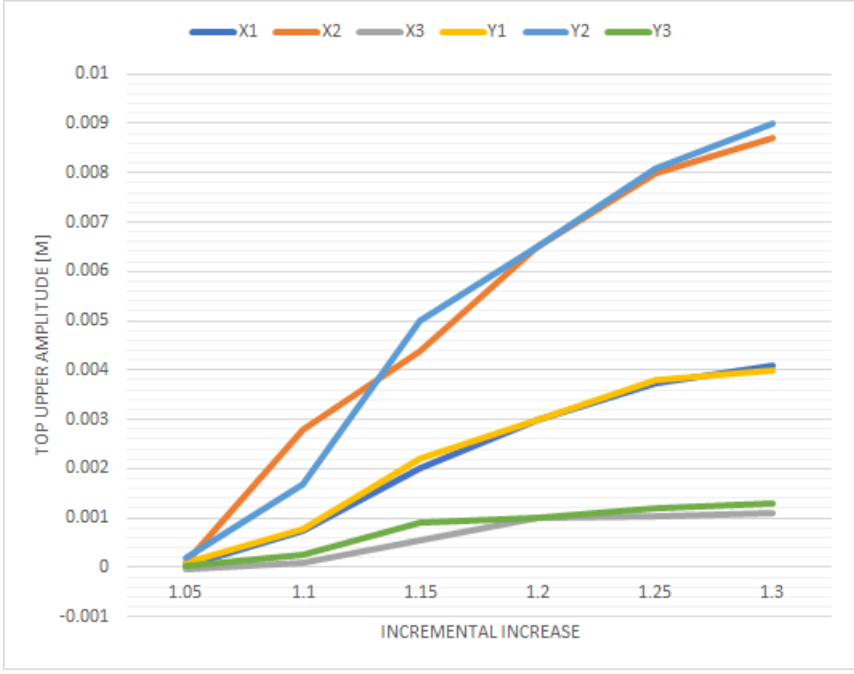

Figure 5.23: Load case 2

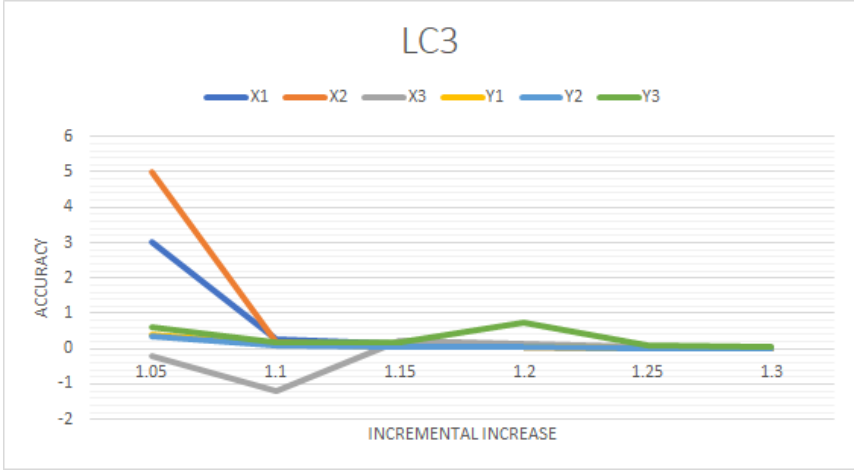

Figure 5.24: Load case 3: At accuracy equal to one, the measured and calculated values are the same

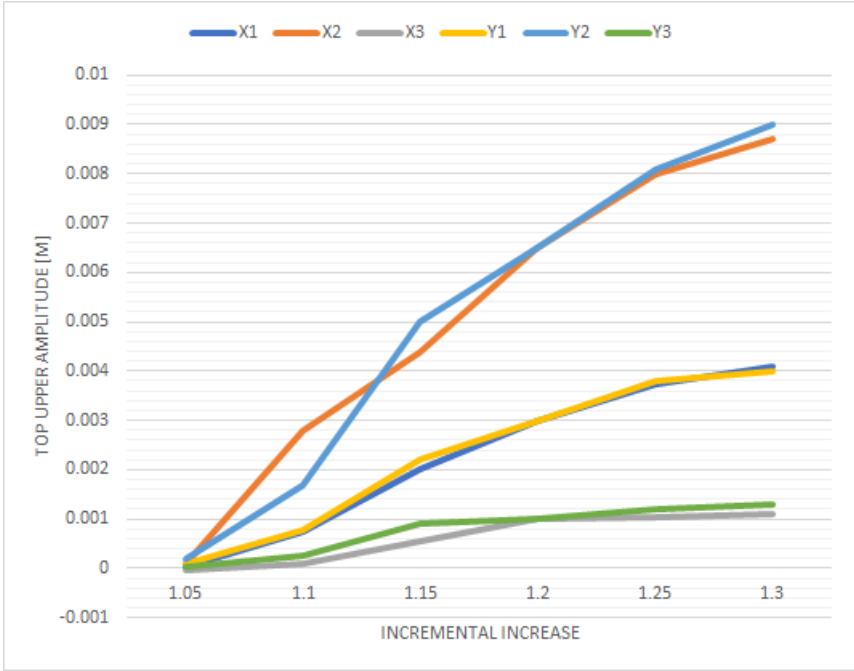

Figure 5.25: Load case 3

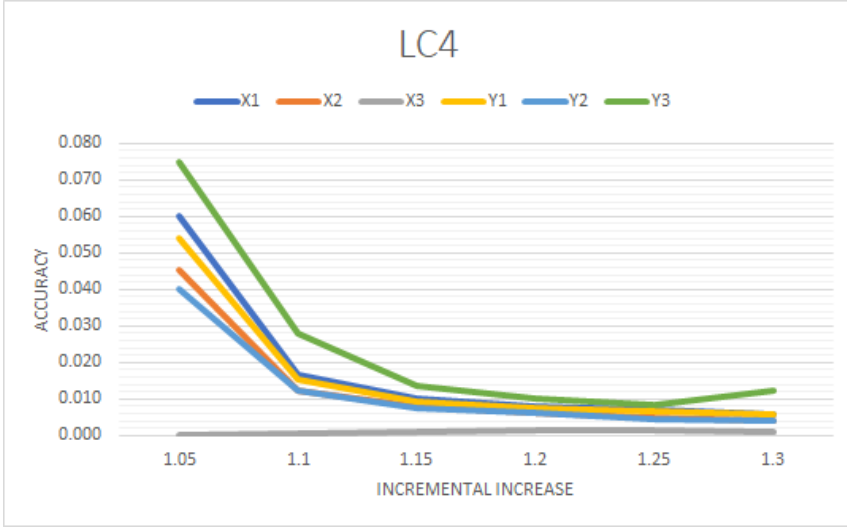

Figure 5.26: Load case 4: At accuracy equal to one, the measured and calculated values are the same

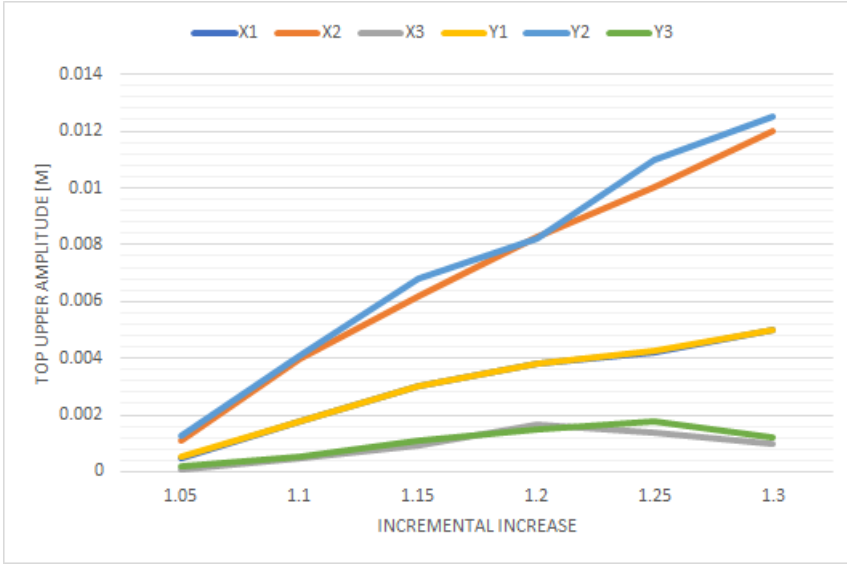

Figure 5.27: Load case 4

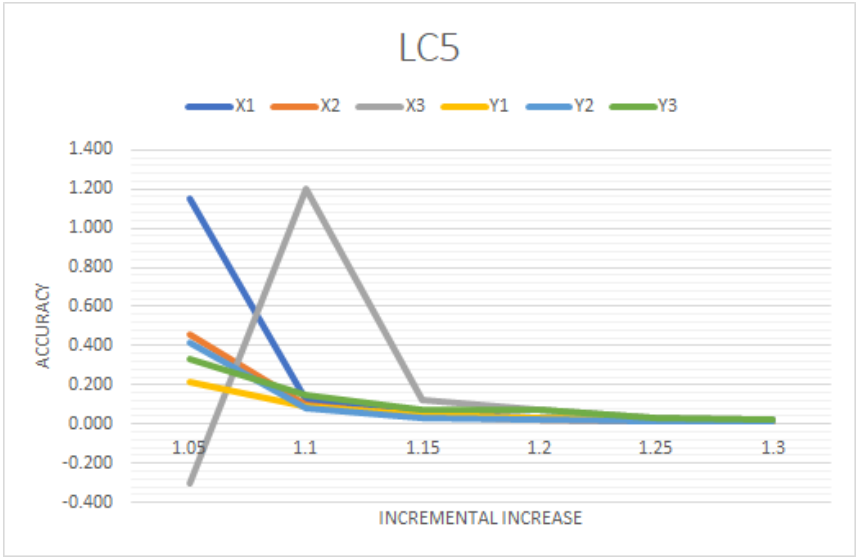

Figure 5.28: Load case 5: At accuracy equal to one, the measured and calculated values are the same

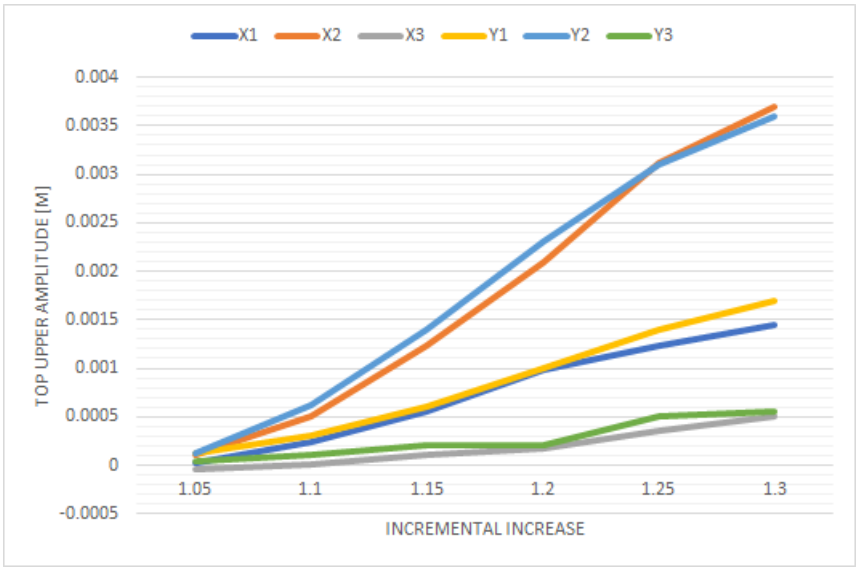

Figure 5.29: Load case 5

Sensitivity

Figure 5.30 shows the different load case sensitivity, where the largest bar represents the largest differential between measured and calculated values.

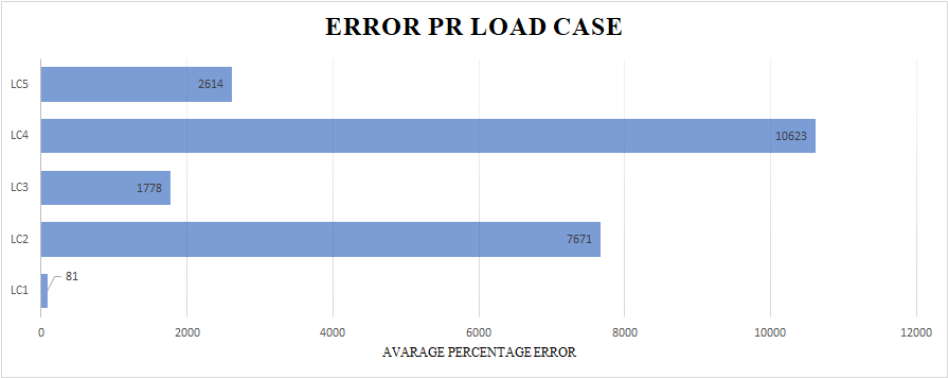

Figure 5.30: The relevant differences for each load case in average percentage

5.3.3 Rigid shaft

Having the bodies in MBS as rigid has effects on the response in the system. In the following section the results from rigid body modelling are shown. This is done with two sets of degrees of freedom, three and five DOF and with the same values as in Table 5.7. The responses in X and Y directions are shown in Figure 5.31, 5.32, 5.33 and 5.34.

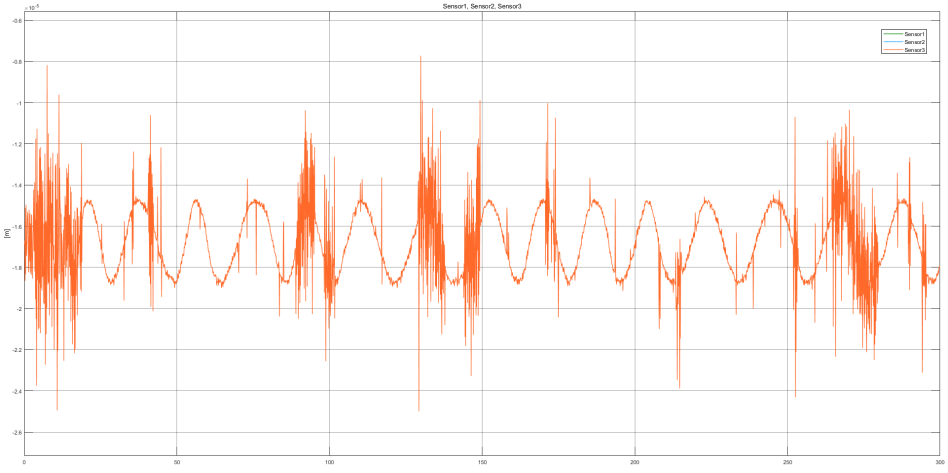

Figure 5.31: 3 DOF Rigid Shaft model response in X-direction

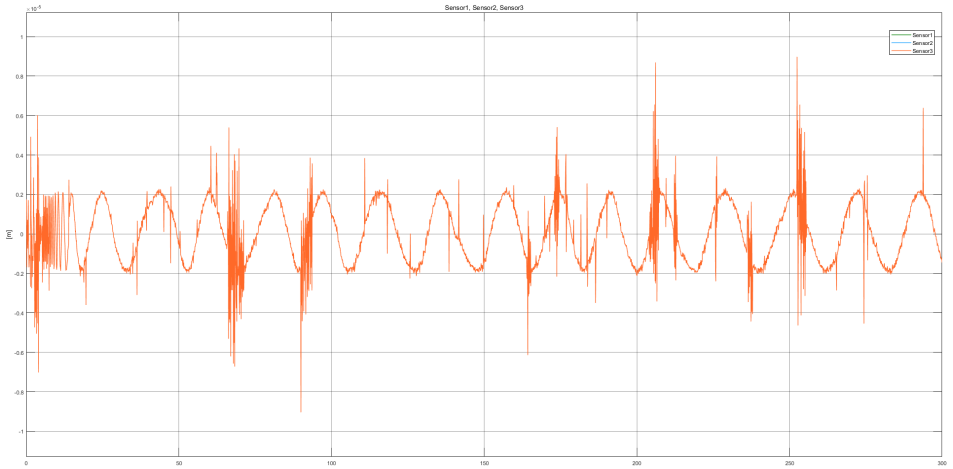

Figure 5.32: 3 DOF Rigid Shaft model response in Y-direction

Experimental Modelling

For the rigid body the response shows minimal change when altering the stiffness. For a 30% increase in stiffness as in load case 1, this resulted in a mere 50% increase in output, which is relatively low compared to the other experimental modelling tests. The model run at 1.30 incremental increase is shown in Appendix E. However, there is detected an increase, as in all the other experimental modelling approaches, when the stiffness is increased.

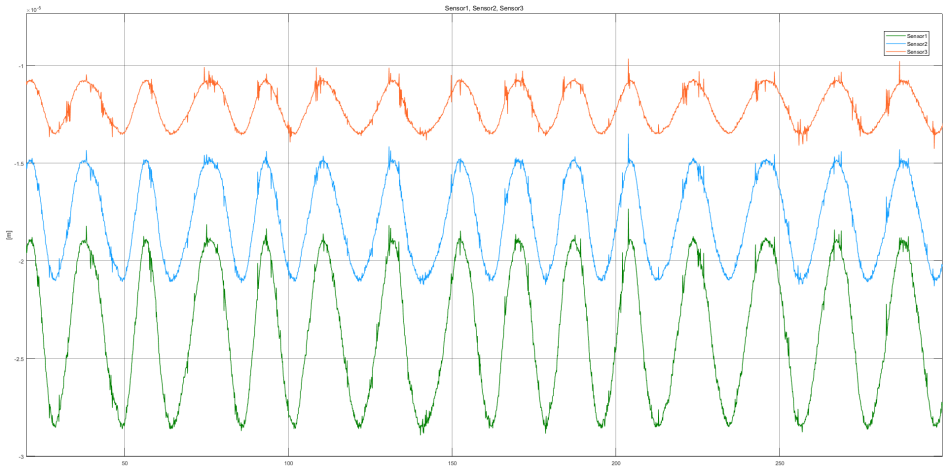

Figure 5.33: 5 DOF Rigid Shaft model response in X-direction

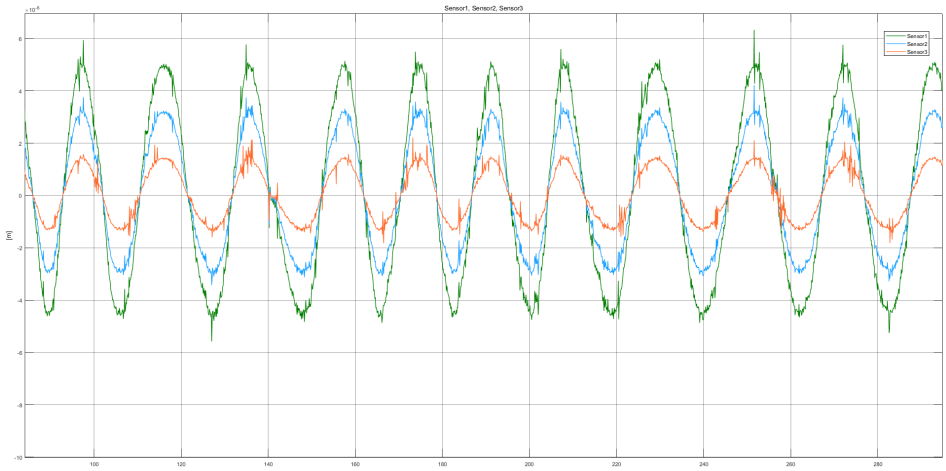

Figure 5.34: 5 DOF Rigid Shaft model response in Y- direction

5.4 Comparative Analysis

5.4.1 1 DOF Model Compared to 5 DOF Model

Figure 5.35 shows the average percentage error per direction in all three sensors for the two models 1 DOF and 5 DOF with flexible shaft. Since the rigid shaft model exhibit systemic errors, this model is discarded for further comparative analysis. This is discussed in Section 6.3.2.

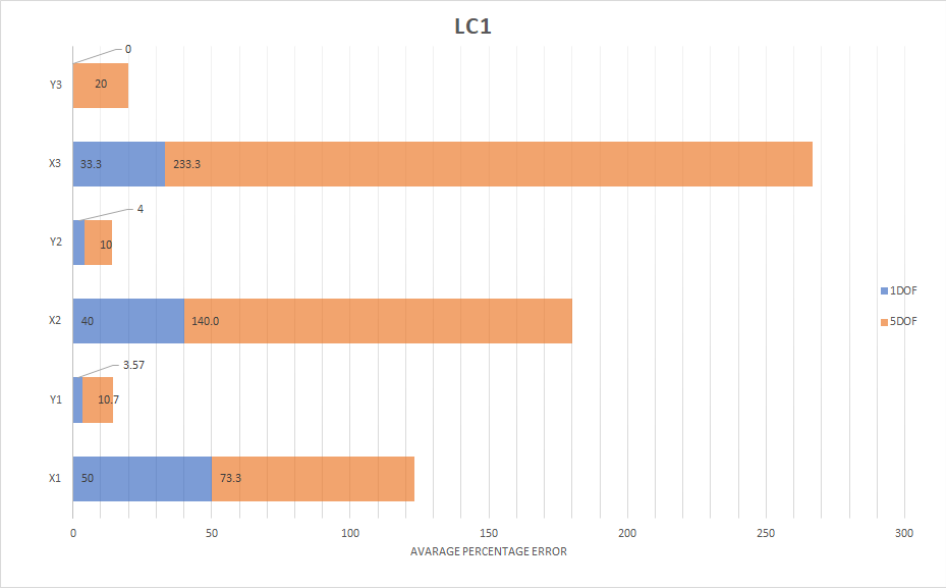

Figure 5.35: Load case 1 for 1 DOF and 5 DOF model

5.5 Force input - 5 DOF

For the force input vector Equation 3.19 was found and implemented. Firstly, the unknown parameters had to be discovered, shown in Section 5.5.1

5.5.1 Values from Monte Carlo method

After running the MATLAB Monte Carlo code for X and Y and for bearing 1 and 2, the following A and B amplitudes and phase values were found, shown in Table 5.9. By comparing the plotted values of the expressions in MATLAB for the EOM and the force response, they were with negligible fault and with as low error as demanded in the code (below 0.0001).

	A	B	Φ
X1	31.0351	8.3311	$\frac{\pi}{2}$
Y1	40.8048	3.4901	$\frac{\pi}{2}$
X2	13.4581	1.5472	$\frac{\pi}{2}$
Y2	22.1783	0.2491	$\frac{\pi}{2}$

Table 5.9: Values found from Monte Carlo process

5.5.2 Response

The response when the force input vector is implemented in the bearing force in SIMPACK, as it is the reaction force, it would be expected to see an accurate or at least similar response as the real life test rig drivetrain. However, the response proved to have a different behaviour in the SIMPACK model. Although it would rotate, it did not stand still, and would have rotation in α direction and also translational movement in vertical direction, yielding it to move out of the plane. A discussion regarding these unexpected results is found in Section 6.5.2.

Chapter 6

Discussion

6.1 Response Real Twin

6.1.1 Existing Faults

The response data shows that there are already existing faults in the model before the modal analysis is performed; shown in the FFT in Figure 5.7, and in orbit plots shown in Figure 5.8 through 5.10. Fault modelling should be done *after* making a digital fault free model that is the exact twin of the real model. Such as, it would be difficult to know the correct data for a the real model without faults. Nevertheless, it is rare that a model rig would be absolutely fault free.

As shown in Figure 5.7 there is one high peak, and two smaller ones in the FFT. These are at 1x-, 2x- and 3xrpm. It is discussed in Section 3.4 that these peaks could imply an unbalance, bent shaft and/or a misalignment in the drivetrain test rig, since the peaks coincides with these fault types shown in Figures 3.14, 3.12 and 3.9. To discover if the faulty condition due to misalignment is caused by parallel or angular misalignment, further investigation should be performed.

In this case it is evident that the experimental modelling is interesting, as this could say something of modelling of further faults through stiffness adjustments in the bearing force.

The orbit plots shows there could be a misalignment or bent shaft, as if there was no fault the center lines would have intersected in origo. None of them do, which shows an indication for fault. Also, the plots reveal a contamination of sorts in sensor 2 and 3. This contamination could be explained by the nature of the sensors, where there are some screws put in place to protect the sensors, and the shaft could be hitting them. Some metal powder found around the drivetrain test rig could be a result of this contact.

The model is faulty, and the stiffness are the same for both bearing 1 and 2 models this

well. This implies that *changing* the stiffness and creating a mismatch between the two bearings will increase the error in the model. The challenge however is not with the fault modelling that could be done with altering stiffness in bearing forces, but with finding the correct stiffness at all.

6.1.2 Root Mean Square

The RMS values are shown to be in the riskier zone boundary layer for sensor 2, as shown in Table 5.2. This could be due to the fact that this is the sensor that is the farthest away from both bearings, and will therefore have higher amplitudes in the displacements values. This is also shown for the response in Figures 5.1 through 5.6 and in Table 5.1. Therefore, sensor 2 is the most exposed for excessive vibration. Thus, it should be carefully observed for unhealthy vibration as it would be central to the shafts health monitoring. Consequently, the values in sensor 2 are critical to the design of the shaft in comparison to 1 and 3.

6.2 1 DOF Model

6.2.1 Response

The response from the 1 DOF model results in minimal error when compared to the measured values, both for X and Y direction. However, this is most apparent in the Y-direction. In order to eliminate the frequency difference (shown in Figure 5.12), faulty vector force inputs were used. Adding phase was also done. Still, the results turned out not to at be the same frequency. This could be the result of human error in the programming part or it could be due to some effects from the calculations and analysis done in advance. Additionally, the weight implied in the code is not necessarily correct. It has been stated from the lab coordinator that the weight could be assumed to be 16 kg, whilst the rotor rig manufacturer states the weight to be 14.3 kg; see Appendix F. These could all be sources of error.

6.2.2 Experimental Modelling

During the experimental modelling stiffness values are increased in X and Y direction (LC2/LC5), as shown in Figure 5.13.

LC2

For LC2 this led to a reduced output response value. This is the only run where an increase in stiffness has led to a decreased response. The stiffness increase leads to a more

rigid shaft that, with a stiffness with limitation to infinity, will be completely rigid. The values actually became more and more accurate when stiffness was increased, which can indicate that the modal analysis calculation were underestimating the stiffness values in X-direction and could, with advantage, be scaled up. This could have been a result of errors in the FFT where X has several high peaks, and perhaps the natural frequency in X-direction in reality is higher, and that the stiffness consequently should be higher.

LC5

For the case when stiffness is increased in Y-direction increasing displacement was observed. It is possible this increase is due to a resonance in the Y- direction.

6.2.3 Uncertainty

When modelling with only one degree of freedom, all other movements are disregarded. Thus, it is not possible to output sensor values at other locations which leads to a model with more uncertainty regarding holistic response and less feasibility towards a holistic high fidelity digital twin. In real life the shaft is not operating as a one DOF system and by modelling it as one it is possible that eigenmodes and natural frequencies from the system are disregarded. The response of the one DOF model was not predicted, however it could be a recommended approach for a lower fidelity model.

6.3 Flexible Shaft

The model utilized in the MBS software SIMPACK with flexible shaft body, results in a relatively similar output to the measured values from testing the drivetrain test rig. The Y-direction sensor values are more similar, due to the tuning that was mainly done with sensor values from Y-direction. Still, values in X- direction are close to the same accuracy, summarized in Figure 5.21. When comparing the values from this five DOF flexible shaft model to that from the one DOF model it shows that the one DOF model turns out to have even more accurate values. These results could be due to the added degrees of freedom in the five DOF model. Especially, having rotational freedom to move in α and β directions, and not measuring any displacements in these directions leads to a significant source of error. Not being able to calculate the stiffness and damping well in these directions interferes both with finding these values, but also the calculated values found from the modal analysis.

It is evident from the results that there is a superior sinusoidal movement. This is present in all the cases of flexible shaft modelling results, and this could be due to coupled effects where two sine waves are added into one response. It would be possible to superposition these sensor values, and extract only one DOF of data at the time, another argument for the coupled effects.

6.3.1 Bearing 1

When considering the different load cases in the experimental modelling for the flexible shaft model case, is is evident that the highest average error lies with LC2 and LC4. This is shown in Figure 5.30. In these cases, the stiffness is increased in the bearing 1, at the end of the shaft. This implies that an elevated sensitivity is present in the bearing furthest from the applied torque. This could be caused by an increased amplitude in displacements by a cumulative effect from the shaft beginning. Thus, it is recommended to carefully state the stiffness, with higher sensitivity with increased distance from the location where the force/torque is applied.

6.3.2 Y- direction

Additionally, for the load cases were the stiffness is increased in Y-direction the error is higher, both in increase in bearing 1 and 2, than the same situation for stiffness in x-direction. This is shown in Section 5.3.2 with associated figures, and also in Figure 5.30. It is therefore possible to say that the model is more sensitive to change in stiffness in Y -direction, and this will increase the displacements significantly. In the case for stiffness change in X-direction, LC2 and LC3 shows less error in the first incremental increase, which maintains an average value below LC4 and LC5. The model is less sensitive for change in stiffness in X- direction, but only for small incremental increase, meaning below 5% increase.

Furthermore, in the case of having a relatively high error for LC4 and LC5, this response could be due to a resonance component. This could be coupled effects coming from both α and β modes, which could not be calculated without obtaining data for these rotational values. Without these data, an iterative process to find the associated values could be performed to design for a more robust model.

6.3.3 Stiffness

Contrary to intuition, the calculated values were not applicable due to output differing from the measured values form the drivetrain test rig. Tuning was performed instead. As discussed, not having data and analysis of data in α and β rotational directions, there are effects that are not accounted for when doing the modal analysis and this could lead to an inaccurate performance when the simulation is run. Especially this could, and in this case it does, lead to inaccuracy at other rpm. Therefore, the tuning could work somewhat better. Tuning is dependent on convergence to see that the model behaviour is considerably reliant and robust, and the tuning starting point was the relation between stiffness and damping, however other model examples also was of influence. This is a significant source of error and in further work it would be of interest to implement sensors and obtaining data for all the directions that have freedom to move in the digital twin.

6.3.4 Uncertainty

For the flexible 5 DOF model, a lot of the uncertainty originates from coupled values and the amount of degrees of freedom. Whilst involving rotation across α and β, without measuring data in these direction it is challenging to achieve the correct values for stiffness and damping here. By performing an iterative process to tune the model instead, it is possible that effects are neglected, such as resonance. Additionally, it could have lead to a less robust model.

It is interesting to see that as the uncertainty increases with added incremental increase, the output also increases. The higher stiffness does in all cases lead to higher output. As discussed, it is reasonable to believe this is due to coupled and resonance effects.

6.4 Rigid shaft

When modelling a shaft in multi-body systems it is recommended to employ flexible bodies for the shaft segment, as discussed in Section 2.3.1 and Table 2.1. On the other hand, by utilizing a rigid model the computational time advantageously decreases, however the accuracy also decreases. Finding the balance between the two depends on the required model fidelity [112].

6.4.1 3 DOF

For the 3 DOF system, the response in all three sensors turns out to have the exact same response. Since the shaft is completely rigid, and there is zero DOF in all joints after the joint that the torque is applied, the rotation and induced in the first joint is identical for the rest of the connected shaft. The model response therefore confirms this, as shown in Figure 5.31 and 5.32.

It is interesting to see that the displacements in X-direction are negative, but following identical response pattern as in Y-direction. This could imply an underestimated value for the stiffness in the X- direction from the modal analysis. This is also shown for the one DOF model.

The jumps in response that the Figures 5.31 and 5.32 show could be coming from the control system it self's limitations. When tuned for a five DOF system, some error will be implied, and this could be the interference observed. However, results from damping value tuning and iterations shows this noise is resolved with higher damping values.

6.4.2 5 DOF

Y-direction

In the rigid shaft in Y- direction the output turns out in correct range of magnitude compared to the measured values. The response is shown in Figure 5.34. However, the sensor data collected from the digital twin seems to have an increasing value further down the shaft. Sensor 3, closest to the rotor, has the most displacement, and sensor 1, at the end of the shaft has the most. By employing a model with five DOF in the joint at the start of the shaft and having zero DOF in the following and attached joints will lead to less displacement closer to the joint with five DOF. As the displacement increases it could be due to a cumulative effect, and that the movement from sensor 3 spreads down the shaft. As the other joints have no degrees of freedom, the only response increased is the one from the joint where the torque is applied. This is the reason for the response pattern being similar for all three sensors. This result is most likely due to the shaft being rigid as well. Iterative and tuning processes shows that the order of the response amplitudes does not change by altering the stiffness, nor the damping values. The rigidity of the system will force the model to respond with these relative amplitudes regardless.

X-direction

In the X- direction the values oscillate around negative values, shown in Figure 5.33. This could indicate that the stiffness in X- direction is underestimated, as discussed earlier. In this case, the movements are also very much separated. This could be due to the fact that the damping in X direction in bearing 1 is set to be 33% of that in bearing 2, making the end of the shaft (closer to bearing 1 and sensor 1) have higher response values. When applying the same value of 33% in Y-direction in bearing 1 compared to bearing 2, the response values were altered for this direction. The values then follows a more separated path and in the same sensor 1, 2 and 3 order as shown in the response in X direction. The response is shown in Appendix E in Figure E.2. Based on this, it is arguable that the damping values lead to this behaviour.

Fault Modelling

To be able to model faults and to perform fault detection, the input values should be able to alter not only the magnitude of the amplitude, but also their relative behavior. When this is not possible, it is difficult to utilize the rigid shaft model for a digital twin, even with a five DOF solution.

6.4.3 Uncertainty

By nature the rigid shaft model has several deflection effects that are neglected. The shaft is too thin compared to its length to be modelled correctly as a rigid shaft. This is shown by the recommendations as discussed, and by the evident errors in the resulting data in the calculated model compared to the measured values.

The resulting response in the rigid shaft in both three and five DOF is not viable for further use as this approach has the largest error in this thesis, both in value and in behaviour. Having all the sensor values to be the same regardless of position makes the model behaviour incorrectly mapped in the three DOF model.

In the five DOF model no further comparative analysis is performed due to the systematic error. Although the error in magnitudes is relatively low when experimental modelling is performed, the systemic errors lead to a consequent uncertainty in both the three and five DOF model, making the rigid shaft model an unfeasible digital twin solution.

6.5 Fault Modelling

6.5.1 Stiffness modification

By only changing the stiffness to model faults, it is shown from the sensitivity analysis that this would not only increase the error of response, not model the existing faults. The model is run at misalignment and unbalance as Figure 5.7 shows. Thus, the fault is captured well in LC1 with K1=K2. Consequently, this fault modelling approach will in this case only lead to added error, not the desired fault modelling. Still, since the model was tuned and calculated based on a faulty model, it is here shown that the fault modelling could also be done with same magnitude stiffness. Additionally, the challenge of this model could be said to be more so with finding the stiffness values that will model the drivetrain test rig as well as possible, than with stiffness modification as fault modelling.

6.5.2 Force Vector Input - 5 DOF

The parameters found through Monte Carlo method proved to give close to identical response when plotted to the EOM. However, when implemented in the five DOF model in SIMPACK, it resulted in a response that first of all had large displacements and rotations in horizontal and vertical direction as well as in α ans β directions. These results implies an inconsistency between the found parameters and what is feasible in the SIMPACK model. This could be because of several sources of error. First of all, the mass in SIMPACK is significantly lower than what is in the real life model and in the code that solves Equation 4.3. Secondly, Equation 4.3 is built on a one DOF model, so in the five DOF model there are values unaccounted for. However, the same values used implemented in

the flexible shaft five DOF model was used in these directions. Thirdly, it is reasonable to say that the mass used in the code and the mass in the SIMPACK model has significant effects as to why this modelling scheme has issues.

Nevertheless, the force vector input has a potential whereas digital twin goes. It is easy to implement the file input in SIMPACK as a dynamic uploaded array pre-processed from the real system. The angular velocity is also easily implemented as a dynamic input in the MATLAB/Simulink model and in the file input force vector. Also, this method allows modal analysis steps to be skipped, which again could allow less computational time.

Monte Carlo method

The Monte Carlo method found several working A's and B's to be implemented, and the resulting plotting of these were almost identical to the EOM. However, there was some phase difference present. This was adjusted for with a phase addition in the expression for the force vector. The A found could then be on the form $\frac{A}{\omega^2} = me$ which would relate the A to the angular velocity. For B, there is no inverse method for finding this with regard to ω. This would be of interest to research inverse methods to find B and its relation to ω.

6.6 Inverse method

By employing SIMPACK for use of inverse method, and to calculate response and performance, it depends on fundamental knowledge of the software. Unless it easily becomes a black box problem. Having extensive knowledge, down to source code level should be present, since user experience with SIMPACK shows reoccurring errors. By experience, there are segments of the software that stores a certain memory, making past fixed error corrupting the response when altered back to working values. This can lead to unintended following errors and increase the overall uncertainties in the modelling. Other software should be considered for validation.

It is also shown that having an input function in the bearing force as the bearings response is a theoretically potential scheme for a digital twin in real-time, dynamic and online modelling. The sensors collects reference displacement values, and for a conversion to happen from reference values to the SIMPACK model an inverse method for finding the input function vector could be implemented. However, the input function could be found through other inverse methods than a stochastic process.

6.7 Methodology

The methodology in question revolves around the modal analysis validity. By collecting values from three sensors, it is possible to attain a sufficient model for one DOF. However,

some issues are raised when a five DOF system is employed. An added number of sensors could fix this issue.

Additionally, by performing the hammer tests, every test showed different values. The average values were used, thus it is evident that the uncertainty of the analysis will decrease by increasing numbers of tests performed.

In the approach there are three sensors that are placed at different locations than where their data are being used as a base of input information. The issue of sensor placement is of interest in most shaft designs, and here it would also be of interest to see the effect a placement of the sensor at the same location as the bearings would aid in accomplishing higher accuracy in the calculated values. A vulnerability map could be performed to know this better. Nevertheless, this model is quite simple and for the purpose of this thesis a method validation is of a prioritized concern and importance.

6.7.1 Flexible Multibody System Dynamics

By employing the discussed approach with floating number coordinate reference frame, it could be argued that the simple modal approach is sufficient. However, for other approaches for flexible modelling, utilization of a more intricate geometry with detailed loads and orientations could result in an increase in accuracy.

6.8 Mass

The mass employed in the modal analysis is the one stated from the lab coordinator, however different from the manufacturer statement. Nevertheless, it will not attain the same values in the model used in the digital twin. This is not an issue in one DOF, when only programming is used to calculate response of the digital twin. However though, for the five DOF model the mass is a problematic parameter to implement well. For further work, the model itself should be changed to have the completely accurate geometrical shape with all details included that do not affect the rotational motion. By doing so it would become easier to achieve closer to identical mass properties as what is present in the real life twin. It would increase the inaccuracy in the model if only increasing the density to achieve the same mass, one should also add volumes to simulate completely similarly.

As discussed, by modelling the mass well in the MBS simulation, the errors in force vector input approach also possibly could be avoided. The inaccurate mass employed in the five DOF model, leads to an issue with the values from the modal analysis, as they will lose their validity. Thus, either doing the modal analysis with wrong mass or increasing the volumes in the digital twin will solve this issue. Nevertheless, doing the modal analysis with the wrong mass would lead to less accurate output. Consequently, it is advisable to consider the model geometry.

Chapter 7

Conclusion

7.1 Concluding remarks

The offshore wind turbine market is growing and many of the maintenance and downtime issues lie in the gearbox, specifically in the bearings. Gearbox sensitivity concerns combined with complex, remote and weather dependent wind turbines, rise a maintenance challenge and potentially significantly elevated O&M costs. Modelling a digital twin of the drivetrain in a MBS software, could be the solution to the challenge and should be investigated further. However, new issues are introduced and needs to be completely addressed by the digital twin model.

For the modelled digital twin of a drivetrain test rig a few concluding remarks are evident. For the one DOF model the results are satisfying, whilst for the five DOF the increased fidelity lead to less accurate simulations. Thus, the increased fidelity leads to decrease in accuracy in this case. For the five DOF models, the flexible shaft model had the least errors, and the stiffness values that led to the best results were the ones from tuning. It has been argued that coupled effects could be part of the reason for this. When the data for α and γ is not collected, there is a hole in the information as to what is modelled. Still, the five DOF model with flexible shaft is close to measured values, especially in Y-direction. Errors in X- direction consequently for all models applied is argued to be related to an error in the modal analysis underestimation of stiffness, coupled effects or resonance, or a combination of these.

Fault modelling could either be done with stiffness change in the bearings or by a force vector input in the bearings. However, in this thesis both proved seems to be inadequate, where stiffness change increased errors and force vector input was unfeasible in the SIMPACK model when the mass was wrongly simulated. Nevertheless, if this issue could be fixed then the force vector input has bigger potential regarding dynamic online modelling, and to become a true digital twin.

7.2 Recommendations for Further Work

For further use of the drivetrain, an implementation of it into a holistic digital twin of the entire wind turbine would be of interest. Additionally, a degradation model should be actualized to consider life expectation sensitives.

While performing the hammer test and gathering data about the decay of the system, an increased number of tests would increase the validity of the modal analysis. A convergence study over several tests could increase the validity and certainty of the analysis.

The mass in the model is given to be about 14.3 kg, however this is not easily implemented in the multi body simulation model due to the simplicity of this kind of modelling. For instance, the bearings are only modelled as force elements, not as a body. By doing so, less of the actual drivetrain is modelled as body and decreasing the mass. It would be useful to either model the mass or model the bearings as bodies as well. It would be helpful to model the mass precisely for fault modelling with use of a force input vector. Then the response from the digital twin could be reliable, stable and with increased accuracy with regards to the real drivetrain test rig response.

By using the SIMPACK model as the inverse and predictive modelling method, it would be interesting to compare the different inverse methods to consider the potency of each approach. Additionally, this could help to disclose SIMPACK flaws and examine its validity.

7.2.1 Stiffness

It was challenges present regarding finding the stiffness that yielded the correct output, and tuning instead of the calculated values for rotational stiffness was used instead. For further work a validation should be done with a more detailed approach like a FEM analysis, experimental data modelling or by other software [106].

Further studies around the values and sensitivity for rotational stiffness in α and β rotational directions should also be performed. By doing so it could be possible to understand the model better without the actual installment of added sensors, or even better, by doing both. Combining this with coupled sensitivities a deep understanding of the stiffness and their effects would be realized.

7.2.2 Sensor data

Issues have been identified concerning the validity of the model with a sensor system of only two DOF analyzing the system. The virtual modelling is done with five DOF, accordingly there is no data for three of the five degrees of freedom utilized. It is evident that this results in deviation in the modal analysis. It would be of interest to develop the model further and implement an increased number of sensors of further tests to consider

it in all five DOF.

7.2.3 Fault modelling and Online Fault Detection

While modeling faults using stiffness alterations could be done, in the approach presented here only a static, offline concept is considered. However, this could be done dynamically and online. By employing sensor data transfers in real time the digital twin will be a dynamic and online model. Nevertheless, the stiffness should be a dynamic parameter in such a case. Therefore, a machine learning approach could be implemented. By doing so the autonomy and connectivity parts are covered as discussed in Section 2.2.2. This algorithm learns by experience with educated assumptions and calculations and will be able to resolve the issue of dynamic and real time digital twin modelling. SIMPACK could be used for real-time data transfers, and perhaps a combination with co-simulation through MATLAB could attain the machine learning function [129]. On the other hand, this would have to a work conducted in cooperation with SIMPACK, because presently the stiffness input in FE43 force component is done manually.

Another approach to perform real time data exchange and online analysis could be done is through input files in SIMPACK and MATLAB/Simulink. For the force vector input approach, the force in the bearings are made as inputs from files. These could automatically be transferred and updated in the input function directory in SIMPACK. Which would in turn be a seamless digital twin online model. As for MATLAB/Simulink, the rotational speed easily could be made to an dynamic input variable that can control the system dynamically. This approach seems easier and more feasible to implement in the nearby future and would be recommended to be pursued.

References

[1] BP P.L.C. Bp statistical review of world energy. Technical report, BP, 2016.

[2] Eurostat. Primary production of energy from renewable sources.

[3] Inc. Encyclopædia Britannica. Wind turbine technology.

[4] Martin O.L. Hansen. *Aerodynamics of Wind Turbines*. Earthscan, London, United Kingdom, 2008.

[5] Global Wind Energy Council (GWEA). Global wind report- annual market update. Technical report, GWEA, 2015.

[6] Douglas Westwood. World offshore wind market forecast 2017-2026. Technical report, Douglas Westwood, 2017.

[7] United Nations. Paris agreement.

[8] Marcel Wiggert and Gerrit Wolken-Möhlmann. Weather window statistics for the operation and installation of offshore wind farms. Technical report, Fraunhofer Institute for Wind Energy and Energy System Technology, 2016.

[9] D Milborrow. Operation and maintenance costs compared and revealed. *Windstats Newsletter*, 19:1–3, 2006.

[10] W Vachon. Long-term o&m costs of wind turbines based on failure rates and repair costs. In *Proceedings WINDPOWER, American Wind Energy Association annual conference, Portland, OR*, pages 2–5, 2002.

[11] A. Matveevb R. Nilssena Z. Zhanga, A. Chenb and A. Nysveena. High-power generators for offshore wind turbines. *Energy Procedia*, 35(1):52–61, 2013.

[12] Peter Tavner, S. Faulstich, B. Hahn, and G J W van Bussel. Reliability and availability of wind turbine electrical and electronic components. *EPE Journal*, 20(4):45–50, 2010.

[13] B Hahn, M Durstewitz, and K Rohrig. Reliability of wind turbines—experience of 15 years with 1,500 wts, wind energy. In *Proc. Euromech Colloquium, Springer, Berlin*, 2007.

[14] LKSH-Landwirtschaftskammer Schleswig-Holstein. Windenergie xx praxisergebnisse 2007, 2008.

[15] J. Ribrant and L. M. Bertling. Survey of failures in wind power systems with focus on swedish wind power plants during 1997 ndash;2005. *IEEE Transactions on Energy Conversion*, 22(1):167–173, March 2007.

[16] Peter Tavner. *Offshore Wind Turbines: Reliability, availability and maintenance*. IET Digital Library, United Kingdom, 2012.

[17] PM Ku. Gear failure modes—importance of lubrication and mechanics. *ASLe Transactions*, 19(3):239–249, 1976.

[18] Shuangwen Sheng, H Link, W LaCava, J Van Dam, B McNiff, P Veers, J Keller, S Butterfield, and Francisco Oyague. Wind turbine drivetrain condition monitoring during grc phase 1 and phase 2 testing. Technical report, National Renewable Energy Laboratory (NREL), Golden, CO., 2011.

[19] Wenxian Yang. Condition Monitoring the Drive Train of a Direct Drive Permanent Magnet Wind Turbine Using Generator Electrical Signals. *J. Sol. Energy Eng*, 136(2):021008–1–8, 2013.

[20] W. Yang. *Offshore Wind Farms - Chapter 18 Condition monitoring of offshore wind turbines*. Woodhead Publishing, United Kingdom, 2016.

[21] Y. Feng, P.J. Tavner, and H. Long. Early experiences with UK Round 1 offshore wind farms. *Proceedings of the Institution of Civil Engineers : energy*, 163(4):167–181, 2010.

[22] R. Isermann and P. Ballé. Trends in the application of model-based fault detection and diagnosis of technical processes. *Control Engineering Practice*, 5(5):709 – 719, 1997.

[23] Liliane Pintelon and Alejandro Parodi-Herz. *Maintenance: An Evolutionary Perspective*, pages 21–48. Springer London, London, 2008.

[24] Unknown. Managing the wind: Reducing kilowatt-hour costs with condition monitoring. *Refocus*, 6(3):48 – 51, 2005.

[25] Kjetil Uhlen Karl Merz Olimpo Anaya-Lara, John Olav Tande. *Offshore Wind Energy Technology*. Wiley, 2016.

[26] Yisha Xiang, C. Richard Cassady, and Edward A. Pohl. Optimal maintenance policies for systems subject to a markovian operating environment. *Computers & Industrial Engineering*, 62(1):190 – 197, 2012.

[27] Fausto Pedro García Márquez, Andrew Mark Tobias, Jesús María Pinar Pérez, and Mayorkinos Papaelias. Condition monitoring of wind turbines: Techniques and methods. *Renewable Energy*, 46(Supplement C):169 – 178, 2012.

[28] Teruo IGARASHI and Shiroji YABE. Studies on the vibration and sound of defective rolling bearings : Second report : Sound of ball bearings with one defect. *Bulletin of JSME*, 26(220):1791–1798, 1983.

[29] DNV-GL. Certification of condition monitoring. *No. DNVGL-SE-0439*, 2016.

[30] J. Nilsson and L. Bertling. Maintenance management of wind power systems using condition monitoring systems mdash;life cycle cost analysis for two case studies. *IEEE Transactions on Energy Conversion*, 22(1):223–229, March 2007.

[31] Sachin Sharma and Dalgobind Mahto. Condition Monitoring of Wind Turbines: A Review. *Global Journal of Researches in Engineering, Mechanical and Mechanics Engineering*, 13(6):17–33, 2013.

[32] Amir Rasekhi Nejad, Zhen Gao, and Torgeir Moan. Fatigue reliability-based inspection and maintenance planning of gearbox components in wind turbine drivetrains. *Energy Procedia*, 53(Supplement C):248 – 257, 2014. EERA DeepWind' 2014, 11th Deep Sea Offshore Wind R&D Conference.

[33] Amir R. Nejad and Torgeir Moan. On model-based system approach for health monitoring of drivetrains in floating wind turbines. *Procedia Engineering*, 199(Supplement C):2202 – 2207, 2017. X International Conference on Structural Dynamics, EURODYN 2017.

[34] T.W. Verbruggen. Wind turbine operation and maintenance based on condition monitoring. Technical report, ECN-C–03–047, 04 2003.

[35] International Organization for Standardization. Condition monitoring and diagnostics of machines – vibration condition monitoring – part 1: General procedures. Standard, International Organization for Standardization, Geneva, CH, February 2002.

[36] International Organization for Standardization. Mechanical vibration - evaluation of machine vibration by measurements on non-rotating parts. part 21: Horizontal axis wind turbines with gearbox. Standard, International Organization for Standardization, Geneva, CH, May 2015.

[37] W.Y. Liu, W.H. Zhang, J.G. Han, and G.F. Wang. A new wind turbine fault diagnosis method based on the local mean decomposition. *Renewable Energy*, 48(Supplement C):411 – 415, 2012.

[38] Zhipeng Feng, Ming Liang, Yi Zhang, and Shumin Hou. Fault diagnosis for wind turbine planetary gearboxes via demodulation analysis based on ensemble empirical mode decomposition and energy separation. *Renewable Energy*, 47(Supplement C):112 – 126, 2012.

[39] Qiang Miao, Lin Cong, and Michael Pecht. Identification of multiple characteristic components with high accuracy and resolution using the zoom interpolated discrete fourier transform. *Measurement science and technology*, 22(5):055701, 2011.

[40] Pratesh Jayaswal and B Agrawal. New trends in wind turbine condition monitoring system. *J Emerg Trends Eng Dev*, 3:133–148, 2011.

[41] S Abdusslam, Mahmud Ahmed, Parno Raharjo, Fengshou Gu, and AD Ball. Time encoded signal processing and recognition of incipient bearing faults. In *Automation and Computing (ICAC), 2011 17th International Conference on*, pages 289–293. IEEE, 2011.

[42] Fardin Dalvand, Asadollah Kalantar, Shoresh Shokoohi, and Hassan Bevrani. Time-domain bearing condition monitoring in induction motors using instantaneous frequency of motor voltage. In *Smart Grid Conference (SGC), 2014*, pages 1–7. IEEE, 2014.

[43] M. Elforjani and D. Mba. Natural mechanical degradation measurements in slow speed bearings. *Engineering Failure Analysis*, 16(1):521 – 532, 2009.

[44] M.J. Ghazali, N.I.I. Mansor, M.Z. Nuawi, and J.A. Ghani. Facile wear failure monitoring of commercial bearing alloys using i-kaz method. *Engineering Failure Analysis*, 35(Supplement C):545 – 553, 2013. Special issue on ICEFA V- Part 1.

[45] B.C. Nakra N. Tandon. Vibration and acoustic monitoring techniques for the detection of defects in rolling element bearings – a review. *Shock and Vibration Digest*, 24(3):3–11, 1992.

[46] N. Tandon, G.S. Yadava, and K.M. Ramakrishna. A comparison of some condition monitoring techniques for the detection of defect in induction motor ball bearings. *Mechanical Systems and Signal Processing*, 21(1):244 – 256, 2007.

[47] K Nienhaus, FD Boos, K Garate, and R Baltes. Development of acoustic emission (ae) based defect parameters for slow rotating roller bearings. In *Journal of Physics: Conference Series*, volume 364, page 012034. IOP Publishing, 2012.

[48] Z. Hameed, Y.S. Hong, Y.M. Cho, S.H. Ahn, and C.K. Song. Condition monitoring and fault detection of wind turbines and related algorithms: A review. *Renewable and Sustainable Energy Reviews*, 13(1):1 – 39, 2009.

[49] Zhen Gao Torgeir Moan Amir Rasekhi Nejad, Peter Fogh Odgaard. A prognostic method for fault detection in wind turbine drivetrains. *Engineering Failure Analysis*, 42(1):324–336, 2014.

[50] Katharina Fischer Diego Coronado. Condition monitoring of wind turbines: State of the art, user experience and recommendations. Technical report, Fraunhofer Institute for Wind Energy and Energy System Technology IWES Northwest, 01 2015.

[51] Christopher J. Crabtree Michael Wilkinson Wenxian Yang, Peter J. Tavner. Cost-Effective Condition Monitoring for Wind Turbines. *IEEE Transactions on Industrial Electronics*, 57(1):263–271, 2010.

[52] Amir Rasekhi Nejad, Erin E. Bachynski, Marit I. Kvittem, Chenyu Luan, Zhen Gao, and Torgeir Moan. Stochastic dynamic load effect and fatigue damage analysis of drivetrains in land-based and tlp, spar and semi-submersible floating wind turbines. *Marine Structures*, 42(Supplement C):137 – 153, 2015.

[53] Rolf Isermann. Model-based fault detection and diagnosis - status and applications. Technical report, Institute of Automatic Control, Darmstadt University of Technology, 2004.

[54] Ranganath Kothamasu, Samuel Huang, and William VerDuin. System health monitoring and prognostics — a review of current paradigms and practices. *The International Journal of Advanced Manufacturing Technology*, 28(9):1012–1024, July 2006.

[55] RV BEARD. Failure accommodation in linear systems through self-reorganization(self-reorganization methods for complex linear dynamic systems to compensate for component failures). 1971.

[56] R.J. Patton and J. Chen. Observer-based fault detection and isolation: Robustness and applications. *Control Engineering Practice*, 5(5):671 – 682, 1997.

[57] David Luenberger. Observers for multivariable systems. *IEEE Transactions on Automatic Control*, 11(2):190–197, 1966.

[58] Rajamani Doraiswami, Chris Diduch, and Maryhelen Stevenson. Kalman filter. In *Identification of Physical Systems*, pages 231–288. John Wiley and Sons, Ltd, Chichester, UK, March 2014.

[59] M Kitamura. Detection of sensor failures in nuclear plants using analytic redundancy. Technical report, Oak Ridge National Lab., TN (USA), 1980.

[60] Ron J Patton and Jie Chen. Review of parity space approaches to fault diagnosis for aerospace systems. *Journal of Guidance, Control, and Dynamics*, 17(2):278–285, 1994.

[61] Silvio Simani. Model-based fault diagnosis in dynamic systems using identification techniques, 2003.

[62] Benjamin Schleich, Nabil Anwer, Luc Mathieu, and Sandro Wartzack. Shaping the digital twin for design and production engineering. *CIRP Annals*, 66(1):141 – 144, 2017.

[63] F.-L. Krause, F. Kimura, T. Kjellberg, S.C.-Y. Lu, van der Wolf, L. Alting, H.A. ElMaraghy, W. Eversheim, K. Iwata, N.P. Suh, V.A. Tipnis, M. Week, and A.C.H. Product modelling. *CIRP Annals*, 42(2):695 – 706, 1993.

[64] Virgilio Quintana, Louis Rivest, Robert Pellerin, Frédérick Venne, and Fawzi Kheddouci. Will model-based definition replace engineering drawings throughout the product lifecycle? a global perspective from aerospace industry. *Computers in Industry*, 61(5):497 – 508, 2010.

[65] S.C.-Y. Lu, D. Li, J. Cheng, and C.L. Wu. A model fusion approach to support negotiations during complex engineering system design. *CIRP Annals*, 46(1):89 – 92, 1997.

[66] Stefan Boschert and Roland Rosen. *Digital Twin—The Simulation Aspect*, pages 59–74. Springer International Publishing, Cham, 2016.

[67] R. Roy, R. Stark, K. Tracht, S. Takata, and M. Mori. Continuous maintenance and the future – foundations and technological challenges. *CIRP Annals*, 65(2):667 – 688, 2016.

[68] Edward Glaessgen and David Stargel. The digital twin paradigm for future nasa and u.s. air force vehicles. Technical report, National Aeronautics and Space Administration, 2012.

[69] Michael Grieves. Digital twin: Manufacturing excellence through virtual factory replication. *White paper*, 2014.

[70] F. Tao and M. Zhang. Digital twin shop-floor: A new shop-floor paradigm towards smart manufacturing. *IEEE Access*, 5:20418–20427, 2017.

[71] Roland Rosen, Georg von Wichert, George Lo, and Kurt D. Bettenhausen. About the importance of autonomy and digital twins for the future of manufacturing. *IFAC-PapersOnLine*, 48(3):567 – 572, 2015. 15th IFAC Symposium onInformation Control Problems inManufacturing.

[72] Oracle. Digital twins for iot applications - a comprehensive approach to implementing iot digital twins. White paper, Oracle, January 2017.

[73] Feng Xia, Laurence T Yang, Lizhe Wang, and Alexey Vinel. Internet of things. *International Journal of Communication Systems*, 25(9):1101, 2012.

[74] Asle Heide Vaskinn Jon Tøndevoldshagen Daniel Zwick, Tomáš Mánik. Technology for a real-time simulation-based system monitoring of wind turbines. *EERA DeepWind Conference 2017*, 2017.

[75] GE General Electric. The digital twin - compressing time-to-value for digital industrial companies. White paper, General Electric, GE, January 2017.

[76] Peter C. Evans and Marco Annunziata. Industrial internet - pushing the boundaries of mind and machines. White paper, General Electric, GE, November 2012.

[77] Henning Kagermann, Johannes Helbig, Ariane Hellinger, and Wolfgang Wahlster. *Recommendations for implementing the strategic initiative INDUSTRIE 4.0: Securing the future of German manufacturing industry; final report of the Industrie 4.0 Working Group*. Forschungsunion, 2013.

[78] Henning Kagermann. Change through digitization—value creation in the age of industry 4.0. In *Management of permanent change*, pages 23–45. Springer, 2015.

[79] M. Hermann, T. Pentek, and B. Otto. Design principles for industrie 4.0 scenarios. In *2016 49th Hawaii International Conference on System Sciences (HICSS)*, pages 3928–3937, Jan 2016.

[80] B Inozu, PG Schaedel, P Roy, and V Molinari. Sharing ships' reliability availability maintainability (ram) information to improve cost effectiveness and safety. *Advances in safety and reliability. Oxford: Pergamon*, pages 1039–46, 1997.

[81] Joo Hock Ang, Cindy Goh, Alfredo Alan Flores Saldivar, and Yun Li. Energy-efficient through-life smart design, manufacturing and operation of ships in an industry 4.0 environment. *Energies*, 10(5):610, 2017.

[82] Machine learning: How will it integrate into the shipping industry? `https://www.morethanshipping.com/machine-learning-will-integrate-shipping-industry/`. Accessed: 2017-10-12.

[83] Ryszard S. Carbonell, Jaime G.and Michalski and Tom M. Mitchell. *An Overview of Machine Learning*, pages 3–23. Springer Berlin Heidelberg, Berlin, Heidelberg, 1983.

[84] Statoil ASA. Putting on digital bionic boots.

[85] Possible uses of virtual singapore by the national research foundation. `https://www.nrf.gov.sg/programmes/virtual-singapore/possible-uses-of-virtual-singapore`. Accessed: 2017-13-12.

[86] Nabil Anwer, Alex Ballu, and Luc Mathieu. The skin model, a comprehensive geometric model for engineering design. *CIRP Annals*, 62(1):143 – 146, 2013.

[87] Benjamin Schleich, Nabil Anwer, Luc Mathieu, and Sandro Wartzack. Skin model shapes: A new paradigm shift for geometric variations modelling in mechanical engineering. *Computer-Aided Design*, 50(Supplement C):1 – 15, 2014.

[88] A. Loving, O. Crofts, N. Sykes, D. Iglesias, M. Coleman, J. Thomas, J. Harman, U. Fischer, J. Sanz, M. Siuko, and M. Mittwollen. Pre-conceptual design assessment of demo remote maintenance. *Fusion Engineering and Design*, 89(9):2246 – 2250, 2014. Proceedings of the 11th International Symposium on Fusion Nuclear Technology-11 (ISFNT-11) Barcelona, Spain, 15-20 September, 2013.

[89] H. Boessenkool, D.A. Abbink, C.J.M. Heemskerk, M. Steinbuch, M.R. de Baar, J.G.W. Wildenbeest, D. Ronden, and J.F. Koning. Analysis of human-in-the-loop tele-operated maintenance inspection tasks using vr. *Fusion Engineering and Design*, 88(9):2164 – 2167, 2013. Proceedings of the 27th Symposium On Fusion Technology (SOFT-27); Liège, Belgium, September 24-28, 2012.

[90] Wenjun Xu Aiming Liu Zude Zhou Duc Truong Pham Qi Zhang, Xiaomei Zhang. Modeling of Digital Twin Workshop Based on Perception Data. *ICIRA: International Conference on Intelligent Robotics and Applications*, 10464(6):3–14, 2017.

[91] Hong Liu Huansheng Ning and Laurence T. Yang. Cyberentity security in the internet of things. *IEEE Computer Society*, 46(4):46–53, 2013.

[92] Saeed Ebrahimi and Peter Eberhard. *Aspects of Contact Problems in Computational Multibody Dynamics*, pages 23–47. Springer Netherlands, Dordrecht, 2007.

[93] Peter Wriggers. *Computational Contact Mechanics*. Springer-Verlag Berlin Heidelberg, second edition, 2006.

[94] Amir R. Nejad, Zhen Gao, and Torgeir Moan. Long-term analysis of gear loads in fixed offshore wind turbines considering ultimate operational loadings. *Energy Procedia*, 35(Supplement C):187 – 197, 2013. DeepWind'2013 – Selected papers from 10th Deep Sea Offshore Wind R&D Conference, Trondheim, Norway, 24 – 25 January 2013.

[95] Olivier A. Bauchau. *Flexible Multibody Dynamics*. Springer Netherlands, 2011.

[96] Joris L. M. Peeters, Dirk Vandepitte, and Paul Sas. Analysis of internal drive train dynamics in a wind turbine. *Wind Energy*, 9(1-2):141–161, 4 2006.

[97] Y. Xing and T. Moan. Multi-body modelling and analysis of a planet carrier in a wind turbine gearbox. *Wind Energy*, 16(7):1067–1089, 2013.

[98] William LaCava, Y Xing, Y Guo, and Torgeir Moan. Determining wind turbine gearbox model complexity using measurement validation and cost comparison. *European Wind Energy Association Annual Event, Copenhagen, Denmark, April*, pages 16–19, 2012.

[99] Yi Guo, Jonathan Keller, William La Cava, Jason Austin, AR Nejad, Chris Halse, Loic Bastard, and Jan Helsen. Recommendations on model fidelity for wind turbine gearbox simulations. In *Gearbox Reliability Collaborative All-Members Meeting, Boulder, Colorado*, 2015.

[100] ISO/TC 60 Gears. Wind turbines – part 4: Design requirements for wind turbine gearboxes. Standard, International Organization for Standardization, Geneva, CH, December 2015.

[101] Ahmed A. Shabana. *Dynamics of Multibody Systems*. Cambridge University Press, forth edition, 2013.

[102] Pascal Ziegler and Peter Eberhard. *Investigation of Gears Using an Elastic Multibody Model with Contact*, pages 309–327. Springer Netherlands, Dordrecht, 2011.

[103] ISO/TC 4/SC 8 Load ratings and life. Rolling bearings – dynamic load ratings and rating life. Standard, International Organization for Standardization, Geneva, CH, February 2007.

[104] Y. Xing, M. Karimirad, and T. Moan. Modelling and analysis of floating spar-type wind turbine drivetrain. *Wind Energy*, 17(4):565–587, 2014.

[105] Zhen Gao Torgeir Moan Amir Rasekhi Nejad, Yi Guo. Development of a 5 MW reference gearbox for offshore wind turbines. *Wind Energy*, 19(6):1089–1106, 2015.

[106] Yi Guo and Robert G. Parker. Stiffness matrix calculation of rolling element bearings using a finite element/contact mechanics model. *Mechanism and Machine Theory*, 51:32 – 45, 2012.

[107] J Balchen, T Andresen, and B Foss. Reguleringsteknikk, 2004.

[108] Singiresu S Rao and Fook Fah Yap. Free vibrations with viscous damping. In Singiresu S, editor, *Mechanical vibrations*, volume 28 of *Cambridge aerospace series*, pages 158–168, Prentice Hall, 1 2011. Prentice Hall Upper Saddle River, Prentice Hall Upper Saddle River.

[109] Michael I. Friswell et. al. Free lateral response of simple rotor models. In *Dynamics of rotating machines*, volume 28 of *Cambridge aerospace series*, pages 22–25. Cambridge University Press, 2010.

[110] Michael I. Friswell et. al. Free lateral response of complex systems. In *Dynamics of rotating machines*, volume 28 of *Cambridge aerospace series*, pages 155–170. Cambridge University Press, 2010.

[111] Michael I. Friswell et. al. Free lateral response of complex systems. In *Dynamics of rotating machines*, volume 28 of *Cambridge aerospace series*, pages 387–389. Cambridge University Press, 2010.

[112] NREL. Recommendations on model fidelity for wind turbine gearbox simulations.

[113] Seung-Kyum Choi and Ramana V. Grannd Rob. Canfield. *Reliability-based structural design*. Springer Verlag, December 2006.

[114] Torgeir Moan. Lecture notes in structural risk and reliability analysis, February 2008.

[115] P Girdhar. Practical machinery vibration analysis and predictive maintenance, 2004.

[116] Singiresu S Rao and Fook Fah Yap. Response of a damped system under rotating unbalance. In Singiresu S, editor, *Mechanical vibrations*, volume 1, pages 287–293. Prentice Hall Upper Saddle River, 2011.

[117] Jason Mais. Spectrum analysis: the key features of analyzing spectra, 2002.

[118] Mahdi Ghane, Amir Rasekhi Nejad, Mogens Blanke, Zhen Gao, and Torgeir Moan. Condition monitoring of spar-type floating wind turbine drivetrain using statistical fault diagnosis. *Wind Energy*, 2018.

[119] N. BACHSCHMID, P. PENNACCHI, and A. VANIA. Identification of multiple faults in rotor systems. *Journal of Sound and Vibration*, 254(2):327 – 366, 2002.

[120] Monte carlo method, April 2018.

[121] International Organization for Standardization. Mechanical vibration - measurement and evalutation of machine vibrtion. part 1: General guidelines. Standard, International Organization for Standardization, Geneva, CH, 2016.

[122] Ahmed A Shabana. Flexible multibody dynamics: review of past and recent developments. *Multibody system dynamics*, 1(2):189–222, 1997.

[123] Stefan Dietz, Oskar Wallrapp, and Simon Wiedemann. Nodal vs. modal representation in flexible multibody system dynamics. *Proceedings of Multibody Dynamics*, pages 1–4, 2003.

[124] Wojciech Cholewa. Inverse vibration modelling for diagnosis of unbalance in machinery, 1995.

[125] Graham ML Gladwell. Inverse problems in vibration, vol. 119 of solid mechanics and its applications, 2004.

[126] John G Ziegler and Nathaniel B Nichols. Optimum settings for automatic controllers. *trans. ASME*, 64(11), 1942.

[127] Simpack with simulink, 2011.

[128] Martin Schulze, Stefan Dietz, Bernhard Burgermeister, Andrey Tuganov, Holger Lang, Joachim Linn, and Martin Arnold. Integration of nonlinear models of flexible body deformation in multibody system dynamics. *Journal of Computational and Nonlinear Dynamics*, 9(1):011012, 2014.

[129] Markus Bachinger, Michael Stolz, and Martin Horn. A novel drivetrain modelling approach for real-time simulation. *Mechatronics*, 32:67 – 78, 2015.

Appendix A

Hammer test

A.1 Hammer test 0

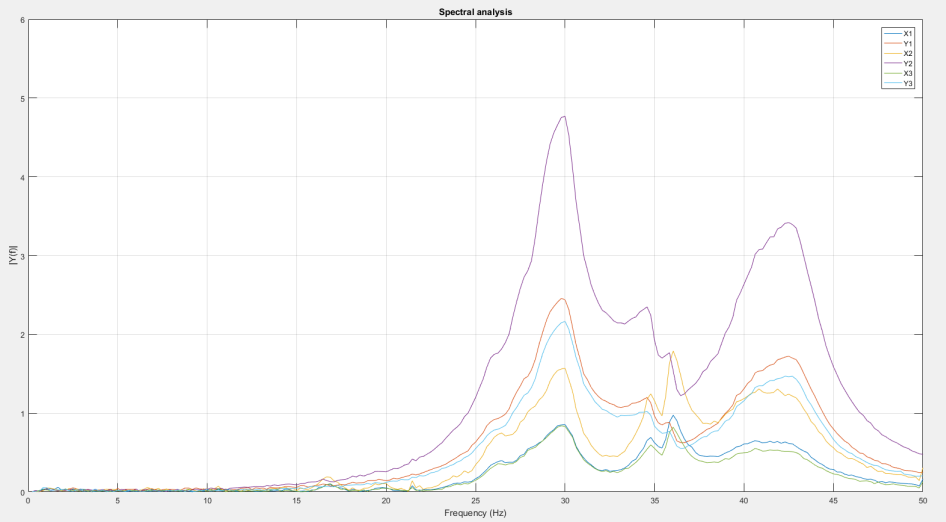

Figure A.1: Spectral analysis hammertest 0

Table A.1: Natural Frequency and Stiffness in hammer test 0

	X1	Y1	X2	Y2	X3	Y3
Damping Coefficient [Ns/m]	45.772	61.803	0.75277	44.919	7.3479	36.965
Natural frequency [Hz]	36.042	29.792	36.042	30	29.792	30
Stiffness [N/m]	7.3334e+05	5.0105e+05	7.3334e+05	5.0105e+05	7.3334e+05	5.0809e+05

A.2 Hammer test 1

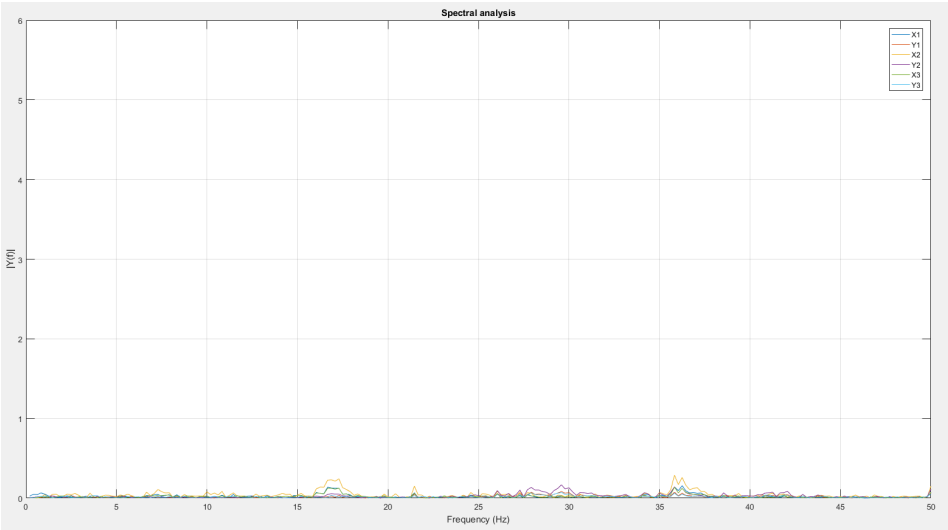

Figure A.2: Spectral analysis hammertest 1

Table A.2: Natural Frequency and Stiffness in hammer test 1. In this run, no impact from the hammer was made and this makes this test invalid.

	X1	Y1	X2	Y2	X3	Y3
Damping Coefficient [Ns/m]	2.718	0.11155	19.565	13.435	0.10144	3.8615
Natural frequency [Hz]	336.042	378.33	873.96	29.583	35.833	202.71
Stiffness [N/m]	7.3334e+05	8.0806e+07	4.312e+08	4.9407e+05	7.2489e+05	2.3197e+075

A.3 Hammer test 2

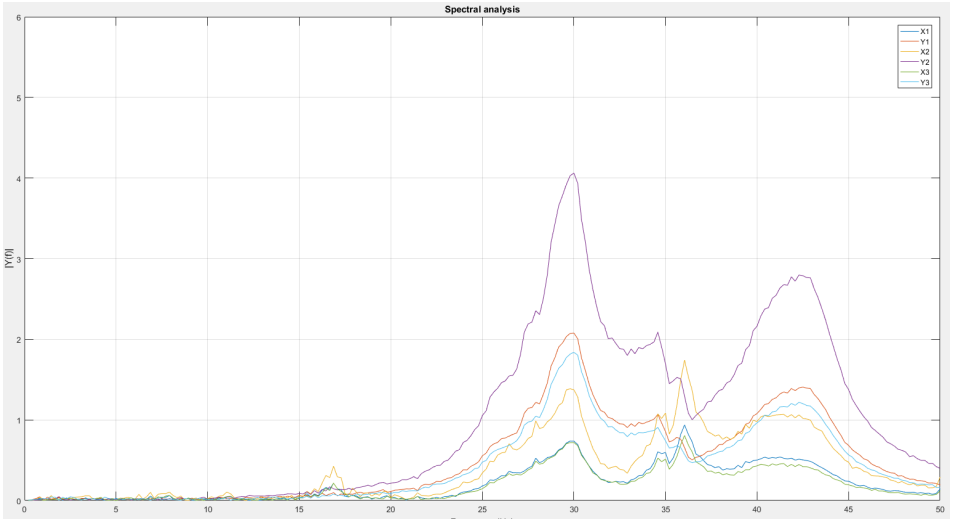

Figure A.3: Spectral analysis hammertest 2

Table A.3: Natural Frequency and Stiffness in hammer test 2

	X1	**Y1**	**X2**	**Y2**	**X3**	**Y3**
Damping Coefficient [Ns/m]	1.5972	78.72	0.15073	54.688	4.7996	37.728
Natural frequency [Hz]	36.042	30	36.042	30	36.042	30
Stiffness [N/m]	8.2052e+05	5.6849e+05	8.2052e+05	5.6849e+05	8.2052e+05	5.6849e+05

A.4 Hammer test 3

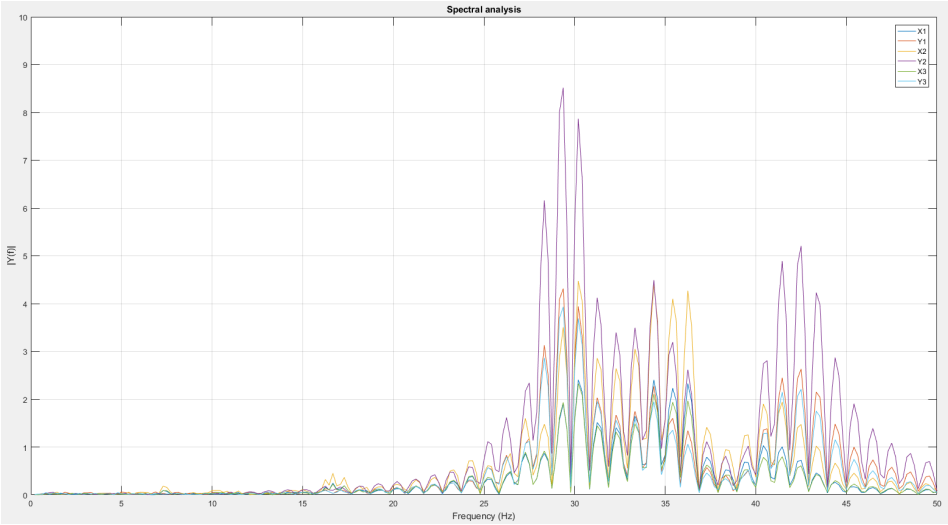

Figure A.4: Spectral analysis hammertest 3

Table A.4: Natural Frequency and Stiffness in hammer test 3

	X1	Y1	X2	Y2	X3	Y3
Damping Coefficient [Ns/m]	6.9883	3.8555	2.1069e-06	8.7901	1.3069	14.761
Natural frequency [Hz]	34.375	29.375	30.208	29.375	30.208	29.375
Stiffness [N/m]	6.6709e+05	4.8714e+05	5.1517e+05	4.8714e+05	5.1517e+05	4.8714e+05

A.5 Hammer test 4

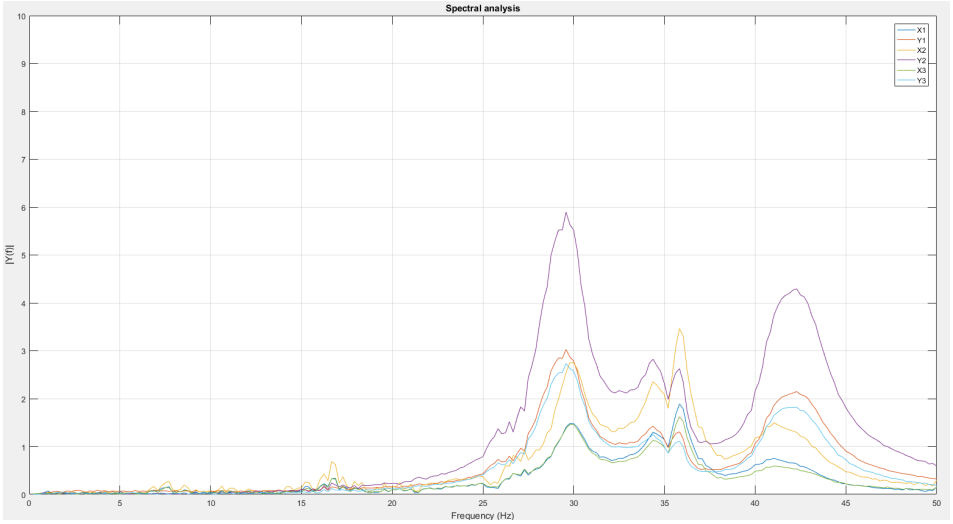

Figure A.5: Spectral analysis hammertest 4

Table A.5: Natural Frequency and Stiffness in hammer test 4

	X1	Y1	X2	Y2	X3	Y3
Damping Coefficient [Ns/m]	8.7031	15.079	0.041107	27.356	5.3289	30.9841
Natural frequency [Hz]	35.833	29.583	35.833	29.583	35.833	29.583
Stiffness [N/m]	7.2489e+05	4.9407e+05	7.2489e+05	4.9407e+05	7.2489e+05	4.9407e+05

A.6 Hammer test 5

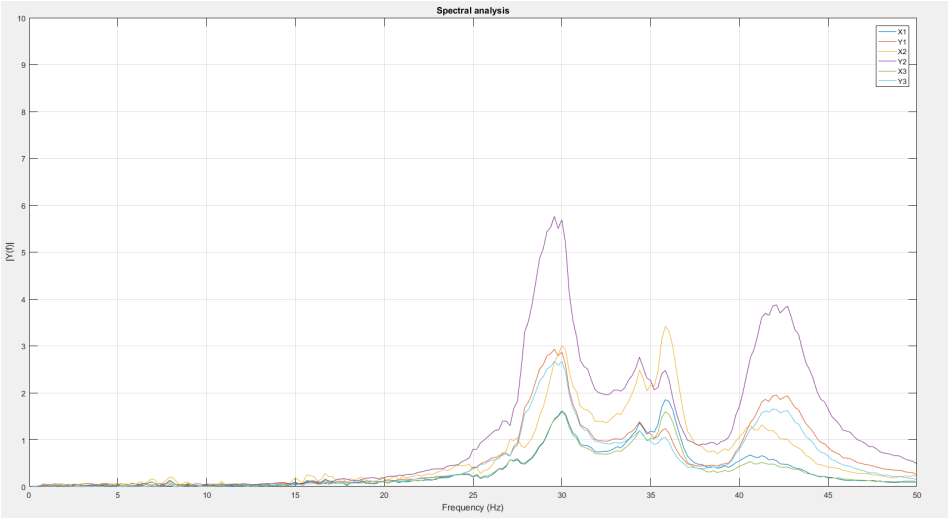

Figure A.6: Spectral analysis hammertest 5

Table A.6: Natural Frequency and Stiffness in hammer test 5

	X1	Y1	X2	Y2	X3	Y3
Damping Coefficient [Ns/m]	0.34565	12.381	2.3069	24.68	5.9279	27.274
Natural frequency [Hz]	35.833	29.583	35.833	29.583	35.833	29.583
Stiffness [N/m]	7.2489e+05	4.9407e+05	7.2489e+05	4.9407e+05	7.2489e+05	4.9407e+05

APPENDIX B. CONTROL SYSTEM TUNING

Appendix B

Control System Tuning

Hz	Kp	Ki
20	12/10	40/8
25	1/10	4/8
30	1/10	4/8
35	1/10	4/8
40	1/10	1/8
45	1/10	1/13
50	1/10	1/550

	20 Hz	125.663706	
	Kp	Ki	
	12/10	40/8	
	25 Hz	157.079633	
	Kp	Ki	
	1/10	4/8	
	30 Hz	188.495559	
	Kp	Ki	
	1/10	4/8	
	35 Hz	219.911486	
	Kp	Ki	
1	12/10	40/8	Crash at 0.3 sec
2	24/10	40/8	Crash at 0.07 sec
3	6/10	40/8	Crash at 0.42 sec
4	5/10	40/8	Crash at 0.52 sec
5	4/10	40/8	Crash at 0.46 sec
6	3/10	40/8	Crash at 0.52 sec
7	2/10	40/8	Crash at 0.6 sec
8	1/10	40/8	Crash at 0.56
9	1/10	30/8	Crash at 0.6 sec
10	1/10	20/8	Crash at 0.85 sec
11	1/10	10/8	Crash at 2.5 sec
12	1/10	8/8	Crash at 2.9 sec
13	1/10	7/8	Crasht at 3.1 sec
14	1/10	6/8	Crash at 3.5 sec
15	1/10	5/8	Crash at 4.5 sec
16	1/10	4/8	OK!
	40 Hz	251.327412	
	Kp	Ki	
1	1/10	4/8	Crash at 3.75 sec
2	1/10	3/8	Crash at 4.6 sec
3	1/10	2/8	Crash at 6.8 sec
4	1/10	1/8	OK!
	45 Hz	282.743339	
	Kp	Ki	
1	1/10	1/8	Crash at 9.2 sec
2	1/10	1/9	Crash at 11.7 sec
3	1/10	1/10	Crash at 15.2 sec
4	1/10	1/11	Crash at 16.7 sec
5	1/10	1/12	Crash at 14.8 sec
6	1/10	1/13	OK!

	50 Hz	314.159	
	Kp	Ki	
1	1/10	1/13	Crash at 11.17 sec
2	1/10	1/14	Crash at 12.3 sec
3	1/10	1/15	Crash at 13.27 sec
4	1/10	1/16	Crash at 14.17 sec
5	1/10	1/17	Crash at 16.6 sec
6	1/10	1/18	Crash at 16.56 sec
7	1/10	1/19	Crash at 17.8 sec
8	1/10	1/20	Crash at 19.7 sec
9	1/10	1/21	Crasht at 21.73 sec
10	1/10	1/22	Crash at 21.39 sec
11	1/10	1/23	Crash at 21.4 sec
12	1/10	1/24	Crash at 22 sec
13	1/10	1/25	Crash at 22.7 sec
14	1/10	1/26	Crash at 23.57 sec
15	1/10	1/27	Crash at 24.4 sec
16	1/10	1/28	Crash at 25.3 sec
17	1/10	1/29	Crash at 26.44 sec
18	1/10	1/30	Crash at 27.3 sec
19	1/10	1/31	Crash at 28.4 sec
20	1/10	1/32	Crash at 29.6 sec
21	1/10	1/33	Crash at 30.8 sec
22	1/10	1/34	Crash at 34.78 sec
23	1/10	1/35	Crash at 35.89 sec
24	1/10	1/36	Crash at 35.89 sec
25	1/11	1/36	Crash at 34.23 sec
26	1/7	1/36	Crash at 42 sec
27	1/5	1/36	Crash at 39.6 sec
28	5	36	Crash at 0.007 sec
29	1/7	1/37	Crash at 39.2 sec
30	1/7	1/38	Crash at 39.6 sec
31	1/12	1/38	Crash at 34.6 sec
32	1/10	1/38	Crash at 36.8 sec
33	1/10	15/38	Crash at 3.2445
34	100	380	Crash at 0 sec
35	1/10	1/40	Crash at 37.95 sec
36	1/10	1/45	Crash at 43 sec
37	1/10	1/50	Crash at 49.4 sec
38	1/10	1/55	Crash at 53.28 sec
39	1/10	1/550	OK!

Figure B.1: K_p and K_i for increasing angular velocity

APPENDIX C. RESPONSE DRIVETRAIN TEST RIG

Appendix C

Response Drivetrain Test Rig

C.0.1 Velocity

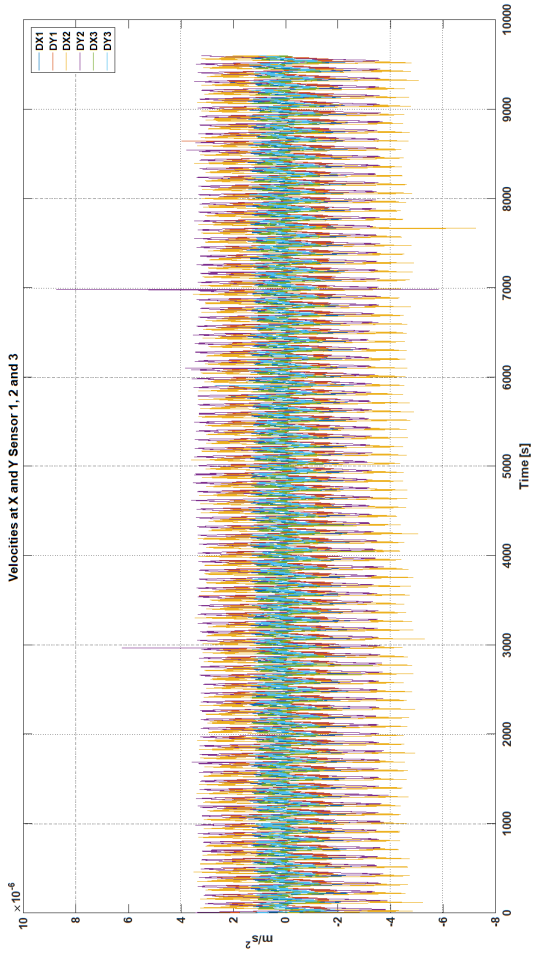

Figure C.1: Velocities in m/s for 20 Hz test run

C.0.2 Acceleration

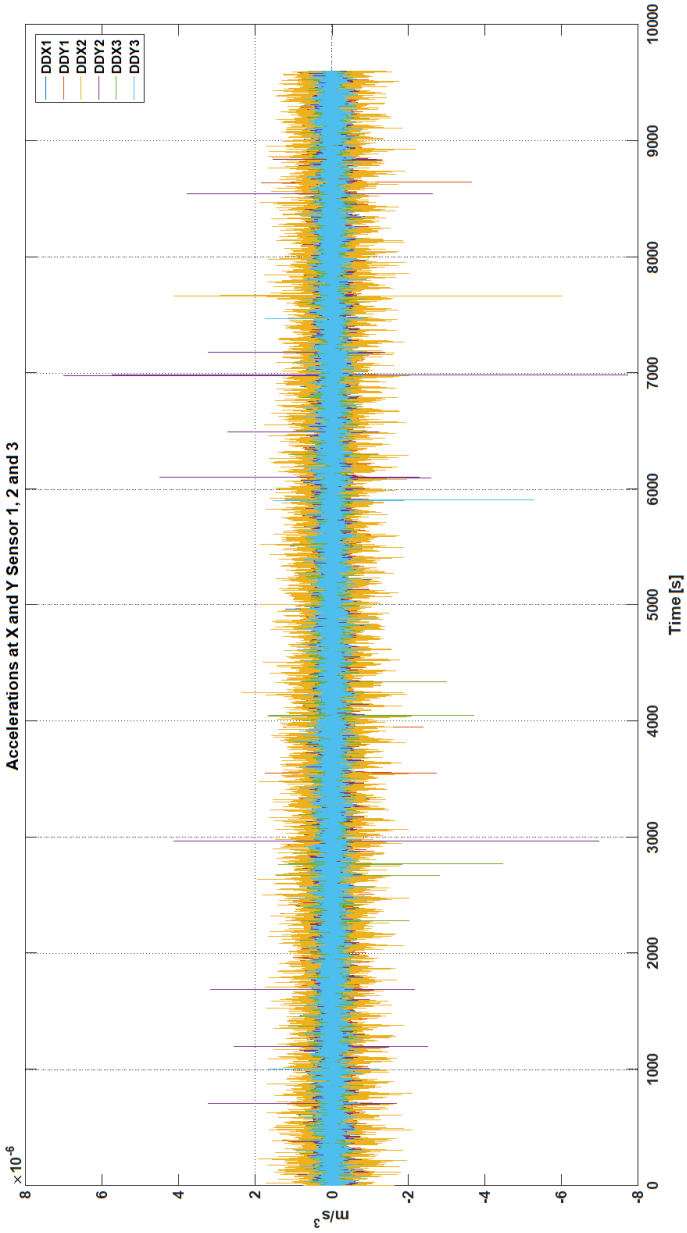

Figure C.2: Accelerations in m/s^2 for 20 Hz test run

Appendix D

Response digital twin - 1 DOF

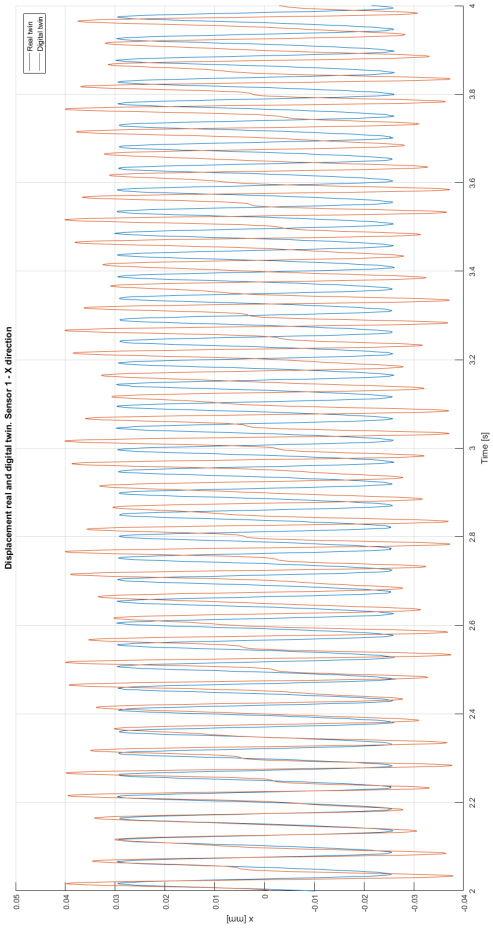

Figure D.1: Performance for Digital Twin 1DOF Sensor 1 - X direction

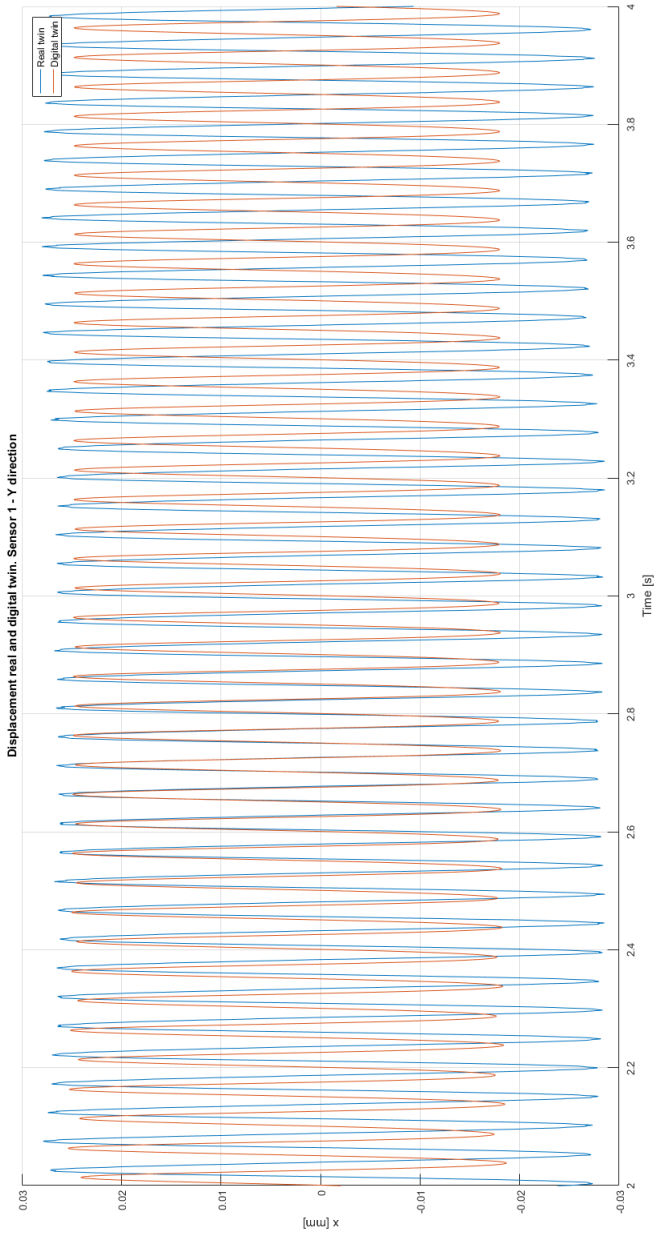

Figure D.2: Performance for Digital Twin 1DOF Sensor 1 - Y direction

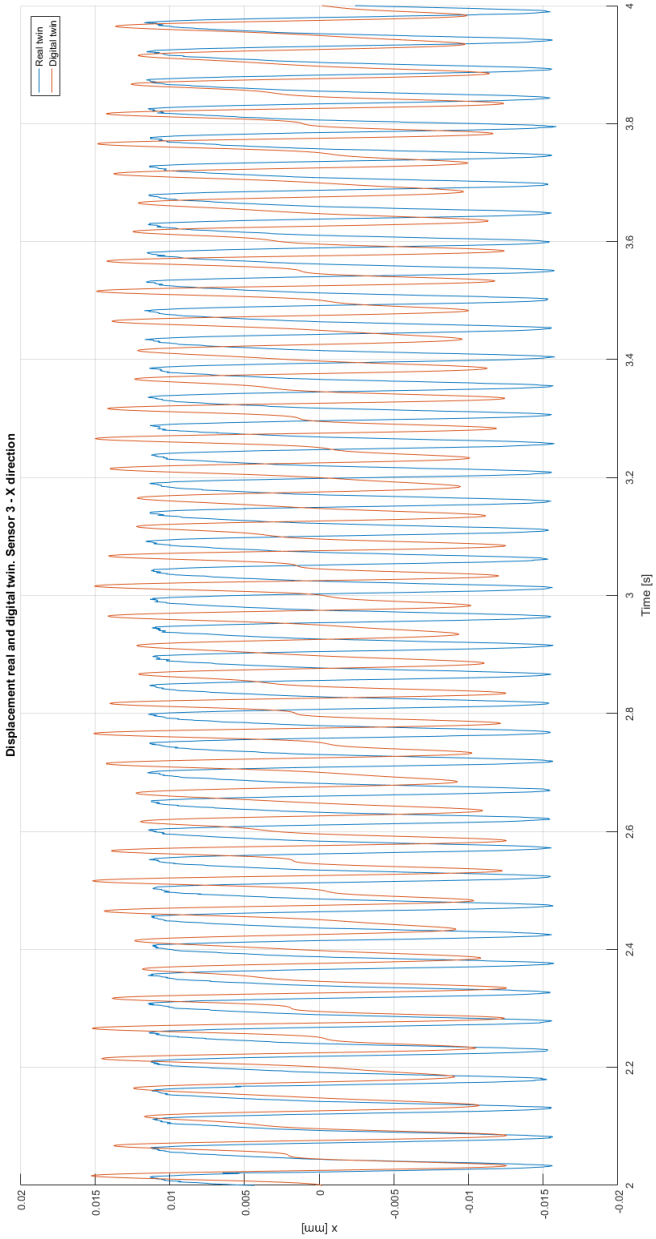

Figure D.3: Performance for Digital Twin 1DOF Sensor 3 - X direction

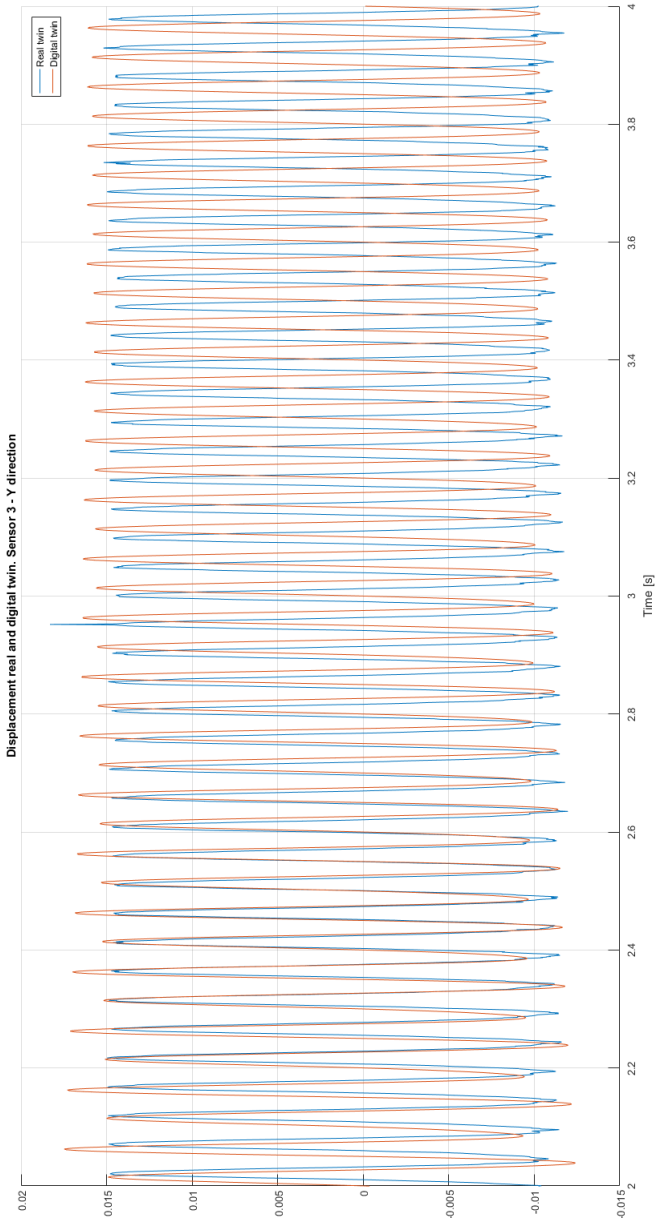

Figure D.4: Performance for Digital Twin 1DOF Sensor 3 - Y direction

Appendix E

Response Rigid Shaft Experimental Modelling

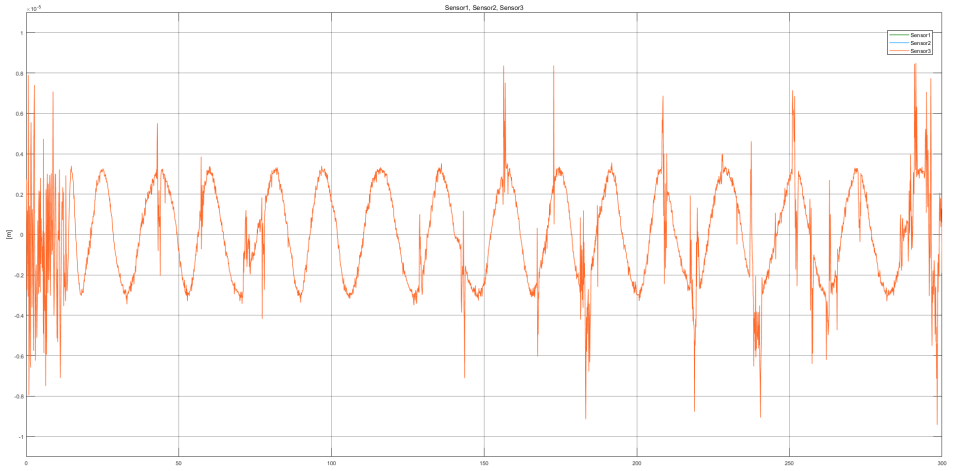

Figure E.1: Response in 3 DOF model with rigid shaft at 1.30 incremental increase of stiffness in X direction

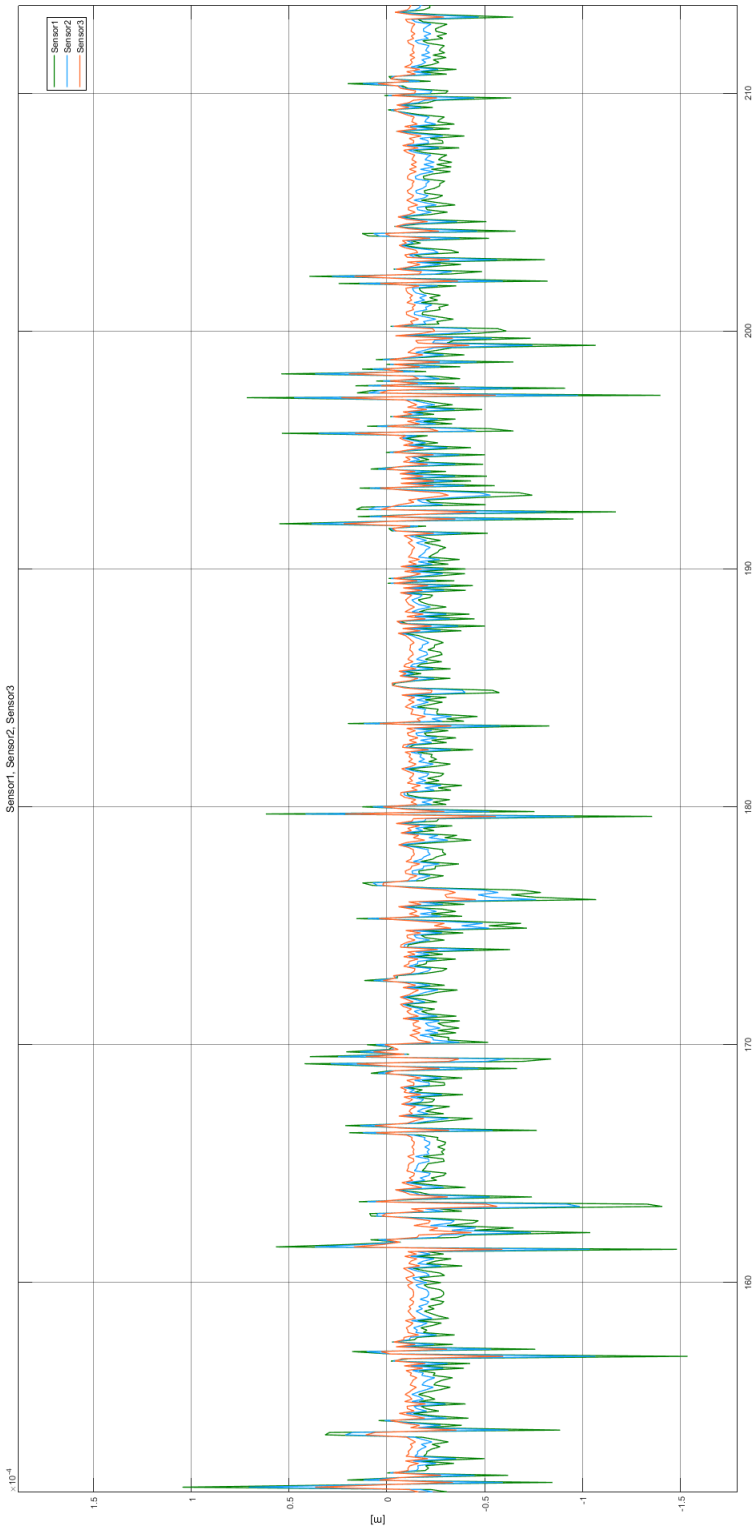

Figure E.2: Response in 3 DOF model with rigid shaft at reduced damping to 30% of bearing 2 values in bearing 1 - X direction

Appendix F

Rotor Kit Bentley Nevada

RK 4 Rotor Kit

Bently Nevada™ Asset Condition Monitoring

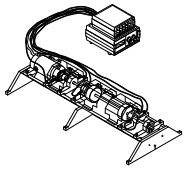

Description

The RK 4 Rotor Kit closely simulates actual rotating machine behavior. Its unique geometry and its ability for users to isolate and control individual machine characteristics make it useful as both a teaching tool and as a laboratory tool for theoretical research.

Machine malfunctions and experiments that can be demonstrated include, but are not limited to:

- rotor unbalance - both single plane and multiplane
- shaft rub condition
- oil whirl and oil whip instabilities
- shaft perturbation

In addition to machinery behavior, the rotor kit can be used to teach the fundamentals of proximity probe placement, gapping, and troubleshooting. It can also help technicians learn how to read and interpret proximity probe signals using an oscilloscope.

Performance and Features

The RK 4 Rotor Kit has a V-frame design that has been developed to provide better control of the housing dynamic stiffness properties. The mechanical tolerances have also been tightened, resulting in more accurate machine behavior modeling. The RK 4 Rotor Kit motor can closely hold the desired speed with changes in loading conditions. This has been accomplished by incorporating a direct current motor and high performance control circuitry. The motor can run in either a clockwise or counter-clockwise direction and has adjustable slow roll speed capability. It can be controlled remotely by using a ±5 volt control input, such as a signal generator or dc power supply, to drive the motor speed control device. Rotor speed is displayed on a digital tachometer with a large LCD readout.

The RK 4 Rotor Kit consists of:

- A mechanical base (including motor, coupling, rotor shaft, two balance wheels, two journal bearings and bearing blocks, six proximity probes, three probe mounts, a rub screw, and three safety covers).
- A Proximitor® assembly that contains five Proximitor units.
- A direct current motor speed control device.

The motor speed control device provides power for both the rotor kit and the Proximitor assembly. A measurement and diagnostic tool, such as an oscilloscope or other diagnostic instrument, should be ordered separately in order to observe the RK 4 machine behavior.

An optional Oil Whirl/Whip kit can be ordered. The Oil whirl kit consists of:

- A high pressure oil pump assembly.
- An oil whirl bearing assembly.
- A rotor kit shaft with oil bearing journal.
- A load frame.

Fluid-induced instabilities (both oil whirl and whip) as well as basic journal bearing behavior can be demonstrated using the oil whirl/whip kit. The oil whirl bearing is made from transparent plastic, allowing the user to view the oil film development during operation. The load frame is used to remove the effect of gravity on the rotor and to position the rotor to any desired eccentricity ratio.

An optional perturbator kit is also available. The Unbalance Perturbator Option applies a precise rotating force to the Rotor Kit shaft independent of the shaft rotative speed. Perturbation testing is a powerful experimental technique used to identify rotor system parameters. The Unbalance Perturbator Option is a 3-in-1 tool that allows the user to perform nonsynchronous, synchronous, and static perturbation experiments on the RK 4 Rotor Kit, with or without the Oil Whirl Option.

The kit includes:

- A mechanical base (including motor, coupling, drive assembly, drive belts, and two proximity probes for motor speed control and Keyphasor® signal pickup).
- A perturbator disk assembly.
- A motor speed control unit.

Specifications

Basic Rotor Kit

Power:

95 to 125 Vac, single phase,
or 190 to 250 Vac, single phase,
50 to 60 Hz at 3.0 A maximum.

Fuse Rating:

250 V at 3 A slow-blow.

Buffered Proximitor Assembly Outputs:

200 mV/mil.

Max Speed:

10,000 rpm, typical.

Max Ramp Rate:

±15,000 rpm/min. typical.

Mechanical Base Dimensions

Height:

165 mm (6.5 in)

Width:

340 mm (13.4 in)

Depth:

789 mm (30.8 in)

Motor Speed Control Dimensions

Height:

115 mm (4.5 in)

Width:

260 mm (10.3 in)

Depth:

325 mm (12.8 in)

Proximitor Assembly Dimensions

Height:

86 mm (3.4 in)

Width:

154 mm (6.1 in)

Depth:

158 mm (6.2 in)

Shaft diameter:

10 mm (0.4 in)

Weight

Rotor Kit Base:

14.5 kg (32 lb)

Proximitor Assembly:

0.9 kg (2 lb)

Motor Speed Control:

2.7 kg (6 lb)

Oil Whirl/Whip Kit

Oil Pump Power:

95 to 125 Vac, single phase

50 to 60 Hz at 1.5 A maximum; or

190 to 250, single phase,

50 to 60 Hz at 0.75 A maximum. User-selectable input voltage.

Oil Pump Fuse Rating:

95 to 125 Vac:

250 V 3.0 A slow-blow;

190 to 250 Vac:

250 V 1.5 A slow-blow.

User-selectable fuse.

Oil Pump Dimensions

Height:

145 mm (5.7 in)

Width:

317 mm (12.5 in)

Depth:

292 mm (11.5 in)

Perturbator Kit

Power:

95 to 125 Vac, single phase,

or 190 to 250 Vac, single phase,

50 to 60 Hz at 3.0 A maximum.

Fuse Rating:

250 V at 3 A slow-blow.

Max Speed:

10,000 rpm, typical.

Max Ramp Rate:

±15,000 rpm/min, typical.

Perturbator Mechanical

Base Dimensions

Height:

165 mm (6.5 in)

Width:

254 mm (10.0 in)

Depth:

305 mm (12.0 in)

Motor Speed Control Dimensions

Height:

115 mm (4.5 in)

Width:

260 mm (10.3 in)

Depth:

325 mm (12.8 in)

Ordering Information

Rotor Kit

123456-AXX-BXX

A: Oil Whirl/Whip Kit

0 0 Not required
0 1 Required

B: Perturbator Kit

0 0 Not Required
0 1 Required

Accessories

Spare Manuals

126376-01

RK 4 Rotor Kit

137482-01

Oil Whirl/Whip Kit

141121-01

Unbalance Perturbator Option

Spare Probes

330903-00-03-10-02-00

Spare 3300 NSv Probe, M8X1, without armor

(Vibration, Keyphasor probes)

330903-00-02-01-02-00

Spare 3300 NSv Probe, M8X1, without armor

(Speed Probe)

Additional Oil Whirl/Whip Option

126379

Oil Whirl/Whip Kit

Additional Perturbator Option

140054

Unbalance Perturbator Option

Option Diagrams

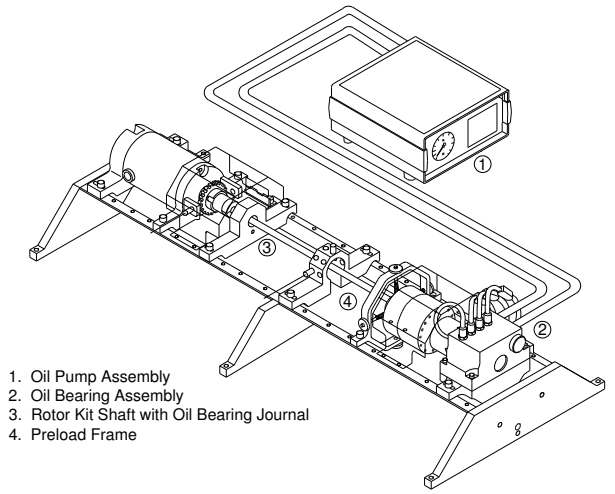

1. Oil Pump Assembly
2. Oil Bearing Assembly
3. Rotor Kit Shaft with Oil Bearing Journal
4. Preload Frame

Figure 1: RK 4 Rotor Kit Base with Oil Whirl Option

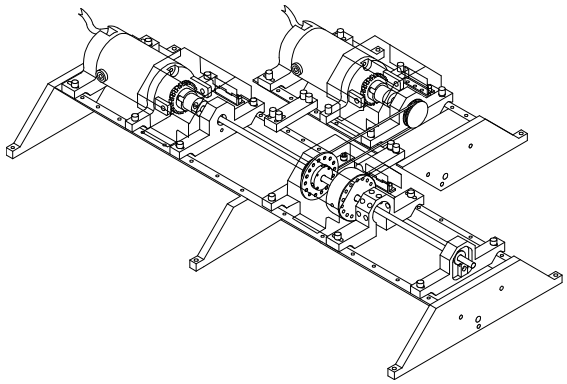

Figure 2: RK 4 Rotor Kit Base with Perturbator Option

Appendix G

Load Case 2, 5 DOF Flexible Shaft

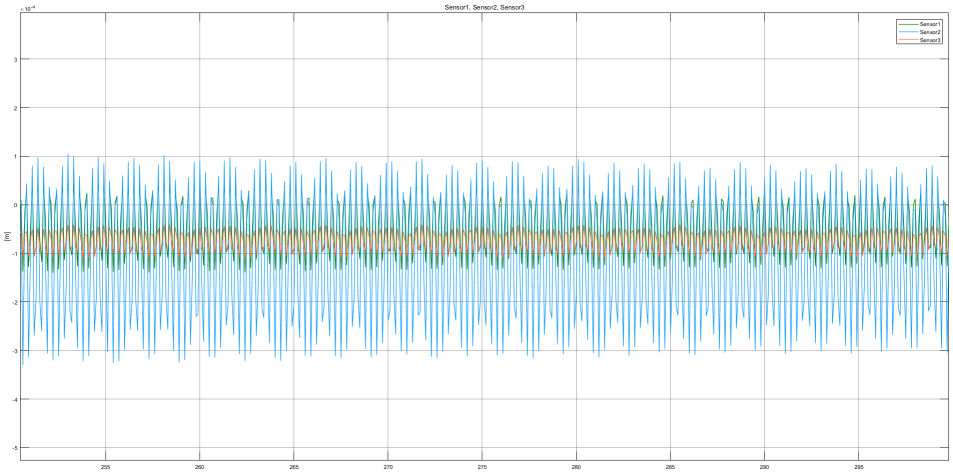

Figure G.1: Incremental increase of 1.05, X-direction

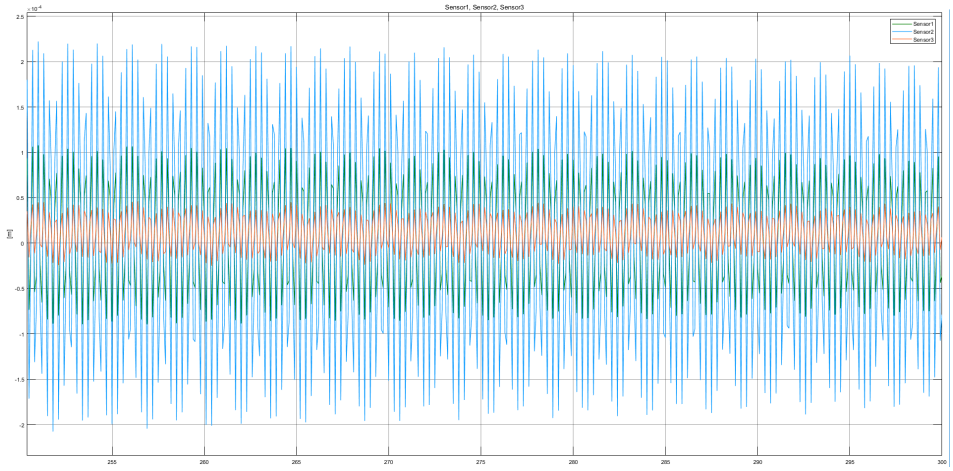

Figure G.2: Incremental increase of 1.05, Y-direction

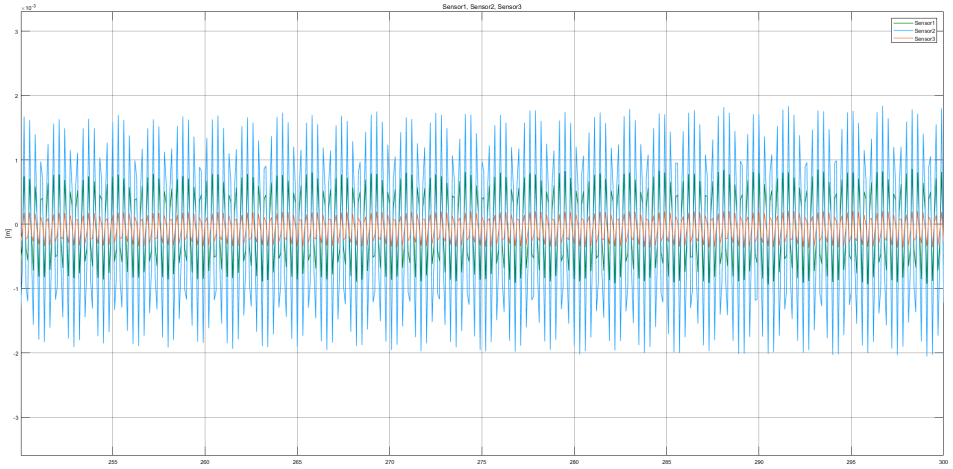

Figure G.3: Incremental increase of 1.10, X-direction

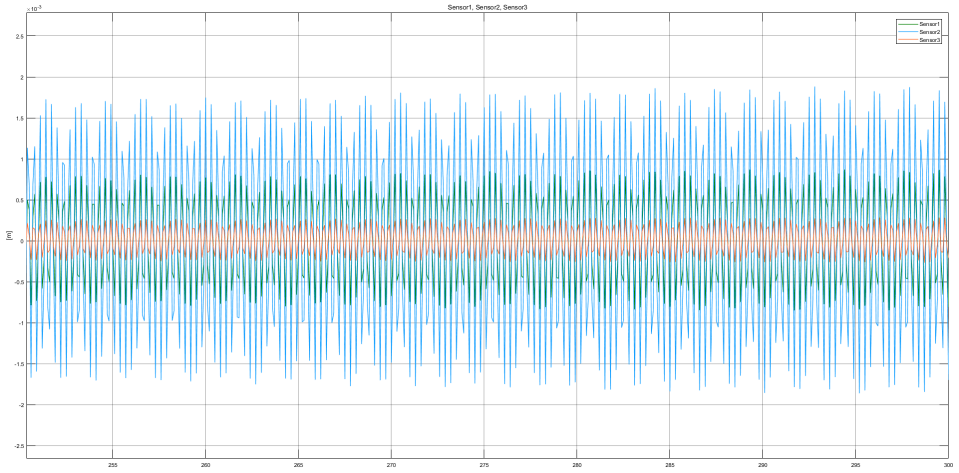

Figure G.4: Incremental increase of 1.10, Y-direction

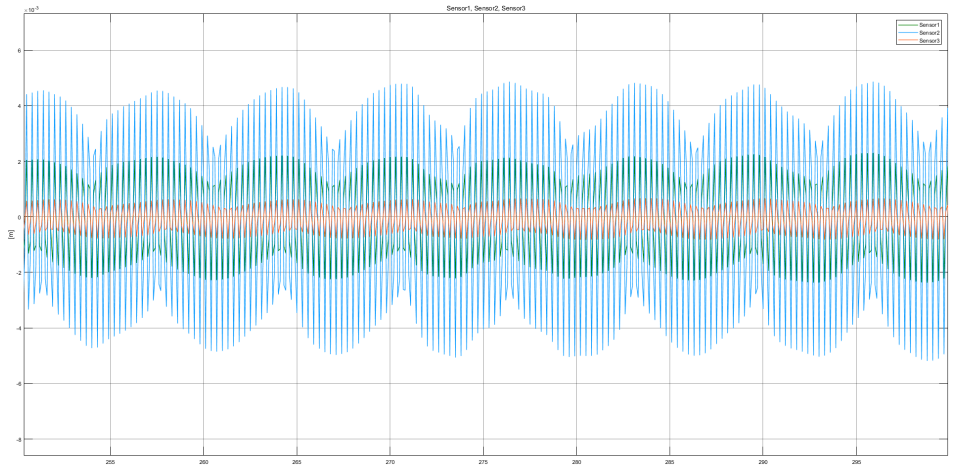

Figure G.5: Incremental increase of 1.15, X-direction

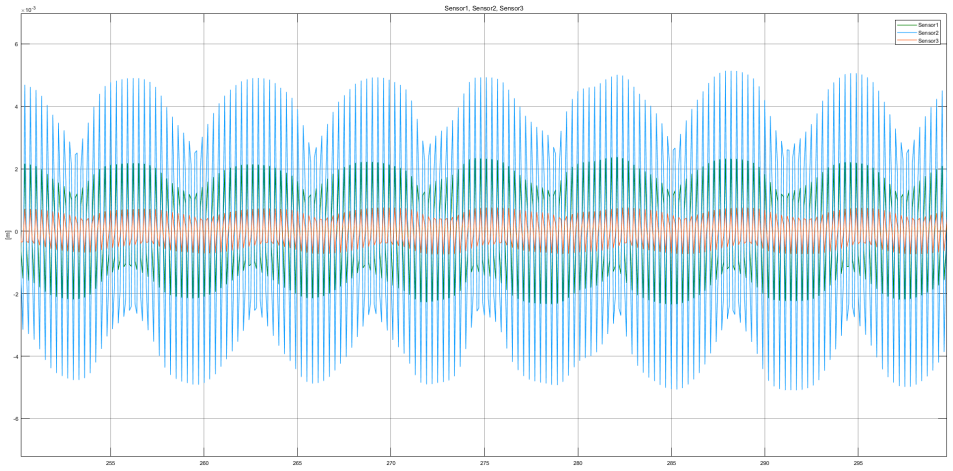

Figure G.6: Incremental increase of 1.15, Y-direction

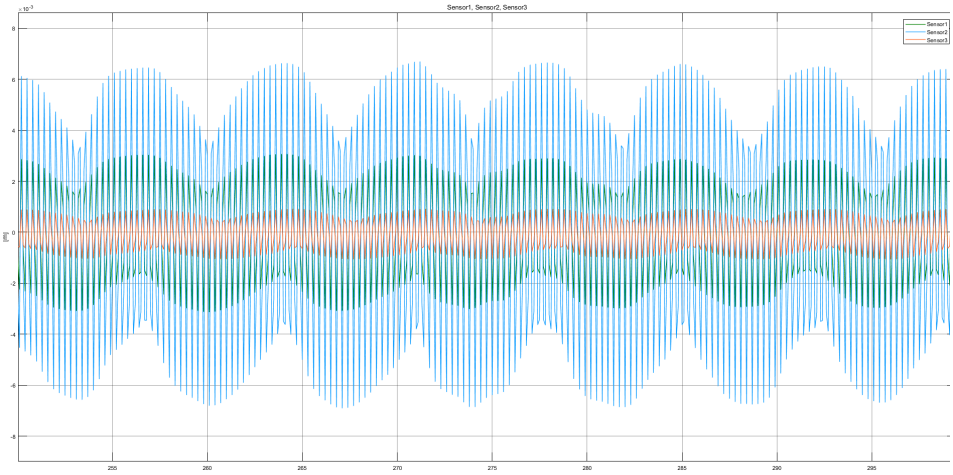

Figure G.7: Incremental increase of 1.20, X-direction

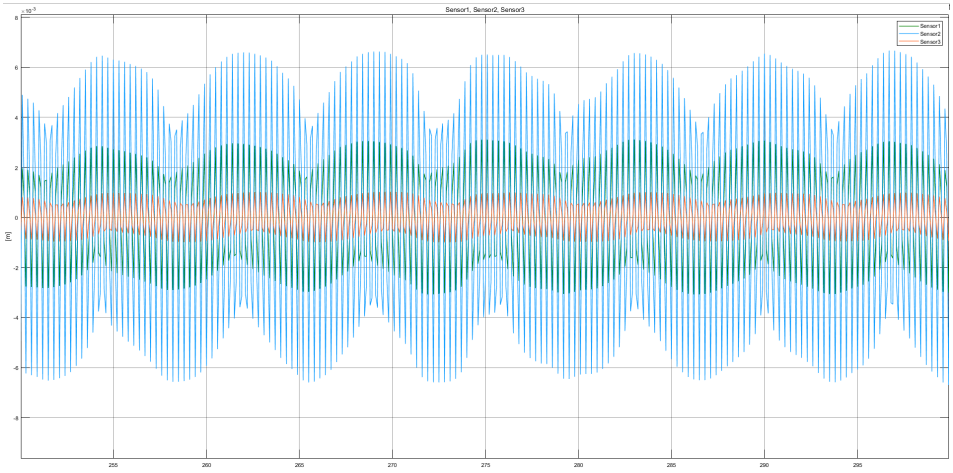

Figure G.8: Incremental increase of 1.20, Y-direction

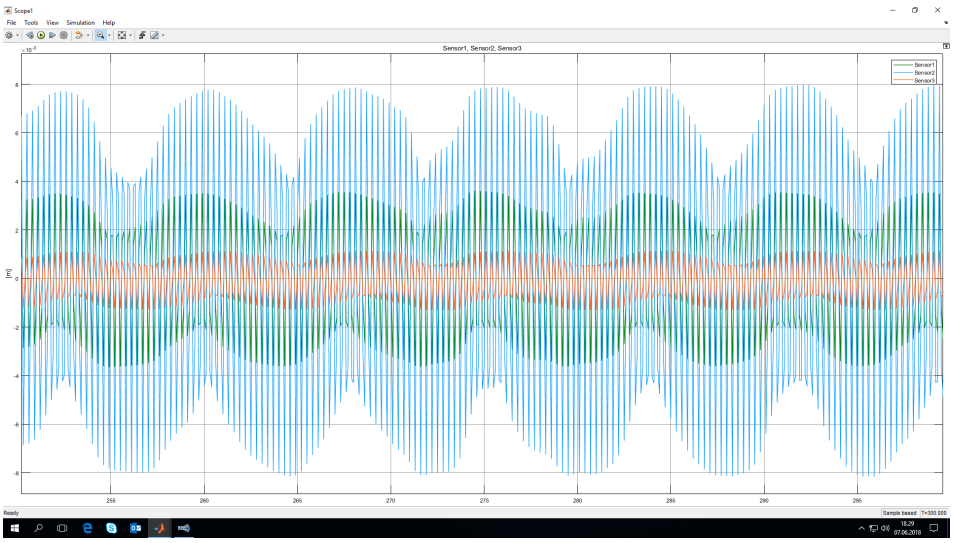

Figure G.9: Incremental increase of 1.25, X-direction

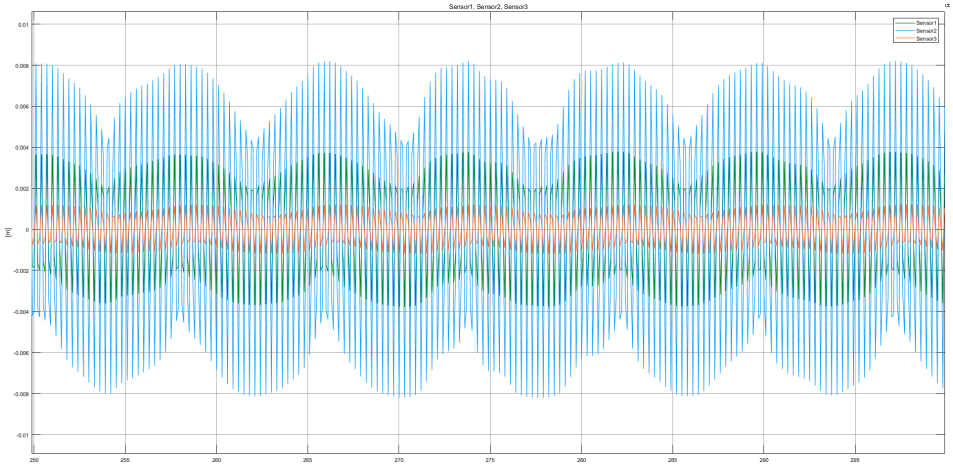

Figure G.10: Incremental increase of 1.25, Y-direction

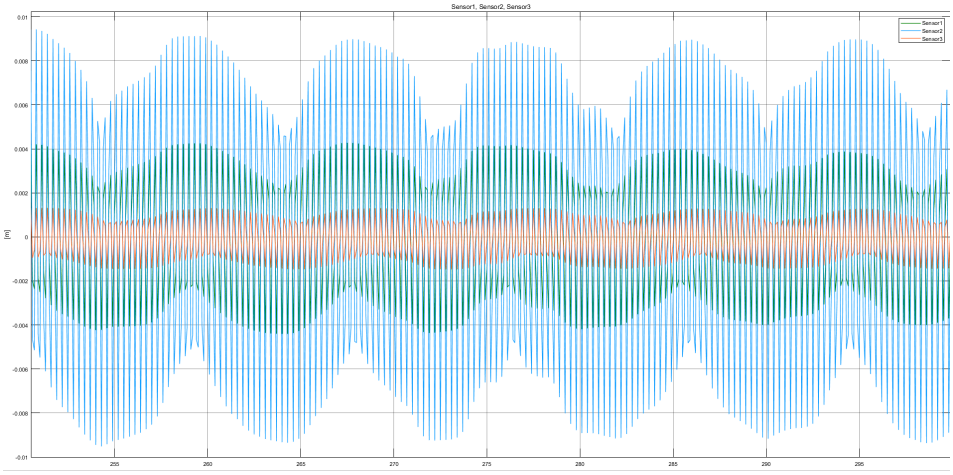

Figure G.11: Incremental increase of 1.30, X-direction

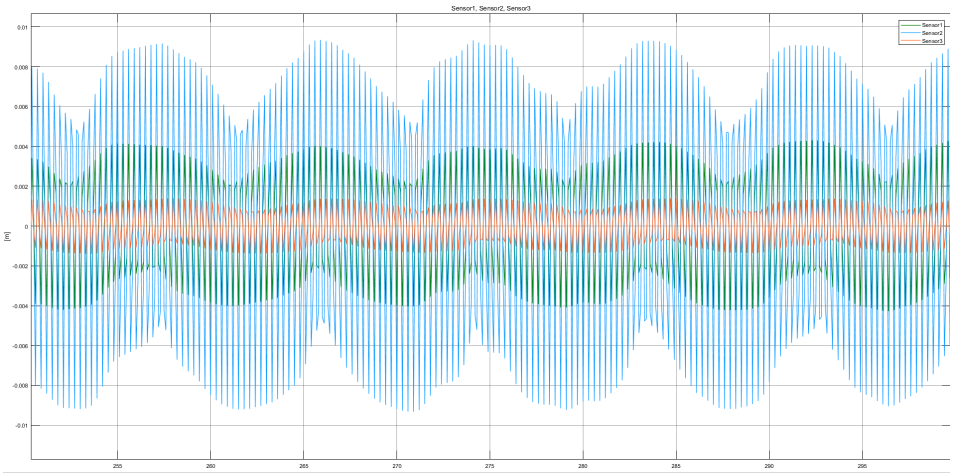

Figure G.12: Incremental increase of 1.30, Y-direction

Appendix H

Speed Increase Drivetrain Test Rig

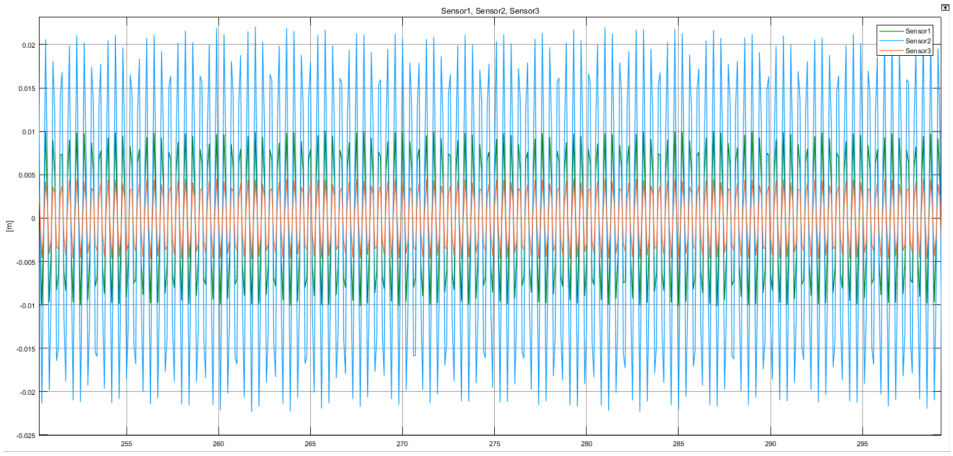

Figure H.1: Flexible 5 DOF SIMPACK Model run at 25 Hz

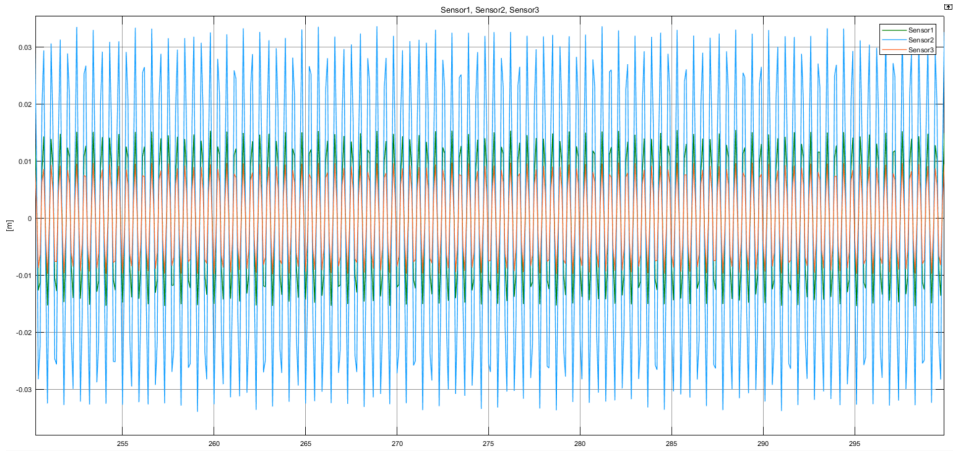

Figure H.2: Flexible 5 DOF SIMPACK Model run at 30 Hz

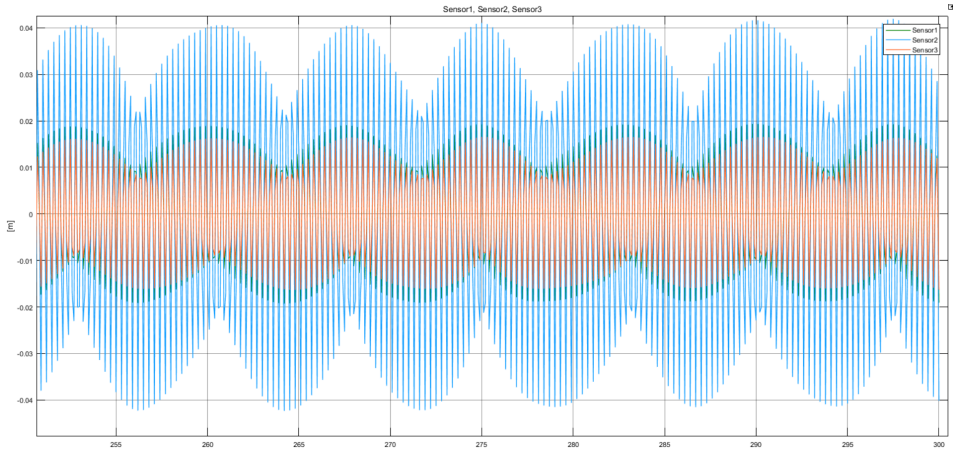

Figure H.3: Flexible 5 DOF SIMPACK Model run at 35 Hz

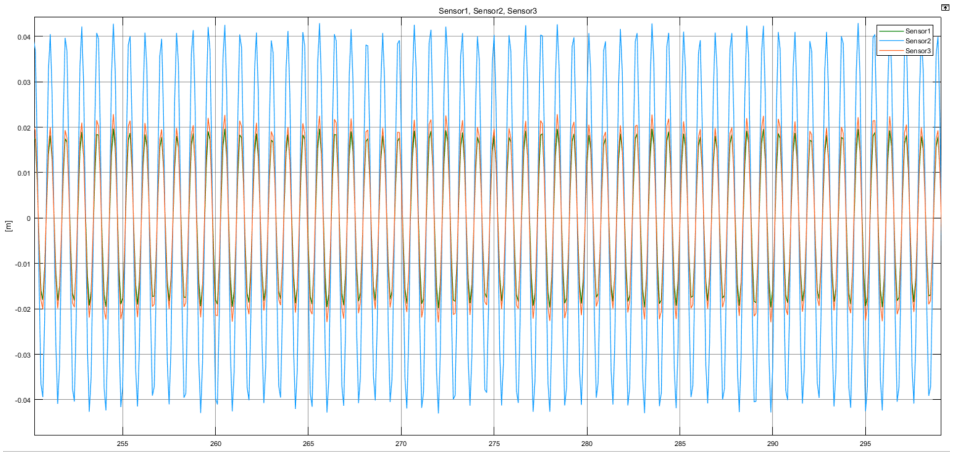

Figure H.4: Flexible 5 DOF SIMPACK Model run at 40 Hz

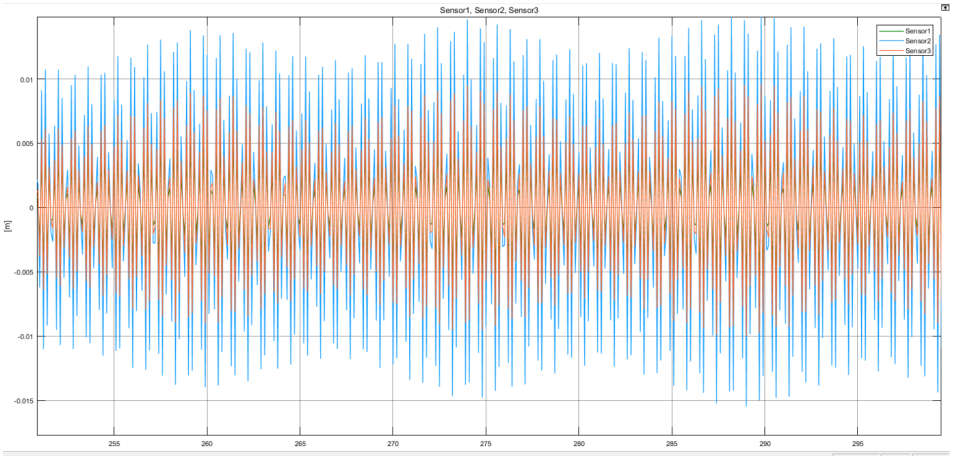

Figure H.5: Flexible 5 DOF SIMPACK Model run at 45 Hz

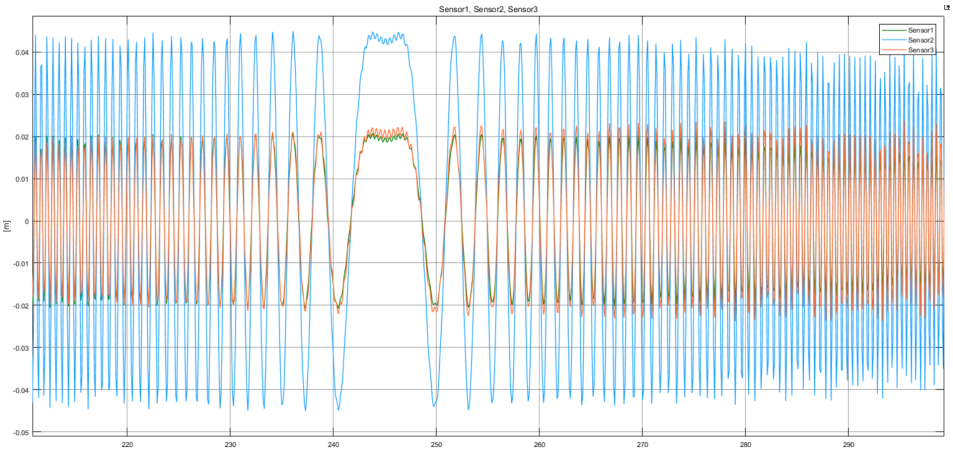

Figure H.6: Flexible 5 DOF SIMPACK Model run at 50 Hz